國 立 交 通 大 學

材料科學與工程學系

博 士 論 文

在金剛烷披覆之矽基材上探討鑽石的成核、成長與結構特性之研究

The study of nucleation, growth, and structural characterization of diamond on adamantane-coated Si substrate

研 究 生 ： Rajanish Nath Tiwari

指導教授 ： 張 立 教授

中華民國 九十九年 十一月

在金剛烷披覆之矽基材上探討 鑽石的成核、成長與結構特性之研究

The study of nucleation, growth, and structural characterization of diamond on adamantane-coated Si substrate

研 究 生: Rajanish Nath Tiwari　　Student: Rajanish Nath Tiwari

指導教授: 張 立 博士　　Advisor: Dr. Li Chang

國 立 交 通 大 學

材料科學與工程學系

博士論文

A Dissertation

Submitted to Department of Materials Science and Engineering
College of Engineering
National Chiao Tung University
in Partial Fulfillment of the Requirements
for the Degree of Doctor of Philosophy
in Materials Science and Engineering

November 2010

Hsinchu, Taiwan, Republic of China

中華民國 九十九年 十一月

在金剛烷披覆之矽基材上探討 鑽石的成核、成長與結構特性之研究

研究生：**Rajanish Nath Tiwari**　　指導教授：張 立 博士

國立交通大學　材料科學與工程研究所

摘要

鑽石薄膜有許多優良的特性，特別是在電子、光電、和光學應用上有極大的潛力。雖然鑽石合成技術已經達到了一個限度，在大面積商品化的需求下還存有一些不明且難以解決的問題，特別是在較低的溫度與壓力下進行鑽石薄膜的合成。因此，在本論文中，我們將會探討如何在較低的溫度(400~700°C)與壓力下進行鑽石薄膜的製備。

我們使用微波電漿化學氣相沉積法(MPCVD)進行成長，通入氫氣與甲烷的混合氣體作為反應用氣體，之後在披覆金剛烷($C_{10}H_{16}$)的單晶矽基材上進行多晶鑽石薄膜的合成，並與在未披覆金剛烷的矽基材上所成長的鑽石薄膜進行比較。

結果我們發現在披覆金剛烷的單晶矽基材上所成長的鑽石薄膜其成長速率比未披覆金剛烷的快上兩倍。在單位面積中，其鑽石的分佈密度約為 $10^3 \sim 10^4$ cm^{-2}，也比未披覆金剛烷的分佈密度高。在中間的成長階段，我們觀察到金剛烷先轉變為與非晶碳相互混合的石墨相。隨後我們藉由 X 光繞射 (XRD) 與 X 光光電子光譜儀(XPS)進行鑽石薄膜的特性分析，證明了在鑽石沉積的過程中會形成碳化矽(SiC)界面層。同時我們使用原子力顯微鏡(AFM)與拉曼光譜儀(Raman)能得知在矽基材上有非鑽石相的存在。而此鑽石薄膜擁有優異的場發射性質：低臨界電壓(55 V/μm)

與高電流密度(1.6 mA/cm^2)。另外，在矽基材(SiO_2/Si)上使用鉑顆粒能夠吸附金剛烷(碳氫化合物)並提升鑽石的成核密度高達 10^{12} ~ 10^{13} cm^{-2}；並且，矽基材表面上的氧化層能避免鉑和基材產生矽化反應，進而避免接下來鑽石的沉積過程中產生碳化矽。在一開始沉積的兩分鐘內，金剛烷的晶種轉變成奈米鑽石和一些未分辨的碳顆粒，並在之後 5 至 15 分鐘的沉積出現了石墨相。之後我們使用高倍率的掃描式電子顯微鏡(SEM)發現以{111}、{100}和許多方向性的碳顆粒成為鑽石成長的成核點。

The study of nucleation, growth, and structural characterization of diamond on adamantane-coated Si substrate

Student: Rajanish Nath Tiwari **Advisor: Dr. Li Chang**

Department of Materials Science and Engineering

National Chiao Tung University

Abstract

Diamond films have been regarded as an active field of science and technology because of their unique properties. Although the technology of diamond film was synthesized to an extent, some problems remain unclear and only their solution can result in wide-scale commercialization, especially as the synthesis of diamond film at low temperature and pressure. Therefore, in the thesis, we will discuss the synthesis of diamond film at relative low temperature (400 ~700°C) and pressure.

The polycrystalline crystalline diamond films were synthesized on adamantane ($C_{10}H_{16}$)-coated crystalline silicon substrates by microwave plasma chemical vapor deposition (MPCVD) from a gaseous mixture of methane and hydrogen gas without any mechanical and electrical pretreatments. Diamonds already grown on Si substrates without adamantane coating have been carried out as well as for comparison.

As a result, we observed that the growth rate of diamond film on adamantane-coated Si substrates were two times faster than without adamantane-coated. The density of diamond on adamantane coated were also ~$10^{3\sim4}$ cm^{-2} higher than that of without

adamantane coated. In the intermediate growth steps, we observed that the adamantane first converts into graphitic phase intermixed with amorphous carbon. The characterization of diamond films by x-ray diffraction (XRD) and x-ray photoelectron spectroscopy (XPS) show that the SiC interlayer have been formed during the diamond deposition. While atomic force microscope (AFM) and Raman spectra show the presence of nanodiamond phase on the Si substrate. The diamond films exhibit a low-threshold (55 V/μm) and high current density (1.6 mA/cm^2) in their field-emission properties. In addition, using platinum particles on SiO_2/Si substrates are adsorb adamantane (hydrocarbon) and increase the nucleation density ~$10^{12\sim13}$ cm^{-2}. The presence of oxide intermediate layer between Pt and Si prevents silicidation as well as SiC in diamond deposition. The seeded adamantane was first transformed into nanodiamond and some unidentified carbon particles in the early stage of deposition within 2 min while, further deposition (5-15 min) shows the existence of diamond and graphite phase. The high-magnification scanning electron microscope (SEM) have shown that the {111}, {100}, and many other orientated carbon particles may act as a nuclei for diamond growth.

Acknowledgements

I am indebted to many people who contributed in several ways to this work, and supported me with their cooperation and timely help.

In particular, I wish to express my sincere gratitude to my research supervisor Prof. Li Chang, for providing me an opportunity to work in his research group. I thank his for unique personal support in every aspect of the experimental work, for all the stimulating ideas, all the deep discussions, for providing support in preparation of various manuscripts for publications, presentations, posters and for the time he spent in reviewing this thesis. He has been a great mentor with his enthusiasm, understanding and willingness to help students professionally and personally.

I am extremely thankful to Mr. K. A. Chiu, Mrs. D. T. Hien, Mr. W.-L. Wang, Mr. W.-C. Chen, Mr. C.-S. Tian, and Mr. C.-Y. Peng, for serving my experimental supports and for their precious suggestions to my study. I would like to express my thanks to all my group members for their friendship: Dr. Y.-H. Wu, Mr. S. R. Sahoo, Mr. P.-H. Wu, and Ms. Y.-C. Chen. I am thankful to all my well-wishers particularly Mr. M. Hornansky and Dr. P.-Y. Kuo, who helped me directly and indirectly, and their emotional support, encouragement and inspiration were instrumental during all these years.

Most importantly, I wish to thank my entire extended family like to dedicate this work to my family particular my parents for their endless love and supports throughout my life. Their encouragement has been a source of inspiration that led to the completion of this thesis. I would like to thank everybody who was important to the successful realization of thesis, as well as expressing my apology that I could not mention personally one by one.

The financial support of my Ph.D. research work by a grant from the NCTU and NSC, Taiwan, R.O.C. is grateful acknowledged.

Contents

Abbreviations

CVD	Chemical vapor deposition
HTHP	High temperature and high pressure
MCD	Microcrystalline diamond
NCD	Nanocrystalline diamond
UNCD	Ultrananocrystalline diamond
MPCVD	Microwave plasma chemical vapor deposition
BEN	Bias enhanced nucleation
3D	Three dimensions
HFCVD	Hot filament chemical vapor deposition
MEMS	Micro-electronic mechanical systems
G.C.	Gas spectroscopy
SEM	Scanning electron microscope
M.S.	Mass spectrometry
SiC	Silicon carbide
CH_4	Methane
C_2H_6	Ethane
C_2H_2	acetylene
$C_{10}H_{16}$	Adamantane
$C_{14}H_{20}$	Diamantane
$C_{18}H_{24}$	Triamantane
AC	Adamantane-coated
Pt	Platinum
TEM	Transmission electron microscope
AFM	Atomic force microscope

XRD	X-ray diffraction
FTIR	Fourier transform infrared spectroscopy
XPS	X-ray photoelectron spectroscopy
OM	Optical microscope
EFE	Electron field emission
Ar	Argon
Mo	Molybdenum
FIB	Focused ion beam
D.F.	Dark field
B.F.	Bright field
EDX	Energy-dispersive X-ray spectroscopy
FFT	Fast Fourier transform
HRTEM	High-resolution TEM
SAD	Selected area diffraction
SAED	Selected area electron diffraction
LTLP	Low temperature and low pressure
N_2	Nitrogen
SCCM	Standard cubic centimeters per minute
WAC	Without adamantane coated
nm	nanometer
eV	electron volt
BOE	Buffer oxide etch
Al	Aluminium
cm	centimeter
$C_6 H_{12}$	Hexane
XTEM	Cross-section TEM

FCC	face centered cubic
F-N	Fowler-Nordheim
mA	milliampere
SiO_2	Silicon dioxide

Table Captions

Figure Captions

Chapter 1

Introduction

1.1 Background

Diamond has always been an outstanding and desirable material. Not only is it famous to the public as gemstones, but also it is attractive to scientists and engineers for its unique, excellent properties. The outstanding electrical, optical, mechanical, chemical, and thermal properties of diamond film have stimulated a great deal of research activities in the growth of diamond thin films using various chemical vapor deposition (CVD) techniques, to study its growth mechanisms, and their wide range of potential applications for optics, microelectronics, tribology, thermal management, DNA sensors, and so on. From the crystal growth viewpoint, synthesis of diamond thin films by CVD in vacuum is a breakthrough in artificial diamond growth compared with using the high temperature and high pressure (HTHP) method [1]. Over the past few decades, different techniques have been developed for the deposition of diamond such as chemical vapor deposition (CVD), pulsed laser deposition, ion beam deposition hydrothermal growth, and oxyacetylene torch or combustion flame method [2-8]. Among all these methods, chemical vapor deposition (CVD) has become a well-established field over the last three decades. CVD diamond materials range in grain size from ultrananocrystalline and nanocrystalline [9, 10] films, through polycrystalline plates and wafers [11], to large single crystals [12, 13]. Ultrananocrystalline diamond (UNCD) is a new special class of nandiamond that has a length of only few nanometers. Due to superior properties of UNCD, the ultrananocrystalline diamonds is most suitable for future biochip and biosensor applications. Nanocrystalline diamond coatings are also promising for certain medical implants such as cardio vascular surgery or coating of certain components of artificial heart valves [14]. Over the past few decades plasma-activated CVD, and

particularly microwave plasma-activated CVD (MPCVD), has become dominant in both industrial and research facilities worldwide for high-quality diamond deposition. A large variety of carbon-containing gases can be employed, including methane, aliphatic and aromatic hydrocarbons, alcohols, ketones, amines, ethers, and etc [15]. Methane is the most frequently used reagents for diamond growth.

Recently, a number of surface pretreatment methods have been developed, including scratching [16], seeding [17, 18], electrical biasing [19], and chemical pre-treatments [20], to improve substrate surface conditions prior to diamond deposition. The scratching and seeding substrate surfaces with diamond powders was very useful for increasing diamond nucleation density. Other forms of carbon, including carbon ions, C_{60} and C_{70} clusters, amorphous carbon, graphite, thin metal coating, and etc. have also been used as a precursor material in various chemical vapor deposition (CVD) methods under low pressures [21, 22].

1.2 Motivation

Recently, substantial attention has been paid to the development of diamond films on non-diamond substrates in particular using methane and hydrogen gases in the CVD plasma. Although the diamond film synthesized to an extent, some problems remain unclear and only their solution can result in wide-scale commercialization, especially as the synthesis of diamond at low temperature and pressure for the non thermal stable substrates. The most important problem is the synthesis of diamond at low temperature and pressure without sacrificing their quality, purity, yield, and so on.

In general, the good quality of diamond film is synthesized at 1% methane in hydrogen as source gas, 700-1000°C deposition temperature and gas pressures in the range 20-300 Torr [23]. However, the high substrate temperature limits the use of

diamond films in many industrially important systems such as electronics substrate. Deposition of diamond at low temperature is desired for technological applications to allow incorporation of the film into electronic and mechanical devices without damage. There have been several reported works for diamond deposition at low temperature and pressure but they are unsatisfactory at the present stage. Therefore, it would be desirable from both scientific and technological points of view to control not only temperature and pressure but also their quality of diamond. This will permit the use of a much wider range of substrate materials of industrial importance such as Al, polyimide, Si, SiC, GaN, GaAs, steel, Ni, and so on in different mechanical, electrical, optical and electronic applications. Lowering of substrate temperature during diamond synthesis could be an important step for deposition on low melting materials as well.

It is well known that for diamond deposition on non-diamond substrates is performed via two major processing steps. The first one, (i) nucleation, corresponds to the formation of diamond nuclei at the substrate surface. Nucleation procedures have been developed by performing either ex situ treatments on the substrate such as scratching, seeding, chemical treatments, or in situ methods before CVD (chemical vapor deposition) growth such as bias-enhanced nucleation (BEN) process. While the first technique leads to non-uniformity while the bias is limited by the conductivity of the substrate. A uniform nucleation throughout the substrate surface along with its density affects the subsequent growth stage. Therefore, we need to find some new and commercially available precursor for the synthesis of diamond at low temperature and pressure. It is also essential to improve the yield purity, and quality of diamond at low temperature and pressure. Chemical precursor is one of the best ways to overcome this problem. It can improve the quality and enhance the diamond yield without damaging the surface. Moreover, an appropriate synthetic route ultimately determines the success or failure of diamond synthesis, because the physical properties and

applications of materials are heavily dependent upon their synthetic method. As a result, there have been tremendous efforts toward the development of new synthetic methodologies for several decades.

In this study, we have proposed very simple and new methods for pretreatment of the Si surface. We used non toxic chemical precursor such as adamantane ($C_{10}H_{16}$) for the synthesis of diamond film by microwave plasma chemical vapor deposition (MPCVD) at low temperature and pressure. Prior to the pretreatment, the substrates were not mechanically abraded/scratched. Adamantane was coated on silicon surface by hotplate method and then external methane and hydrogen gas used for diamond growth. The experimental results have shown that the synthesized diamond films are in high yield along with good quality at low temperature. Moreover, noble materials adsorb the hydrocarbon. Therefore, using platinum thin interlayer can enhance the diamond density.

Chapter 2

Literature Review

Carbon is an important element in nature and its allotropes include the hardest naturally occurring substance are the tetragonal bonded (sp^3) diamond and also one of the softest substances are the trigonally bonded (sp^2) graphite graphite trigonally bonded (sp^2). With recent advancement in nanotechnology, new structure of carbon and synthetic production of diamond [24], fullerenes (C_{60})[25], carbon nanotubes[26], carbon fibers[27], diamond-like carbon[28], diamondoid hydrocarbons[29], as well as the development of graphene[30] are few examples of this continuously expanding research area.

This thesis concentrates specifically on the lower diamondoid hydrocarbons (particularly on adamantane) to the diamond growth. The following chapter and contents is a brief introduction to the study of diamond and related materials, particularly focusing on the topics mentioned above. As we brief discussed above about the various structure of carbon, however, now we are going to discuss about graphite and diamond.

2.1 Graphite

The mineral graphite is one allotropes of carbon. Graphite has a sheet like structure where the atoms all lie in a plane and are only weakly bonded to the graphite sheets above and below, as shown in Figure 1(a). While, diamond has a framework carbon structure where the carbon atoms are bonded to other carbon atoms in three dimensions (3D). In the diamond lattice structure, hybrid sp^3 orbital forms strong covalent bonds with four neighboring carbon atoms, tetrahedrally arranged with equal angles of 109° 28’ to each other. This three-dimensional network of covalent bonds gives diamond its unique hardness and resistance to wear. Unlike the tetrahedral arrangement of atoms in diamond, the carbon atoms in graphite are arranged in the form of hexagonal rings in layers. In the graphite crystal structure, each carbon atom combines with its three neighbors by sp^2 covalent bond with a bond order of 1.5.

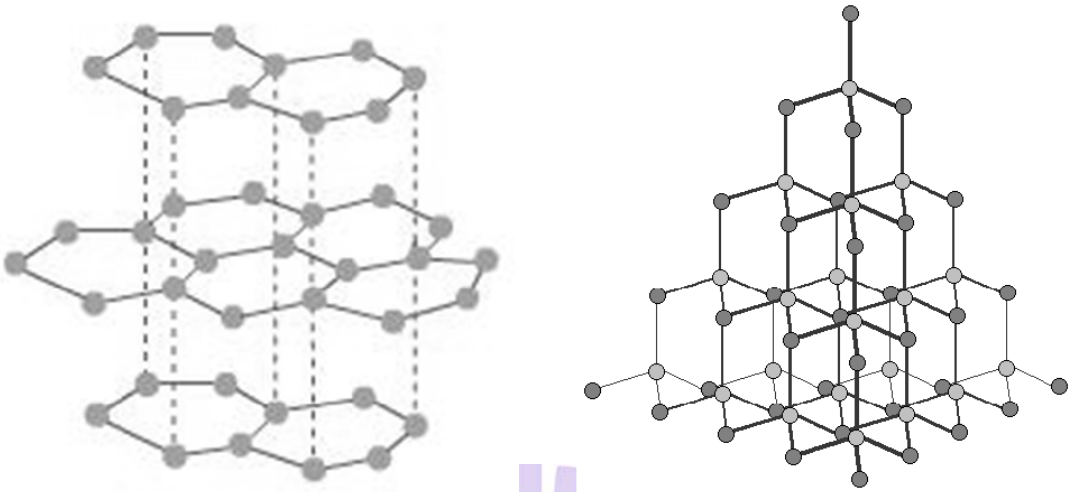

(a) Graphite (b) Diamond

Figure 2.1: Structure of (a) graphite and (b) diamond.

Table 2.1: Comparison of the bond strengths, crystal structure, transparency, thermal conductivity, and electrical resistivity of diamond and graphite [31, 32].

Property	**Diamond**	**Graphite**
C-C bonding	Covalent sp^3	Covalent sp^2 and Van der Waals
Bond Energy	711 kJ/mol	524 kJ/mol and 7 kJ/mol
Crystalline form	Cubic and hexagonal	Hexagonal and rhombohedral
Transparency	From UV to IR range	Opaque
Thermal Conductivity (W/m.K)	~2000	$< 4182_{(//)}$ and $2_{(\perp)}$
Electrical resistivity (Ω cm)	10^{14}	$10^{-4}{}_{(//)}$ and $1_{(\perp)}$

The carbon-carbon bonds in the graphite mineral are actually quite stronger than those in diamond (Table 2.1). Graphite and graphite powder are valued in industrial applications for its self-lubricating and dry lubricating properties. Graphite is a soft, opaque, lubricious material while diamond is hard, transparent and abrasive. This difference in properties of these materials is determined by the nature of the chemical bonds and structure. There is a common belief that graphite's lubricating properties are solely due to the loose interlamellar coupling between sheets in the structure. The properties of graphite are highly anisotropic. Graphite can conduct electricity due to the vast electron delocalization within the carbon layers. Graphite is able to conduct electricity due to the unpaired fourth electron in each carbon atom. The structure of diamond and graphite are shown in Figure 2.1 and some interesting properties of diamond and graphite are summarized in Table 1. This unpaired 4th electron forms delocalised planes above and below the planes of the carbon atoms. These electrons are free to move, so are able to conduct electricity. However, the electricity is only conducted within the plane of the layers. However, no electronic pathway exists between adjacent graphene layers since the 3.35 Å spacing between graphene layer planes acts as an electrically insulative “vacuum” to electron transfer. The thermal conductivity perpendicular to the planes is very low by comparison due to the weak van der Waals bonding, as shown in Table 2.1. For this reason, graphite is not conductive between layers (parallel with “c” crystallographic axis). There are three principal types of natural graphite:—lump, crystalline, and amorphous. Lump graphite occurs in veins and is believed to be hydrothermal in origin. It is typically massive, ranging in particle size from extremely fine to coarse, platy intergrowths of fibrous or acicular crystalline aggregates with the long axis parallel to the enclosing wall rock. Crystalline flake graphite consists of isolated, flat, plate-like particles with angular, rounded, or irregular edges. It is usually found in layers or pockets in metamorphic rocks. In some deposits, the flake graphite occurs as massive accumulations in veins, lenses, or pods. And amorphous graphite is formed by the thermal metamorphism of coal. The designation amorphous is a misnomer. Its relatively low degree of crystalline order and very fine particle size make it appear amorphous. It is usually of lower purity than the crystalline flake graphite and, therefore, commands a lower price than its more ordered counterpart [33].

Figure 2.2: Photographs of different kind of graphite [http://en.wikipedia.org/wiki/Graphite]

2.2 Diamond

Diamonds were first mined in India over 4000 years ago. For centuries diamonds have captured the hearts and minds of millions, including scientists. For most, the word diamond immediately relates to a brilliant gem, wealth, status and/or prosperity. For scientists, diamond is known as one of the strongest and most chemically inert material. Diamond is something superb, the peerless "king of gems" that glitters, dazzles, and symbolizes purity and strength. The structure of diamond is shown in Figure 2.1(b). It can be regarded as a 3D network of carbon atoms tetrahedrally bonded by sp^3

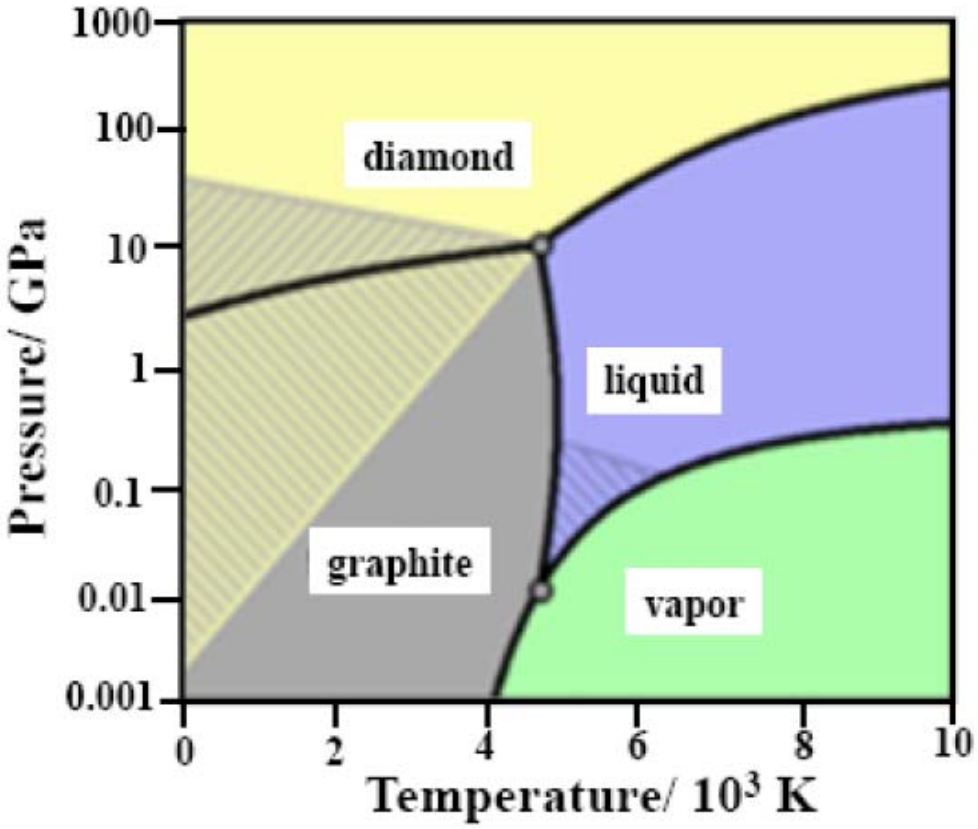

Figure 2.3: Theoretically predicted phase diagram of carbon [http://en.wikipedia.org/wiki/Diamond].

hybridized bonds. Since each carbon atom in the diamond lattice is firmly "supported" by four neighboring atoms, this structure makes the extreme properties of diamond. The extreme properties of diamond such as high mechanical strength, exceptional chemical inertness, outstanding thermal stability, and many other excellent properties made it as a supreme material for diverse applications [34, 35]. Despite being harder and denser than graphite, under ambient conditions, diamond is less stable by 2.9 kJ/ mole. Fortunately, a large activation barrier prevents an appreciable rate for interconversion from diamond to graphite. Since diamond is only metastable at standard temperature and pressures, the production of diamond from other forms of carbon is difficult. Before progressing further let us discuss how diamonds are formed in some more detail.

2.2.1 Natural production

Figure 2.1 (b) shows the structure of diamond. Diamond is the stable solid form of carbon at high pressure. Diamonds are formed deep inside the earths interior where crushing pressure and blistering heat work together for a long period of time to create the diamond lattice. At depths below 150-200 km, the pressure and temperature are such that diamond becomes the most thermodynamically stable form of carbon. Scientists believe that, narrow volcanic pipes running down into the earths interior allows diamonds to be transported via violent explosions to the earth's surface. It is believed the time taken to form a natural diamond is approximately billions of years.

2.2.2 Synthetic production

Apart from being the hardest known naturally occurring material till presently, diamond also enjoys several other superior properties. Diamond has very high wear resistance and a low coefficient of friction. Diamond is also inert to most chemical environments and hence diamond coatings can be used for corrosive and/or corrosion-erosion applications as well. It is also a bio-compatible material. The high carrier mobility [36], wide band gap and thermal stability [37] of diamond means that electronic devices would be able to operate faster and under much more extreme conditions than silicon based devices. It has very low thermal expansion coefficient at room temperature. Diamond also has low or negative electron affinity [37]. By virtue of these commendable properties, diamonds have a potential for wide ranging applications for wear and corrosion resistant applications, field emission, heat sinks, optical windows etc [37]. However the high costs of natural diamonds severely restricts their application potential. Scarcity and cost of the natural diamond led scientists to find means of making diamond in the laboratory. Although there have been several attempts to synthesize diamond from various sources of carbon since it was discovered to be an allotrope of carbon, two main techniques were invented in 1950; (i) High pressure and high temperature (HPHT) synthesis and (ii) chemical vapor deposition (CVD) synthesis.

2.2.2.1 High-Pressure High-Temperature Synthesis

With the realization in the nineteenth century that natural diamonds are produced deep under the earths crust under conditions of high temperature and high pressure, scientists started experiments to imitate this condition in laboratories. The first success in synthesising diamond particles by HPHT probably belongs to Swedish in about 1953 and in the Unites States by General Electric in 1955 [24]. They used pressures of 10 GPa and temperatures in excess of 2300 K to produce diamond crystals with an edge length of over 1 mm. HPHT, a process which mimics the way in which natural diamonds are formed by geophysical processes deep in the earth, has allowed synthetic diamond to become a key material in the cutting and abrasive business, being widely used in the machine tool industry, oil and gas drilling, mining, quarrying, and construction. Over the years the process has been refined, and it is now possible to produce different types of diamonds of several carats in mass [38]. It can be seen from the carbon phase diagram (Figures 2.3 and 2.4) that the diamond structure is stable at very high temperatures and pressures. Today, the diamond synthesis by HPHT process remains the dominant manufacturing process for industrial diamond, as shown in Figure 2.5.

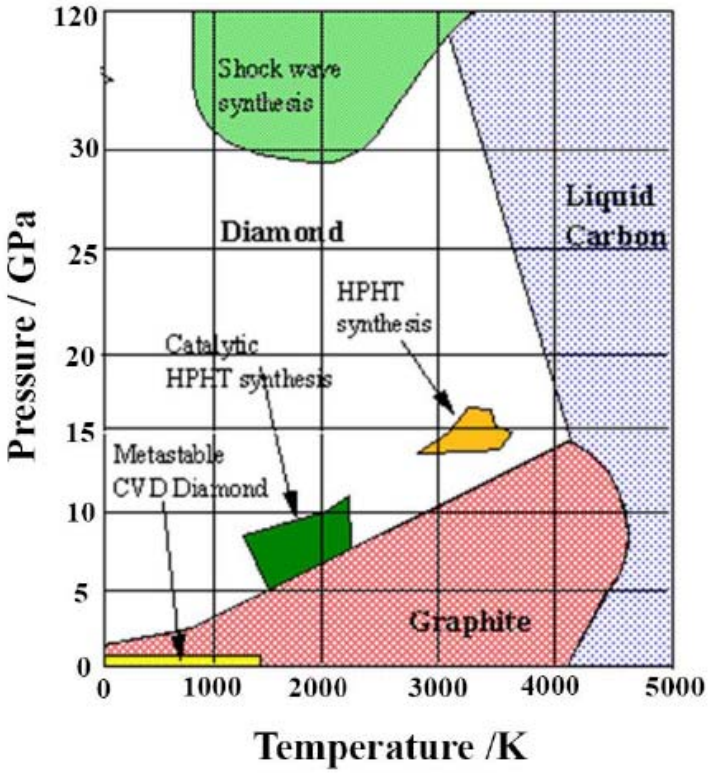

Figure 2.4: Carbon phase diagram with temperature and pressure ranges corresponding to various diamond synthesis process [39].

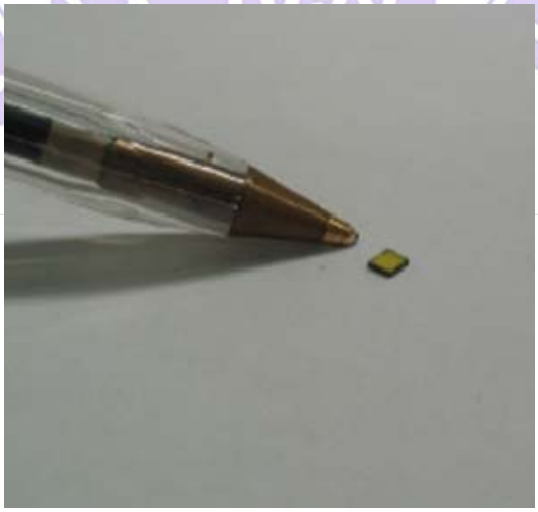

Figure 2.5: Photograph of commercial HPHT diamond (ball point pen for scale).

2.2.2.2 Shock-wave Synthesis

Figure 2.6 shows the schematic diagram of Shock-wave for diamond synthesis. Shock-wave synthesis methods are better than traditional HPHT methods. These methods only produce small grain size (nano) diamond powders. In 1961, Decarli et al. had observed diamond from graphite after explosive shocks at 300,000-atmosphere and Greiner et al also noticed diamond crystals with soot after the detonation of carbon-containing molecules at high explosive in an inert atmosphere [40, 41]. The nanocrystals of diamond are formed by shock-wave synthesis due to the incredibly short reaction time [42].

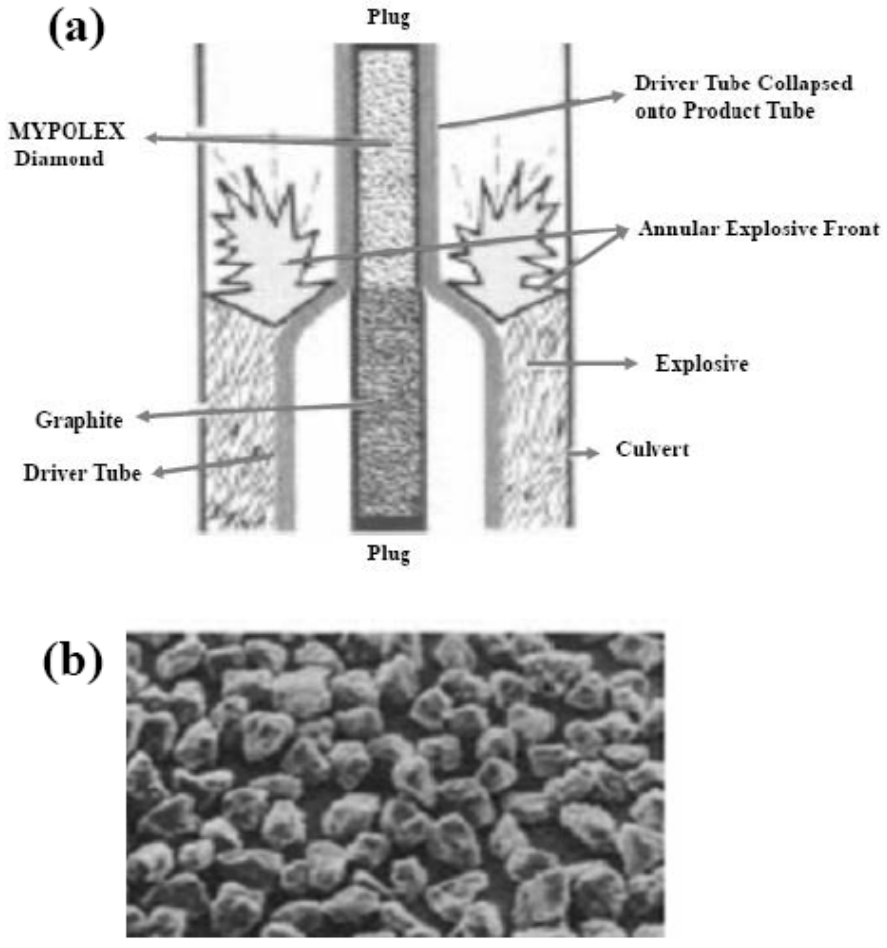

Figure 2.6: (a) Schematic diagram of the shock-wave for diamond synthesis (b) The synthesis of nanocrystalline diamond [43].

2.2.2.3 Chemical Vapor Deposition (CVD)

Synthesis of diamond by Chemical Vapor Deposition (CVD) uses a low pressure process. This technology opens the possibility of making new shapes, coatings, films and qualities that can exploit diamond's unique properties in a breath-taking array of industries. The possible growth of diamond by CVD was first shown by Angus et al. in 1968 [44]. It is a process which includes both gas phase reactions and gas-solid surface reactions. The process relies on decomposing carbon-containing gas molecules, such as methane, acetylene or carbon dioxide at sub-atmospheric pressure and depositing diamond as a film on a substrate. Figure 2.7 shows the appropriate ratio of each elements such as C, H, and O for the diamond growth [45]. The importance of CVD methods is that they do not require the huge pressures required for HPHT synthesis and can create diamond that can be tailored for a wide range advanced engineering applications.

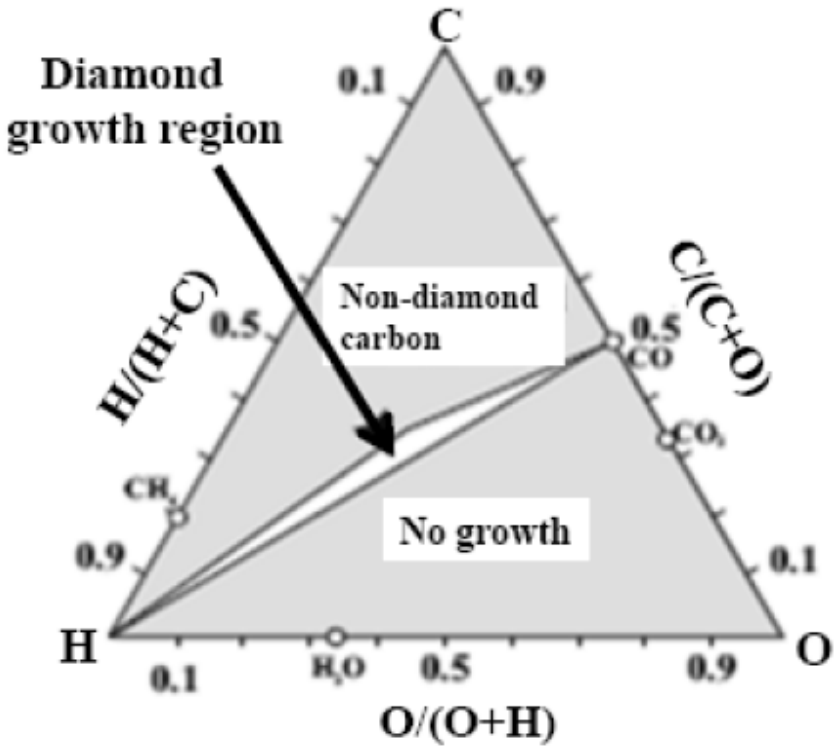

Figure 2.7: The Bachmann Diagram [45]. This diagram shows the relative proportions of C, H, and O required in the gas phase for CVD diamond growth to occur.

Recently, there are four main CVD methods used to create diamond films. The CVD techniques, classified by means of how the energy is coupled into the system (called gas activation), which will be briefly introduced in the following sections.

2.2.2.3.1 Hot filament

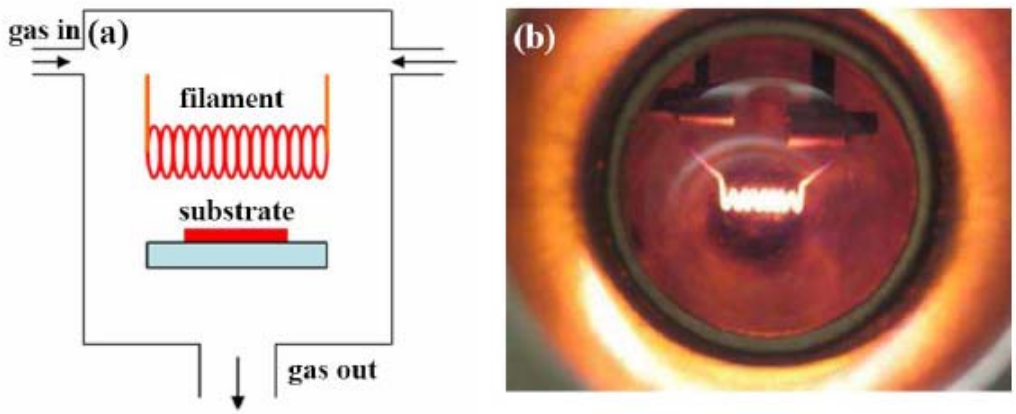

Figure 2.8: (a) Schematic and (b) Photograph of hot filament CVD reactor[http://www.chm.bris.ac.uk/pt/diamond/end.htm].

In 1976, Soviet scientists have successfully diamond synthesized on non-diamond substrates by hot filament CVD (Hot Filament Chemical Vapor Deposition, HFCVD). The schematic diagram of HFCVD is shown in Figure 2.8. It uses a metal coil, resistively heated to around 2000~2500 K to activate the gas phase reactions. In the HFCVD, normally researchers are using the mixture of methane and hydrogen. The filament works as a power source and catalyst at the same time to help dissociate the H_2. The resulting H atoms then initiate most gas phase reactions with the hydrocarbon and finally lead to diamond deposition on the Si substrate, which is heated separately by an electric heater to 1000~1200 K. Therefore, the properties of the filament are very important for HFCVD. The commonly used filament material is a kind of chemically-inert metal, e.g. tungsten or tantalum. However, under the high temperature, it will inevitably react with carbon-containing species and gradually degrade, and finally become more brittle and resistive. This then will influence both the power coupling efficiency and the catalysis activity. Also, due to the presence of the filament in the reactor, the input gas for HFCVD cannot

contain oxidizing or corrosive gases. Even so, the contamination from the filament material is still difficult to avoid. Thus, usually, HFCVD-grown diamond has low quality and is suitable for mechanical, but not for electronic applications.

2.2.2.3.2 Arcjet plasma

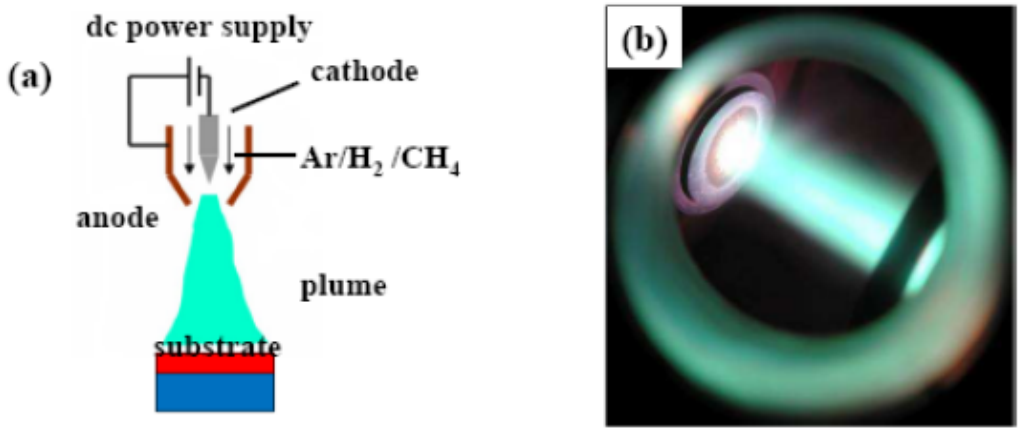

Figure 2.9: (a) Schematic and (b) Photograph of a DC arcjet reactor[http://www.chm.bris.ac.uk/admin/tpw.htm].

The DC arcjet is another CVD method to produce diamond. The schematic diagram of Arcjet plasma is shown in Figure 2.9 In this system, an anode and a cathode are connected by a DC power supply. Between the two electrodes a discharge region is formed. When the mixture of gases flow through this region, ionization occurs and a jet of plasma is generated and accelerated by a pressure drop towards the substrate, where the diamond film is deposited. The advantage of this technique is its high growth rate, which is usually unobtainable by other methods. The maximum can be 1mm/hr [47]. However, this method cannot grow diamond over large areas and, again, metal contamination (from the cathode) tends to impair the diamond purity and quality.

2.2.2.3.3 Microwave plasma

Microwave plasma is now the most popular way to produce high quality diamond film. The two most common types of MWCVD reactor are shown in Figure 2. 10. The first microwave plasma CVD reactor was designed at NIRIM [32] using quartz tube of 45-55 mm in diameter that perpendicular penetrates the waveguide for 2.45 GHz, as schematically in Figure 2.10 (a). By this reactor a diamond film coating is possible on a 1-inch Si wafer at maximum, but in most cases, a piece of Si that is only less than 1 cm^2 is used as the substrate. In contrast, uniform diamond film coating on large area (2-inch square) is possible using an ASTeX-type reactor, which is shown in Figure 2.10 (b). In a microwave reactor, the gases mixture is introduced. The microwave power is coupled into the chamber through a quartz window. Firstly, electrons will pick up energy from the electromagnetic field. Then, through their collisions, the energy is transferred to the heavy species, making them dissociated, excited or ionized. The "active" species so produced then react on the substrate surface and form the diamond film. The advantage of this method is that there is no electrode or filament in the reactor. This provides a clean environment for diamond growth. Also, the diamond growth rate is relatively fast due to high input power and the immersion of the substrate into the plasma. The main drawback is that such systems are usually expensive. Therefore, we are now entering a new phase for CVD diamond where companies are exploring a raft of new applications. Improvements in plasma-type CVD processes are allowing the growth of polycrystalline and single crystal CVD diamond films with fewer defects and with consistent characteristics.

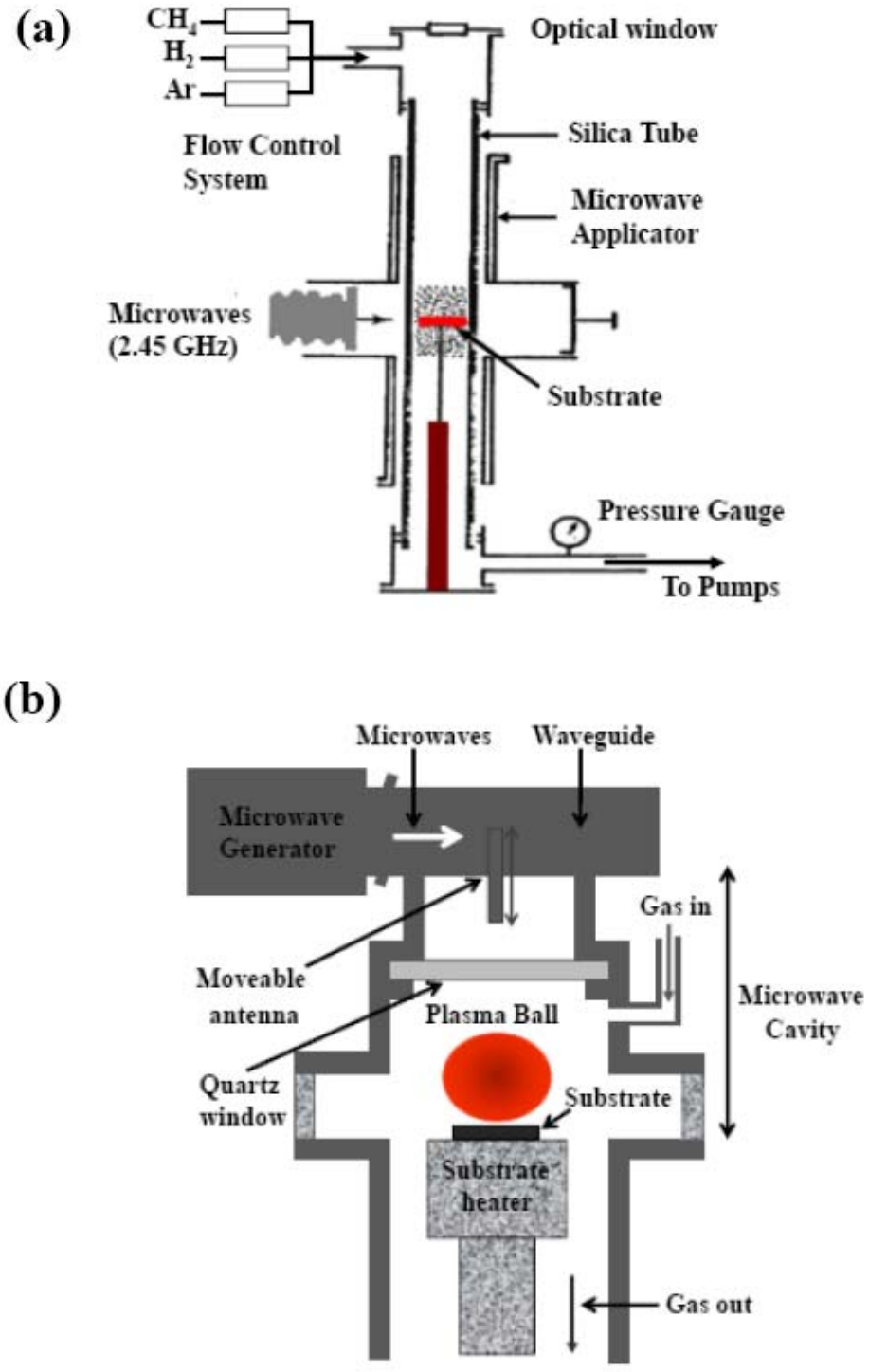

Figure 2.10: Schematic diagram of (a) NIRIM type [48] and (b) ASTEX type microwave reactor [http://www.chm.bris.ac.uk/pt/diamond/stuthesis/chapter1.htm].

2.3 Properties and applications of diamond

The synthetic diamonds are manufactured in a laboratory by various processes (as described above) for more than half a century. However, in recent years it has become possible to produce gem quality synthetic diamonds of significant size. The large size, high thermal conductivity, low thermal expansion, and low dielectric constant of diamonds makes them excellent as heat sinks [37]. As stated above, they are also the substrate of choice for homoepitaxial diamond CVD. Microcrystalline CVD diamond films are the most versatile form of synthetic diamond. They can be used as protective coatings, for heat dissipation, and even as windows in fusion reactors [37, 49, 50]. The high surface roughness of microcrystalline diamond (MCD) is not well suited for optical, wear and thermal management applications. However, nanocrystalline CVD diamond (NCD) films are increasingly studied due to their smooth surface and relatively homogeneous structure compared to MCD films. The low surface roughness of NCD is being used in optical coating, wear and thermal management applications. The low abrasiveness and antiwear properties of nanodiamond powders make them promising solid lubricants [37]. Moreover, NCD films not only being smooth but also being more adaptive to the CVD diamond applications and having enhanced electronics and other properties. This is reflected in their cost effective and superior performances in the areas of protective coating, tribology, SAW devices, and micro-electronic mechanical devices (MEMS), as shown in Table 2.2. One of the most interesting properties of diamond is the negative electron affinity of the hydrogen-terminated surface [51]. A negative electron affinity implies diamond could be used as a cold cathode in electron emitting devices. Indeed, nanodiamond powders have been shown to produce stable electron emission, with low turn-on voltages (3.2 V/μm) and high current densities (~95 mA m^2 under the applied field of 5 V/μm) [52]. Moreover, as the size of grains in changing from micrometer to nanometer, a factor of a million in volume, new properties have started emerging, exploring new areas of applications [37], for example, in X-ray optics, X-ray physics, particle physics, and so on.

Table 2.2: Diamond properties and its applications [37].

Properties	Diamond (MCD/NCD)	Applications
Electronic properties		
1. Band gap	5.5/ 2-5.5	Electronic devices
2. Electron affinity	Negative	Flat panel displays
3. Doping	p-type/ both p-type and n-type possible	Electrochemical electrode
Optical properties		
1. Transmission	transparent from UV to far IR/ ~78-84%	Optical coating
2. Refractive index	2.41/ ~2.27-2.35	IR windows
Mechanical properties	>100/ >90	
1. Hardness (GPa)	1054/ ~1000	Wear resistant
2. Young's modulus (GPa)	<0.1/ 0.1 to 0.01	Protective coating
3. Coefficient of friction		MEMS/NEMS
Other properties		
1. Thermal conductivity (W/cm k)	20/ 12	Thermal devices
2. Thermal stability (°C)	>1000/ >800	SAW devices bioelectronic sensing system
3. SAW phase velocity (km/s)	10/10	

2.4. Nucleation and growth of diamond in CVD

2.4.1 Nucleation

The diamond nucleation on the non-diamond substrates is usually very difficult and thus growth of diamond is very slow. Because of very low nucleation density, only of the order of 10^4 cm^{-2} on non-scratched substrates [53] is observed. Therefore, unlike diamond substrate, a non-diamond substrate often needs a pretreatment prior to diamond deposition. Several surface pretreatment methods have been developed, such as manual scratching, ultrasonic abrasion, and bias enhanced nucleation, and so on. The substrate scratching was found to be most simple, yet very powerful method for achieving a high nucleation density and uniform grain size. Substrate seeding can be achieved by applying the ultrasonic abrasion technique using a mixture of diamond powder and alcohol. In this method we can achieve a 10^8 cm-^{2} diamond nucleation density. The diamond powder was mixed with Cu, Al_2O_3, Ti, Fe, c-BN. TaC, and SiC, diamond nucleation enhanced ~10^9 to ~10^{10} cm^{-2} [54]. Nucleation enhancement by scratching is attributed to a number of factors. One of them is the change in the surface morphology due to the formation of defects, breaking of a number of surface bonds and removal of surface oxides. The defects are suggested to be chemically active sites, which preferentially adsorb precursors (diamond) and thus accelerate the nucleation process. Another opinion is that residual fragments of diamond powder act as nuclei for the diamond growth during CVD deposition. This is known as the seeding effect. Unfortunately, these abrasion techniques cause considerable damage to the surface and hence are not practical for electronic device applications. In contrast to the commonly used scratch methods, bias enhanced nucleation pretreatment does not cause mechanical damage to the substrate but still can induce a high nucleation density. The bias treatment is an in-situ method, where plasma is generated by biasing the substrate positively and negatively with respect to the chamber prior to the growth stage. This method is only good for semiconductor and conductive substrates. In 1991, Yugo et al. had successfully increased diamond nucleation by bias treatment [55]. There have two types of bias (i) negative bias and (ii) positive bias. In the negative bias, the positively charged ions in the growth chamber are accelerated towards the surface and bombard it, thereby removing the contamination and facilitating cluster

formation on the surface, as shown in Figure 2.11 (a). While Figure 2.11 (b) shows the positive bias effect where negative electrons are adsorbed and impact on the substrate and carbon atoms. Figure 2.12 shows the schematic diagram of bias enhancement nucleation and epitaxial growth of diamond.

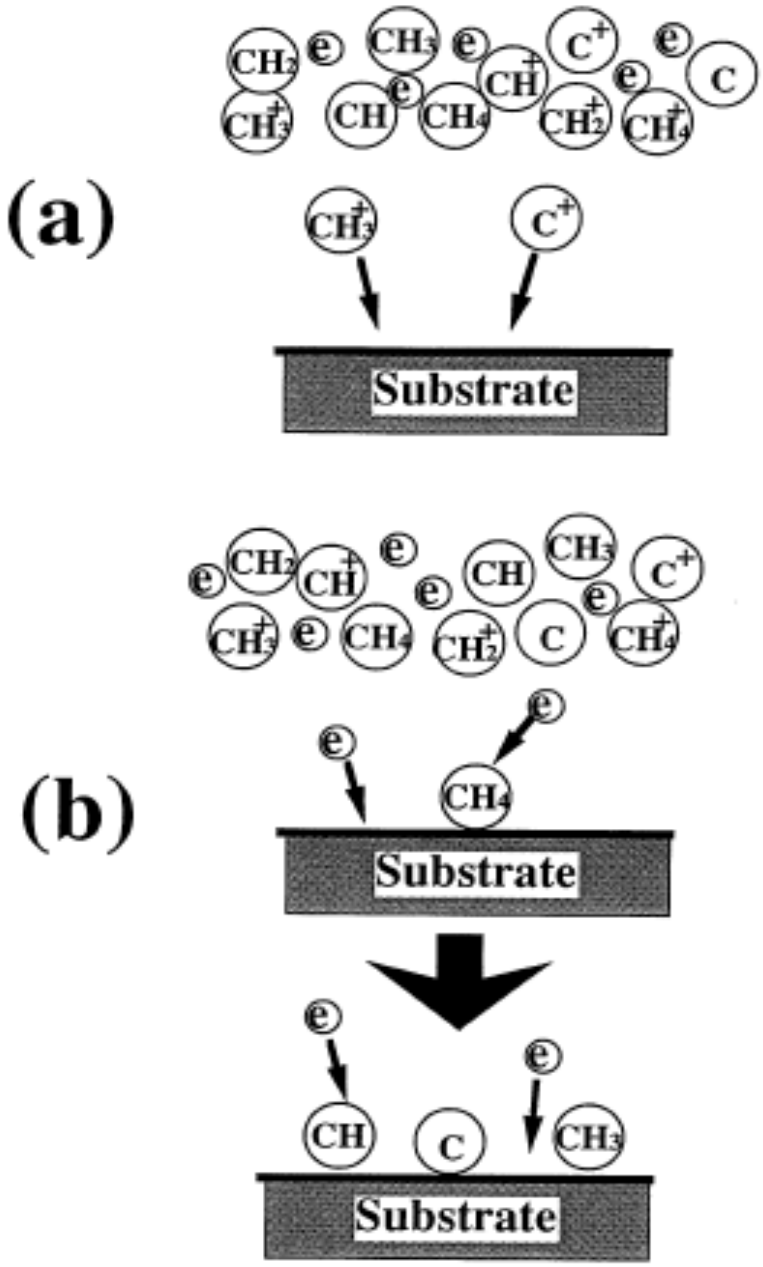

Figure 2.11: Diamond nucleation by (a) negative (b) positive bias method [56].

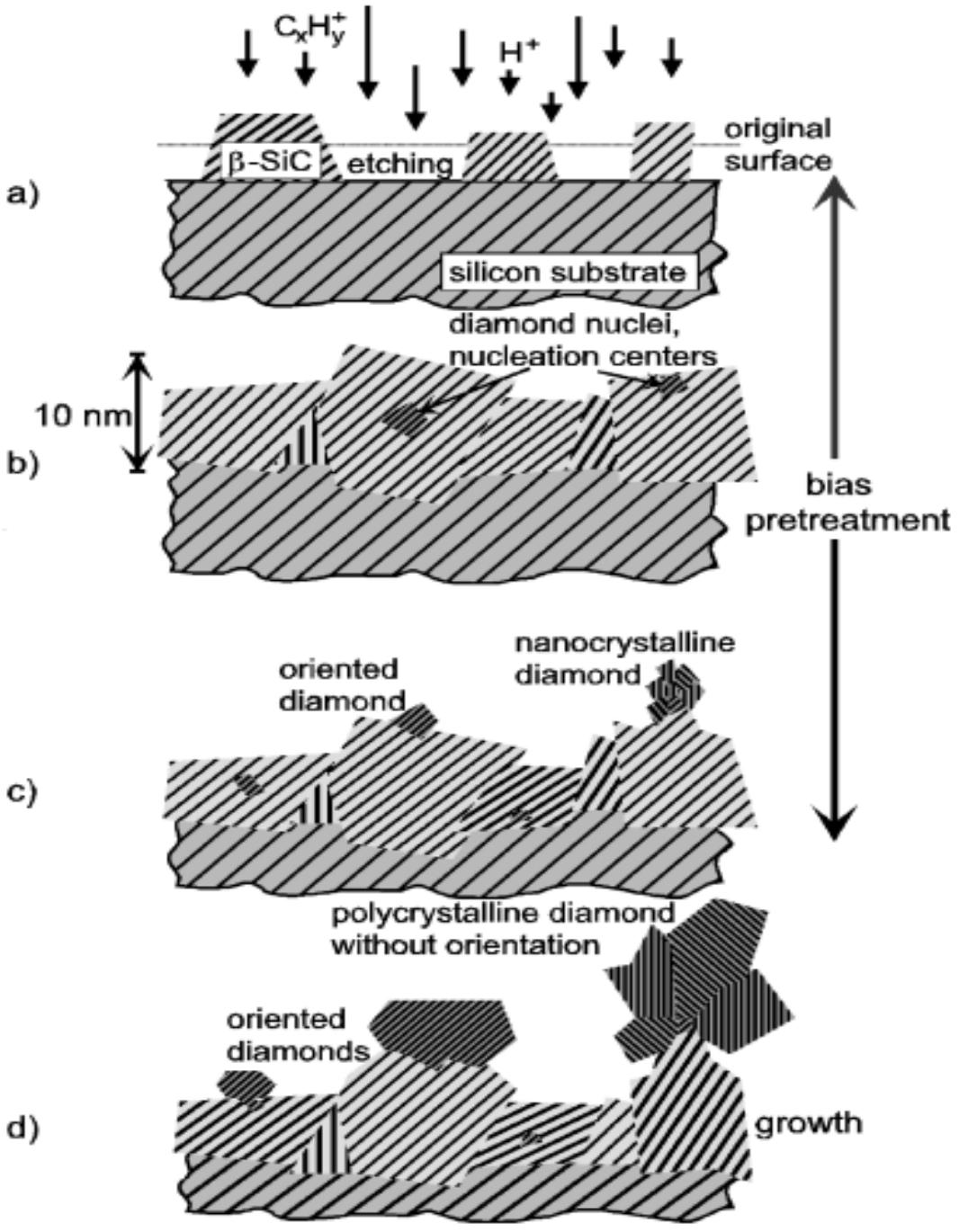

Figure 2.12: Mechanism of bias nucleation and epitaxial growth of diamond film [57].

2.4.2 Diamond growth mechanism

For the diamond deposition, various types of carbonaceous gases as sources were investigated for their potential on CVD diamond deposition, such as CH_4, C_2H_6, C_2H_2, C_2H_4, CO, CH_3OH, C_3H_6O, CCl_4, and CCl_2F_2. However, in present work, methane gas was used as a source gas [54]. The chemistry behind the diamond growth is very complicated. It can be divided into gas-phase chemistry and surface chemistry.

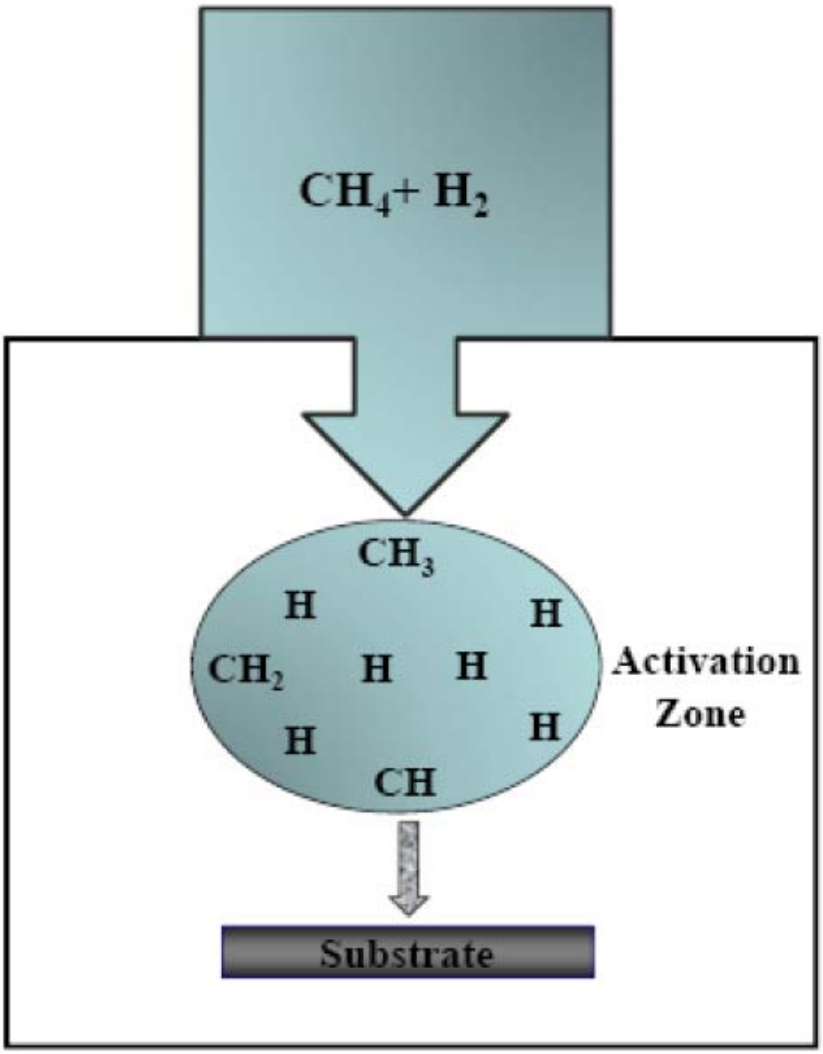

Figure 2.13: Schematic representation of the diamond CVD process.

2.4.2.1 Gas phase chemistry

A general schematic of the CVD diamond deposition process is shown in Figure 2.13. It is believed that hydrogen atoms usually play a crucial role in initiating the relevant gas phase reactions [58]. In a CVD diamond deposition process, when a H_2 and CH_4 mixture is introduced into the reactor, H_2 is dissociated by collisions. This results in an H-abundant environment. Under high atomic hydrogen concentration, CH_4 reacts with H through a series of abstraction reactions, producing many radicals like CH_3, CH_2, CH, C, and etc. These can also react with one another through "self-scavenging" reactions, producing C_2 species, like C_2H_6. Then, following similar H abstraction reactions, species like C_2H_5, C_2H_4, etc are also formed. Among them, C_2H_2 is the thermodynamically favored hydrocarbon species. Some of the species will act as precursors for diamond growth in the following gas-solid surface interactions.

2.4.2.2 Surface Chemistry

The H atoms also play an important role in surface reactions. During the surface reaction diamond and non-diamond carbon phases are formed. Graphite phases on the surface are simultaneously etched by hydrogen. Hence, atomic hydrogen plays a very important role in the formation of diamond and in preferential etching of non-diamond carbon phase. They can continuously create and re-terminate (thereby preventing the reconstruction to non-diamond forms) the reactive surface sites necessary for the propagation of the diamond lattice sites. H atoms can also selectively etch any graphitic (sp^2) carbon through so-called β-scission processes [59], as shown in Figure 2.14.

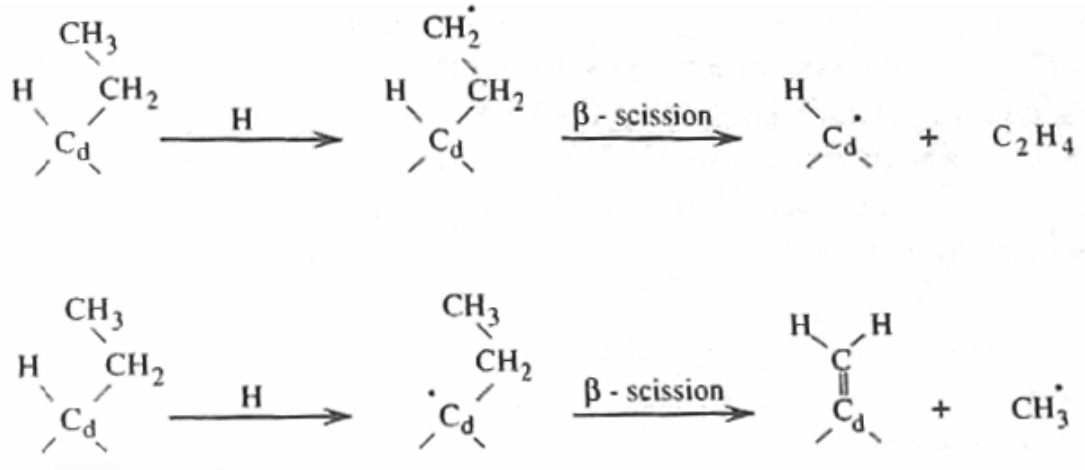

Figure 2.14: Two β-scission processes to attack a surface-bonded ethyl group [59]. C_d represents the carbon atom on the diamond surface.

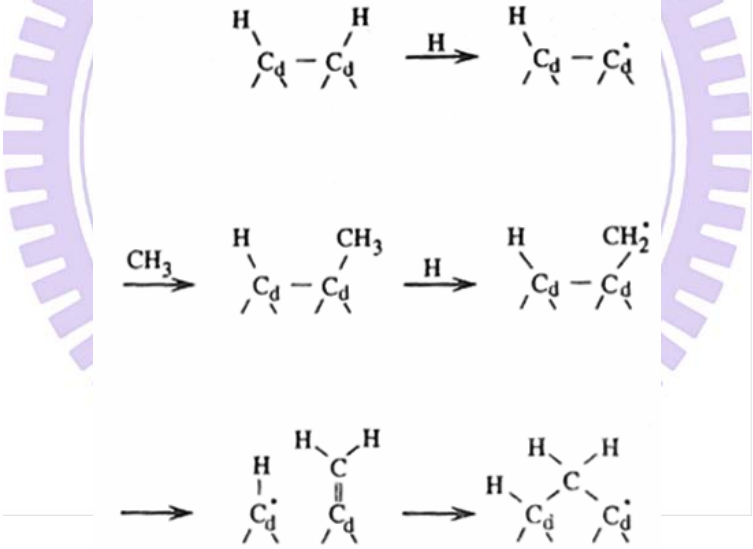

Figure 2.15: The GDSB mechanism for methyl insertion [59].

Recently, C1 and C2 mechanisms are two accepted mechanisms for diamond growth. In C1 mechanisms (Figure 2.15), the usually assumed growth species is CH_3 due to its abundance in the gas phase. In 1992, Garrison, Dawnkaski, Srivastava, and Brenner suggested a so-called GDSB mechanism, as shown in Figure 2.15 for methyl addition to

the (100) surface [60]. While in C2 mechanism is shown in Figure 2.16 for the addition of acetylene to the (100)-(2×1):1H surface [58, 61].

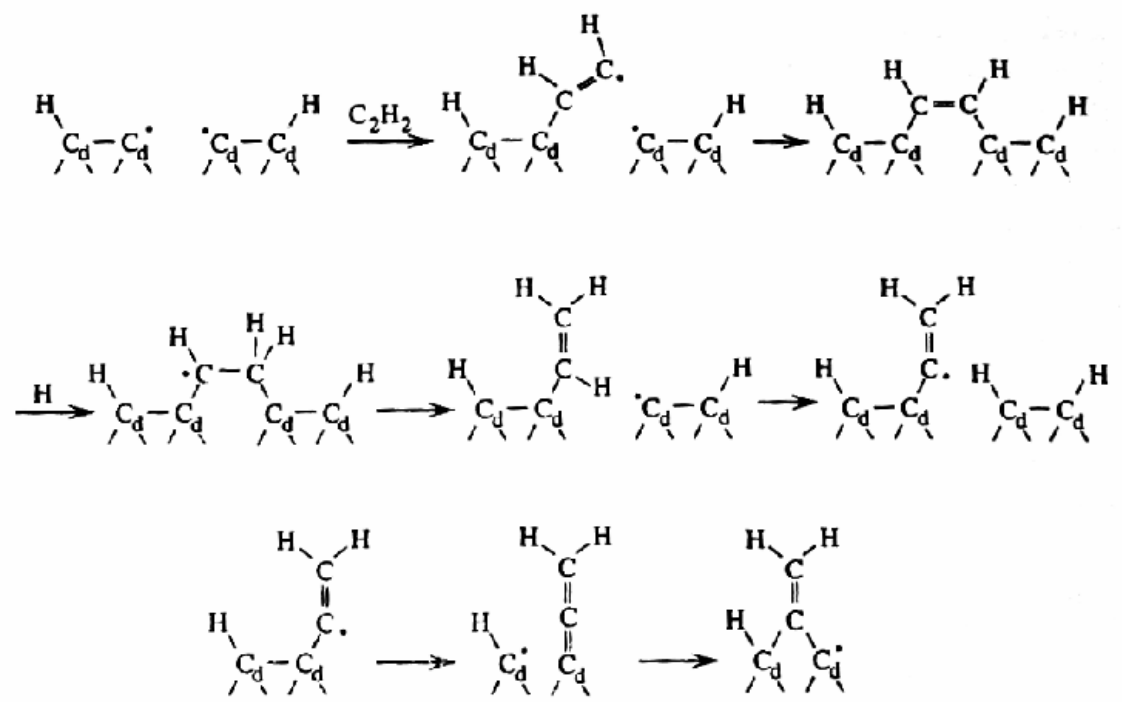

Figure 2.16: C2 mechanism for the addition of acetylene [58, 61].

2.5 Diamondoid Hydrocarbons

Diamondoids are saturated hydrocarbons and its molecules are totally or largely super imposable on diamond lattice [62]. Adamantane ($C_{10}H_{16}$) is a cycloalkane and also a lowest unit of diamonoids. The diamondoid can be split into two groups; (i) Diamondoids that are only partly superimposable on the diamond lattice, and (ii) Diamondoids which are completely superimposable on the diamond lattice. The carbon skeleton of adamantane comprises a small cage structure. Because of this, adamantane and diamondoids in general are commonly known as cage hydrocarbons. An additional diamond cage is face-fused to the 10-carbon adamantane structure, a molecule of diamantane ($C_{14}H_{20}$), and another adamantane fusing with diamantane it forms trimantane ($C_{18}H_{24}$) and so on [63]. The higher adamantane molecules (diamantine, trimantane and etc) are also know as polymantanes.

2.5.1 Lower diamondoids

Diamondoid was first discovered and isolated from Czechoslovakian petroleum in 1933 [64]. The isolated substance was adamantane and the name came from the Greek for diamond (adamas). This name was chosen because it has the same structure as the diamond lattice, highly symmetrical and strain free. The rigidity, strength, and assortment of their three dimensional (3D) shapes make them valuable molecular building blocks. The simplest of these polycyclic diamondoids is adamantane, followed by its homologues diamantane, tria-, tetra-, penta- and hexamantane. The lower diamondoids have chemical formulas of $C_{4n+6}H_{4n+12}$, where n equals the number of diamond-cage subunits [65]. Adamantane was first synthesized in five stages by Prelog in 1941 from Meerwein's ester and had a yield of about 0.16% [66]. Schleyer (in 1957) found 30-40% yield, when he had used catalyst and then this method become an affordable source of adamantane [67]. The two cage structure (Diamantane) was first produced in 1965 by Cupas et al. [68], although it was isolated from petroleum a year later [69]. While, trimantane was discovered in 1966 [70], however, the synthesis of progressive polymantanes (higher diamonoids) became increasingly difficult. The formation mechanism of the higher diamondoids in petroleum remains a mystery. So far, it has not been possible to synthesize higher diamondoids except antitetramantane, a tetramantane isomer. Certain higher diamondoids are now available in multi-gram quantities through Molecular Diamond Technologies, Inc. on a collaborative basis. By comparison, lower diamondoids (adamantane, diadamantane, and triadamantane), extracted from crude oil much earlier than larger members of the diamondoid series, are currently available in kilograms quantities and can be synthesized. Figure 2.17 shows the structures of lower diamonoids in different models such as 3D stick, 3D ball and stick, and 3D space filling models.

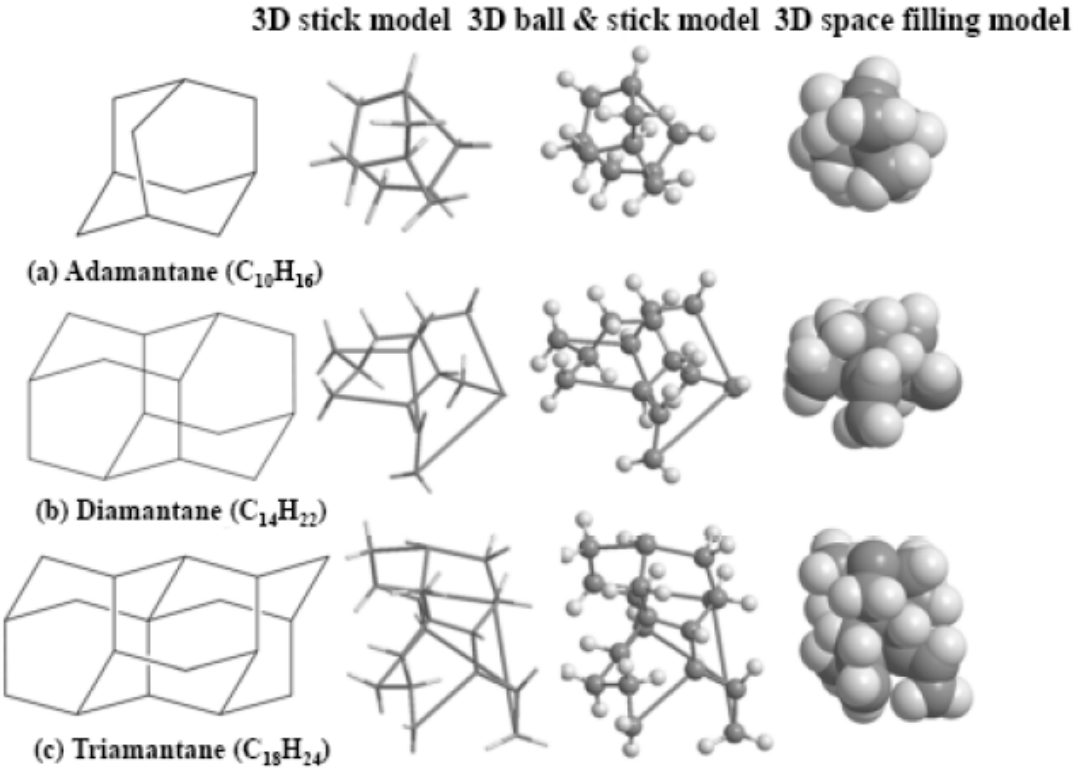

Figure 2.17: Structure of lower diamonoids (a) adamantane, (b) diamantane, and (c) triamantane in different models.

2.5.2 Higher diamondoids

After the discovery of lower diamondoids, the higher diamondoids were sought, however, the synthesis of progressive polymantanes (higher diamonoids) became increasingly difficult. In 1955, a group of higher diamondoids, including tetramantane, pentamantane, and hexamantane, was first discovered in a gas condensate produced from a very deep (~ 6800 m below the surface) petroleum reservoir located in the US Gulf Coast [71]. These polymantanes and their isomers were identified by gas chromatography/mass spectrometry (GC-MS). In 2003 Dahl et al. [72] published a paper in *Science* announcing the isolation and crystallization of large selection of higher diamonoids (C_{22} and higher polymantanes) from petroleum. In total they isolated and

crystallized all four tetramantanes, nine pentamantanes, one hexamantane, two heptamantanes, two octamantanes, one nonamantane, one decamantane, and one undecamantane.

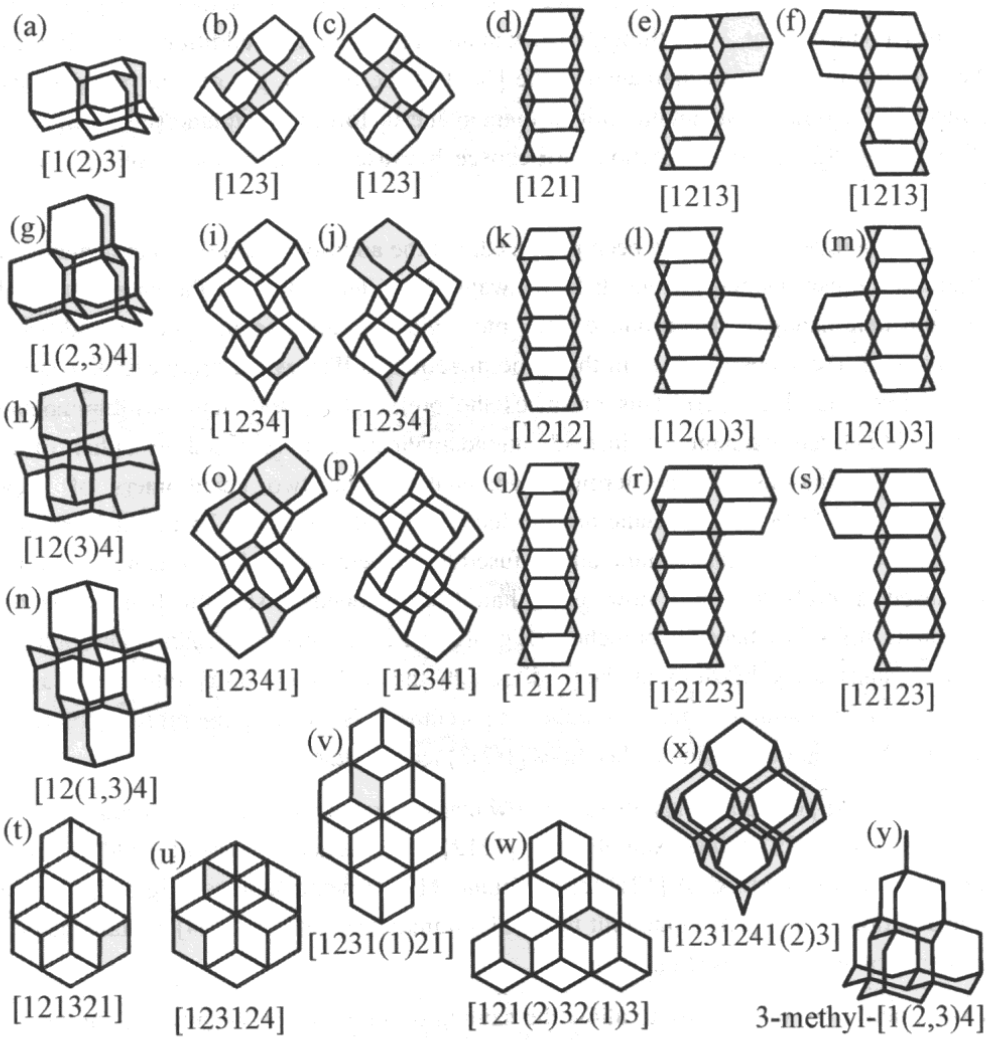

Figure 2.18: Diamondoids isolated; tertamantanes (a,b,c,d), pentamantanes (e,f,g,h,i,j,k,l,m), hexamantanes (n,o,p,q,r,s), heptamantane (t,u), octamantane (v), nonamantane (w), decamantane (x), and the alkylated pentamantane (y) [72].

2.5.3 Properties and applications of lower diamondoids

As we described above that the adamantane is the smallest unit of diamondoids. Adamantane molecule consists of three condensed cyclohexane rings fused in the chair conformation. The carbon-carbon (C-C) bond length is 1.54 Å and is almost identical to that of diamond, and the carbon-hydrogen (C-H) distance is 1.11 Å. The structure of adamantane is shown in Figure 2.19. Adamantane has face-centered cubic crystal structure.

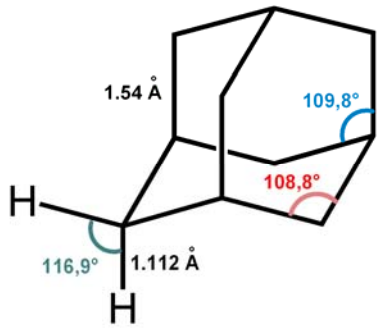

Figure 2.19: Structure of adamantane [http://en.wikipedia.org/wiki/Adamantane].

The density of adamantane at room temperature is ~1.08 g/cm^3. The adamantane is a colorless solid crystalline with camphor smell. It is insoluble in water but soluble in hydrocarbon solvents. Adamantane slowly sublimates at ambient temperature and its melting point is ~ at 270 °C [73]. The exact boiling point of adamantane is impossible to be determined due to its sublimation property.

Diamondoids show remarkable rigidity, strength, and thermodynamic stability, as well as interesting electronic properties [74], which may be of use in chemical, polymer, and pharmaceutical applications, as well as in nanotechnology. The adamantane structure is similar to diamond lattice, therefore, adamatane derivative (2-adamantanone) has been used for the nucleation and growth of diamond at 850°C and 40mbar [75]. The SEM image of synthesized diamond is shown in Figure 2.20. The characterization of the synthesized diamond has shown that the quality and crystallinity is good. They also shown that the during diamond deposition silicon carbide (SiC) interlayer formed on the Si substrate [75].

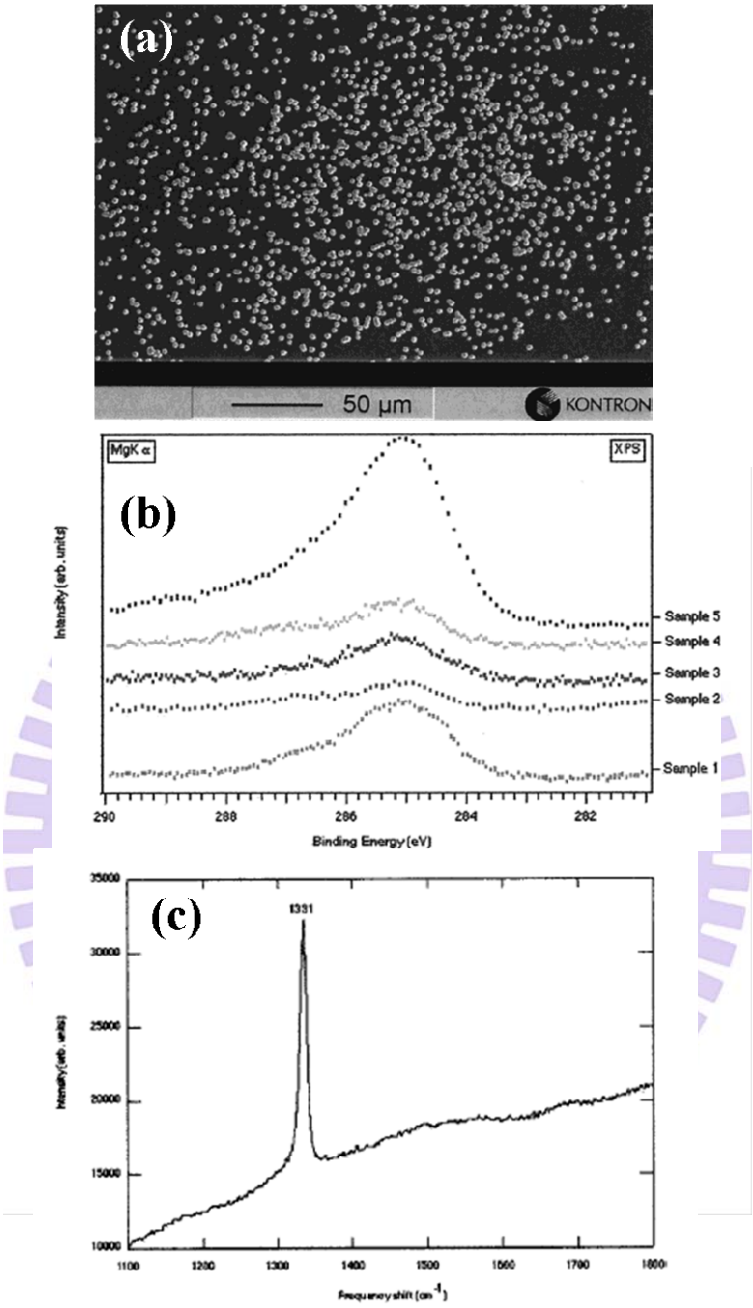

Figure 2.20: (a) SEM image, (b) XPS spectra, and (c) Raman spectrum of synthesized diamond using adamantane derivative for the nucleation and growth of diamond [75].

2.6 Structure of the thesis

The remainder of this thesis consists of six chapters and is organized as follows: In chapter 3, gives a detailed description of the experimental methods and procedures used in this study, and the materials and chemical chosen to accomplish the research work. Chapter 4 shows the diamond deposition at low temperature along with we described that the adamantane first converted into graphitic phase. Further, the graphitic phase acts as a diamond nuclei and its growth. Their excellent field emission property is also shown. While in chapter 5 shows the role of platinum particles. Platinum particles adsorb hydrocarbon (adamantane) and enhances the diamond density. The adsorb hydrocarbon (adamantane) convert into clusters of oriented graphite or carbon crystals in high density. Finally, Chapter 6 gives an overview and conclusions of the present study, and future works.

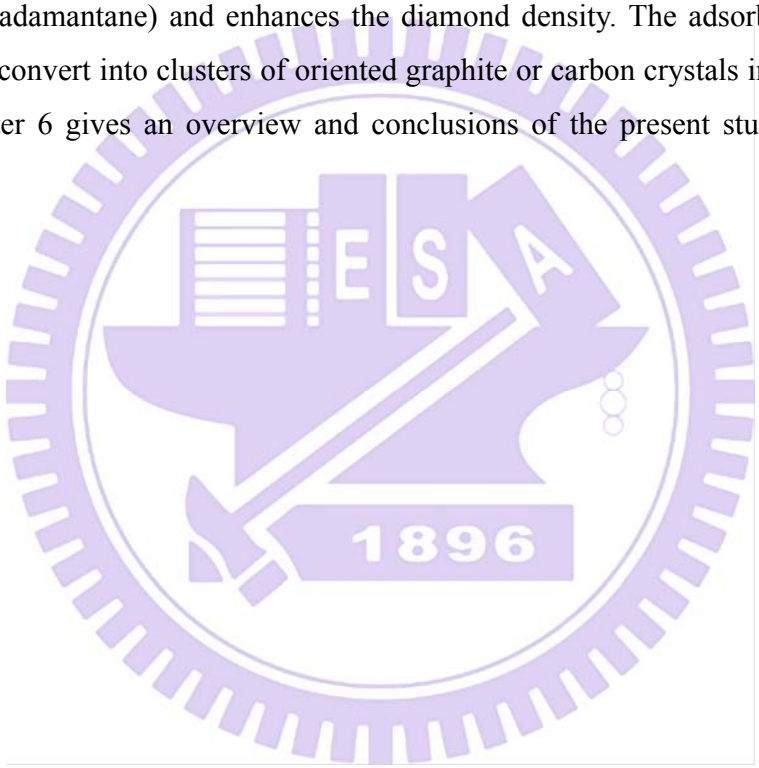

Chapter 3

Experimental methods

We have developed a several convenient techniques for the synthesis of diamond thin film. The processes include the pretreated Si surface with adamantane ($C_{10}H_{16}$) by hotplate method and ultrasonication method for diamond deposition. This chapter contains detailed descriptions of all the experimental techniques and their structure analysis for each process employed in this study.

3.1 Experimental flowcharts

Figure 3.1 shows the experimental flow chart of synthesis and characterization of diamond film on adamantine-coated Si substrates at low temperature and pressure. Prior to diamond film deposition, the adamantane were coated on Si surface by hotplate method.

Figure 3.2 shows the role of platinum (Pt) particles on interface layer for diamond deposition. The admantane deposited on Pt/SiO_2/Si layer by ultrasocation process, where Pt coated SiO_2/Si substrate by sputtering process.

In both process (Figures 3.1 and 3.2), diamond films were deposited by 1.5 AsTeX type microwave plasma chemical vapor deposition MPCVD from a gas mixture of methane and hydrogen without the application of a bias voltage to the substrates. In addition, the Si substrates were not mechanically scratched/abraded.

The surface morphology, bonding structure and chemical composition were analyzed by scanning electron microscopy (SEM), transmission electron microscopy (TEM), x-ray photoelectron spectroscopy (XPS), atomic force microscopy (AFM), Raman spectroscopy, x-ray diffraction, Fourier transform infrared spectroscopy (FT-IR), and optical microscopy. The field emission measurements of specimens were performed at room temperature.

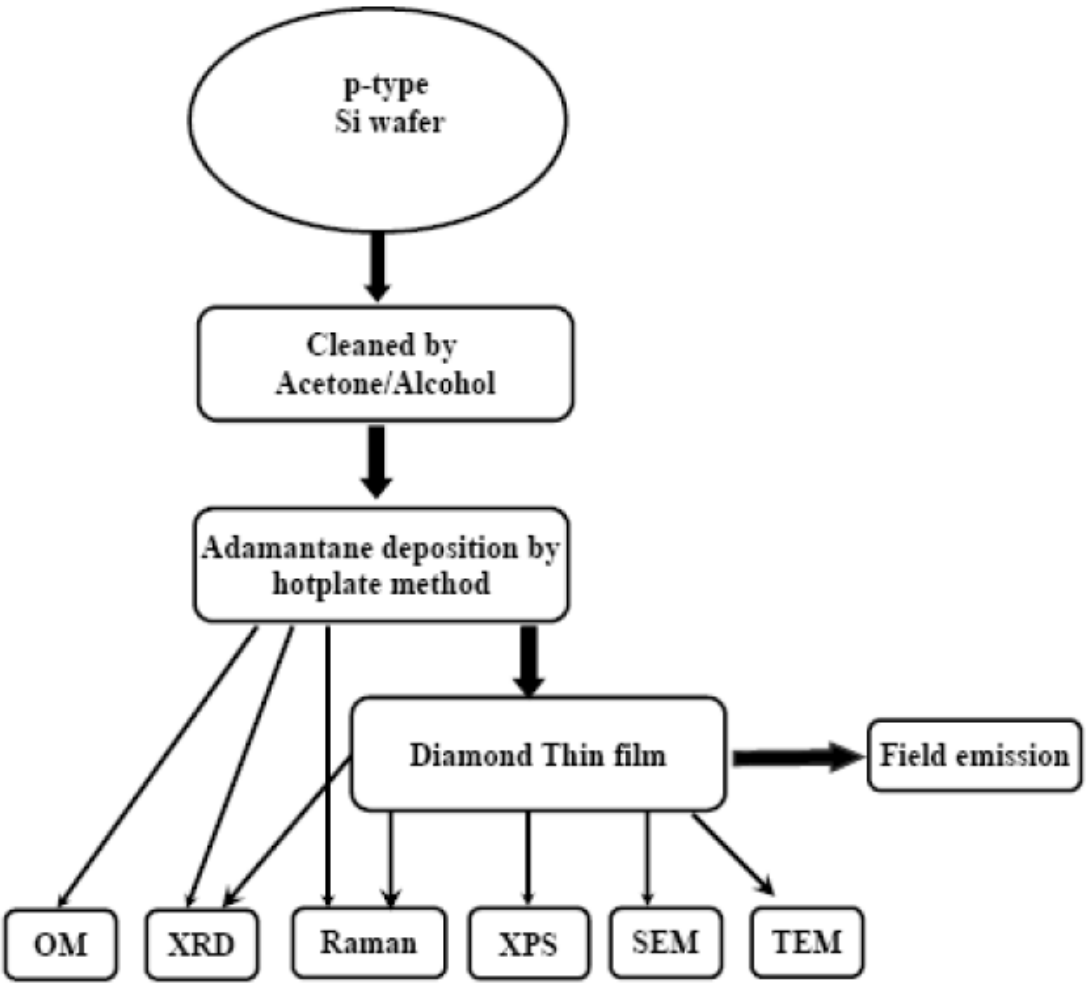

Figure 3.1: Experimental flowchart of the synthesis and analysis of diamond film on Si substrate and its application in field emission.

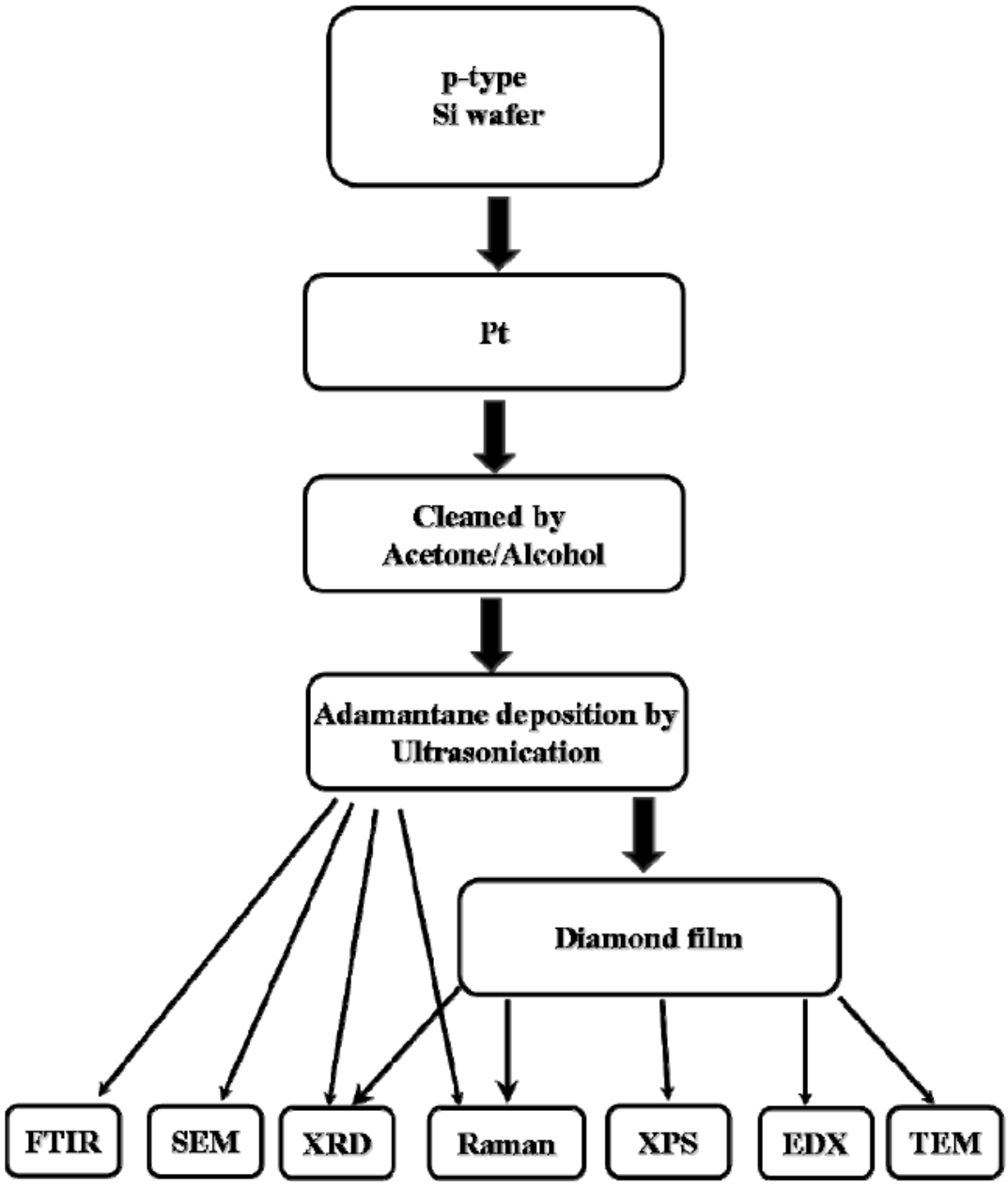

Figure 3.2: Experimental flowchart of the synthesis and analyses of diamond film on $Pt/SiO_2/Si$ substrate.

3.2 Substrate holder

We used molybdenum (Mo) holder for diamond growth in all experimental process. The schematic diagram of Mo holder is shown in Figure 3.3.

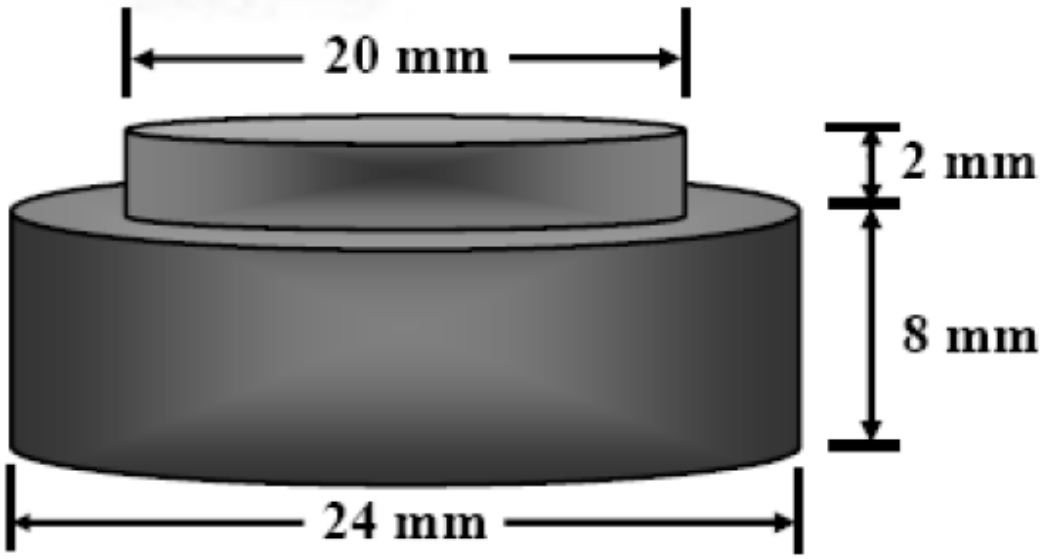

Figure 3.3: Substrate holder for diamond deposition

3.3 Microwave plasma chemical vapor deposition (MPCVD) system

The deposition of diamond film was carried out in a microwave plasma chemical vapor deposition system. The photograph of 1.5 kW ASTeX type MPCVD is shown in Figure 3.4 (a). In this system we can increase the power up to 1000W. The schematic diagram of MPCVD reactor is shown in Figure 3.4 (b). The basic structure of MPCVD consists of the following parts, as shown in Figure 3.4 (a):

(i) Microwave generator: The function of microwave generator is to produce microwave. The magnetron in 1.5 ASTeX system generates high frequency (2.45GHz) microwave.

(ii) Wave guide: After generating the high frequency microwave, it delivered within square waveguide and finally gets into the microwave chamber through antenna.

(iii) Circulator: This device is mainly use to control the reflected power from the system.

(iv) CVD Reactor Chamber: It is mainly made of stainless steel to sustain a high

temperature and pressure. There is optical quartz glass at the top of chamber while base is made of stainless steel. The unique properties (low microwave absorption coefficient and high thermal stability) of quartz glass are made to use in CVD chamber.

(v) Multi-Gas Controller: It is use to the control the flow of gases into the reaction chamber to generate plasma.

(vi) Pressure Controller and Vacuum System: the function of pressure controller is the control the pressure in the chamber. The vacuum system is mainly dominated by the mechanical pump such as rotary pump.

(vii) Bias System: In laboratory has the additional DC power supply (Model: LABORATORY DC power supply GPR 50H10D) and it can be use in the system as maximum voltage at 450V. The use of positive and negative bias can increase the density and quality of diamonds.

(viii) Cooling System: The main function of this system is to cool the system at room temperature.

\

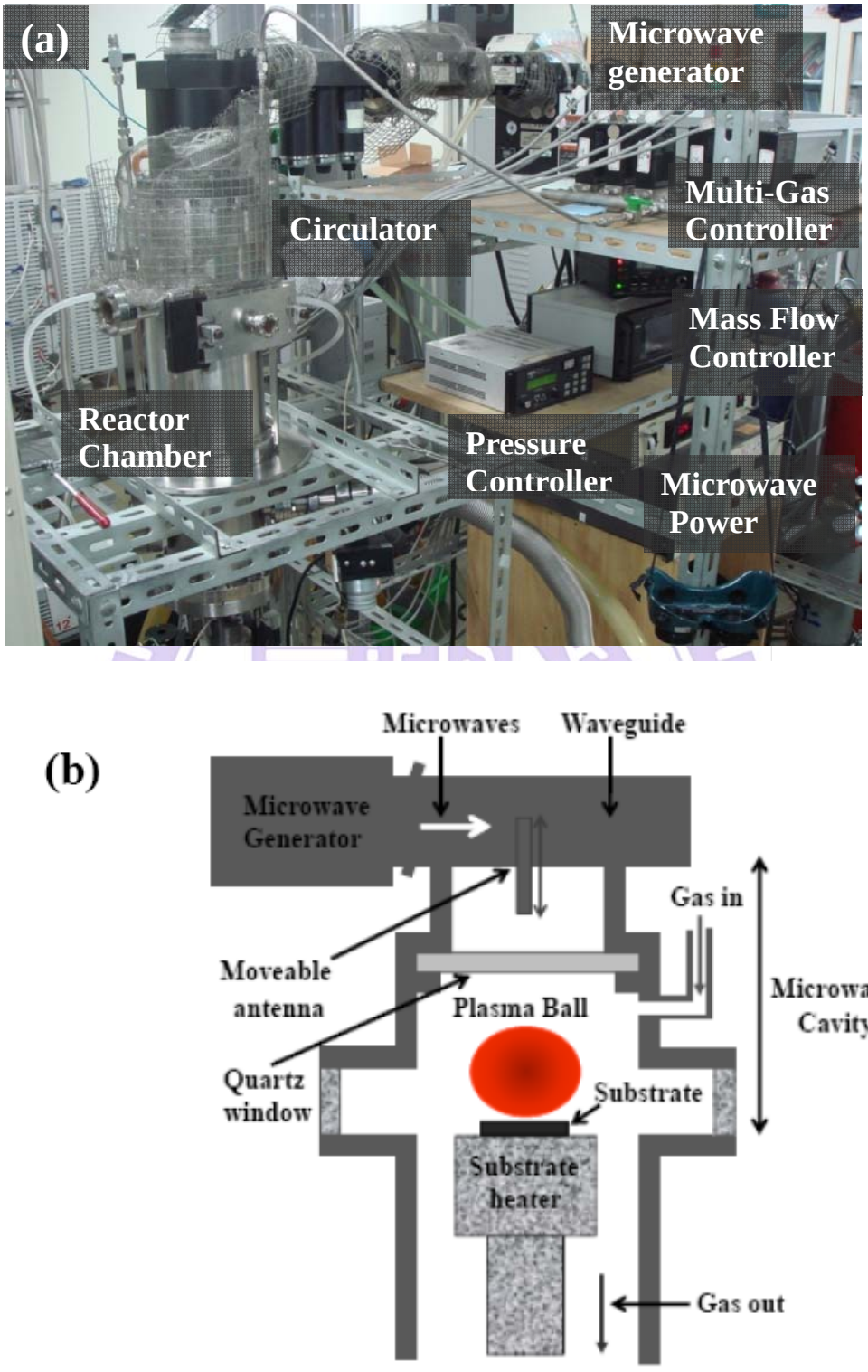

Figure 3.4: (a) Photograph and (b) schematic diagram of CVD reactor of 1.5 kW ASTeX type MPCVD system.

3.4 Material analysis methods

3.4.1 Scanning electron microscopy (SEM)

Scanning electron microscopy (SEM) is used to examine the surface morphology of the samples at a high magnification. The high magnification range of the SEM is achieved due to its resolving power of approximately 3-6 nm. The SEM is useful and popular for many reasons. One of the great advantages of SEM is its large depth of field (the amount of sample that is in sharp focus at one time). This makes it possible to examine surfaces with a relatively high level of surface variability (and at much higher magnifications). This is because the depth of field of the SEM can be up to four hundred times greater than that of a light microscope. Moreover, it has the advantage of easy sample preparation, and high image resolution. A common SEM is equipped with an electron gun to generate an electron beam to be accelerated under 0.4-40 kV voltage. By deflecting the incident beams with scanning coils, a two dimensional image can be obtained by detecting secondary electrons and backscatter electrons.

The microscopes mainly engaged are field emission type SEM JEOL-6500 and 6700. Accelerating voltage is 15 kV with emission current of 10μA. Working distance is 10mm and 8mm under 9.63×10^{-5}Pa. Here, we used SEM to see the morphology of our films at low and high magnification. We also have taken top-view along with cross-section image.

3.4.2 Micro Raman spectroscopy

Raman spectroscopy is a simple and non-destructive technique for the analysis of carbon materials. Raman spectroscopy has been used to study vibrational, rotational, and other low-frequency modes. In this system, a laser is focused through a microscope onto the specimen and the scattered light is passed to a spectrometer, which is dispersed by the light grating onto a charged coupled device (CCD) detector. The choice of laser wavelength can be varied depending upon the required applications usually from a laser in the visible, near infrared, or near ultraviolet range. The Raman spectra of carbon species is shown in Table 3.1.

We used micro Raman spectroscopy (LABRAM HR 600) with a spatial resolution of the order of 1 μm^2 for the analysis of our specimen. In this system, we used Ar and He-Ne lasers with the wavelength of 514.5 and 632.82nm, respectively to the analysis of our specimen. The schematic diagram of the basic working principle of Raman spectrometer is shown in Figure 3.5.

Table 3.1: Raman characteristics of different carbon species of carbon [76].

Wavenumber (cm^{-1})	**Different carbon species**
1150	Nanodiamond or trans-polyacetylene v_1-band (C=C)
1332	Diamond (sp^3)
1350	D-band (sp^2)
~1450	Trans-polyacetylene v_3-band (C=C)
1580~1600	Graphite G-band (sp^2)

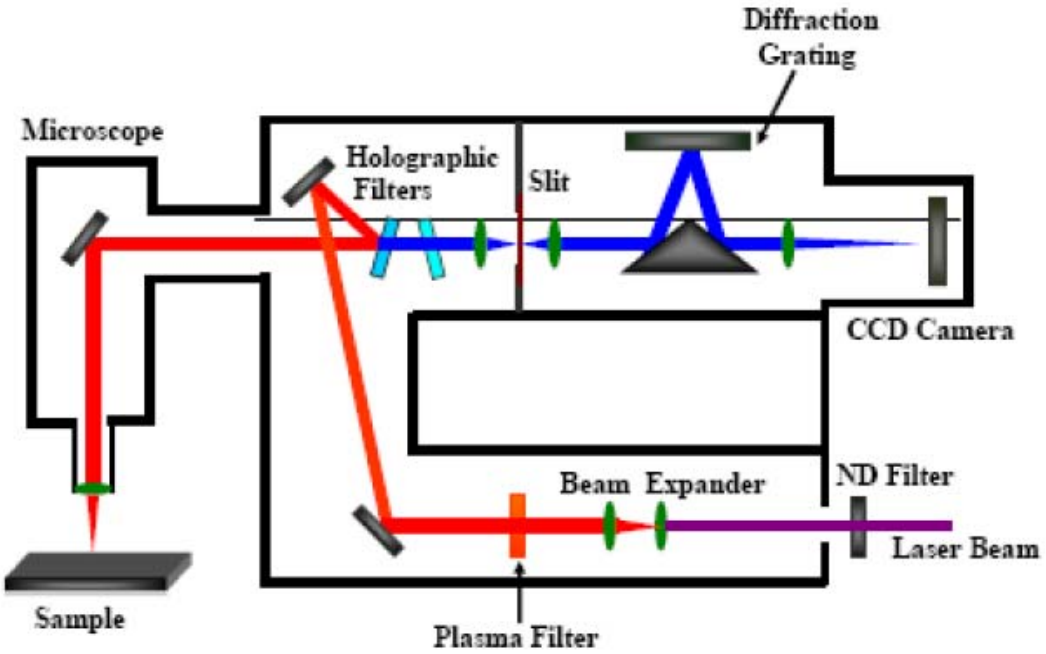

Figure 3.5: Schematic diagram of the Raman spectrometer.

3.4.3 Transmission Electron Microscopy (TEM)

Transmission electron microscopy (TEM) (JEOL JEM-2010F; Philips Tecnai20) is operating at 200 kV accelerating voltage. This is the most important instrument to study defects in detail. Transmitted and diffracted electrons are recombined by objective lens to form a diffraction pattern in the back focal plane of that lens and a magnified image of the sample in its image plane. A number of intermediate lenses are used to project either the image or the diffraction pattern onto a fluorescent screen for observation. The screen is usually lifted and the image is formed on photographic film for recording. The schematic diagram and different image modes in TEM are shown in Figure 3.6. The cross-sectional TEM specimen was prepared using a focused ion beam (FIB; FEI Nova 200 dual-beam FIB). For the protection of the TEM specimen against damage from the high-energy ion beam (30 keV Ga^{+}), the specimen was coated with platinum.

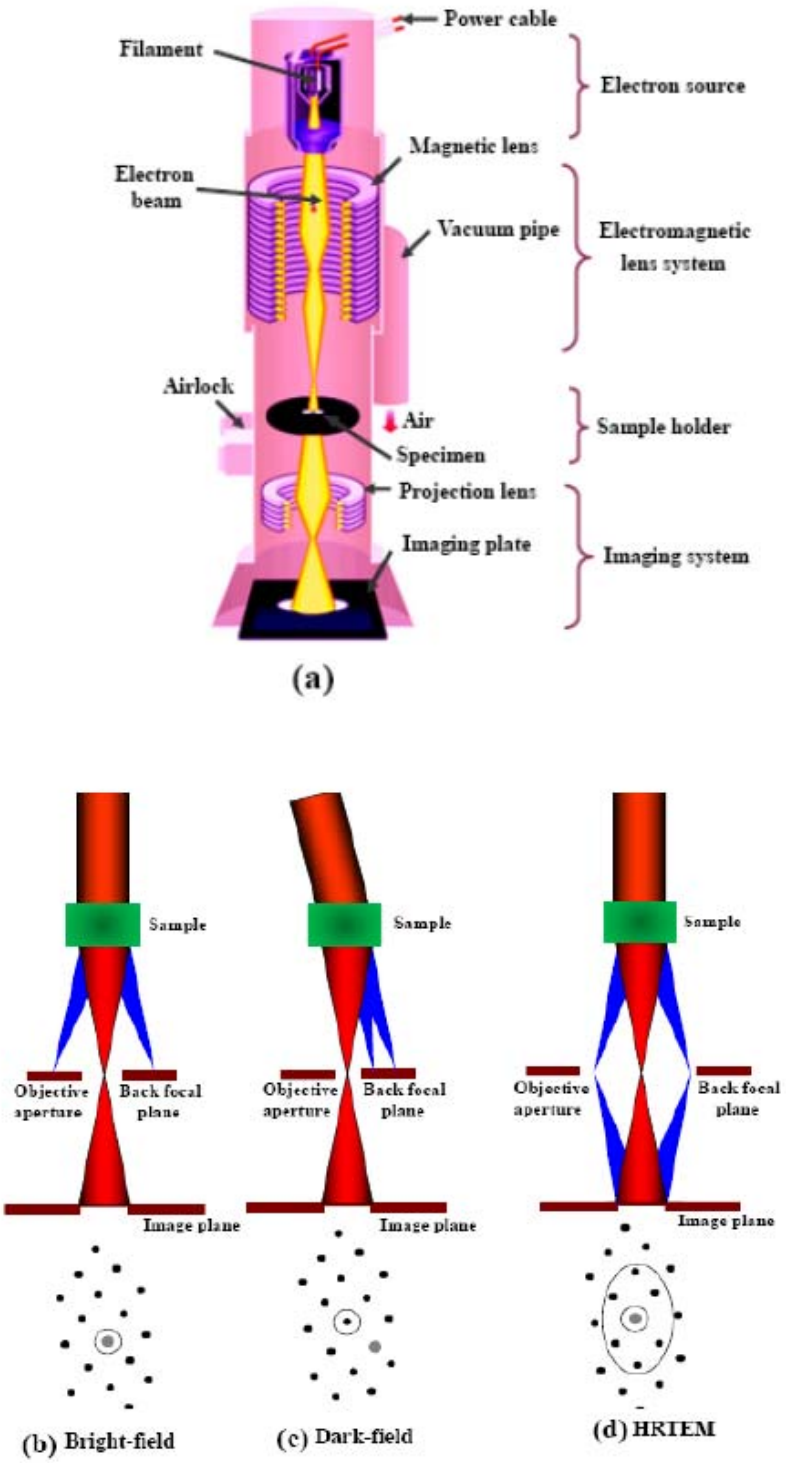

Figure 3.6: Schematic diagram of (a) TEM [http://www.hk-phy.org/atomic_world/tem/tem02_e.html], (b) Bright field image, (c) Dark field image, and (d) HRTEM image.

The cross-sectional TEM specimens were placed onto a holey-carbon copper grid. Energy-dispersive X-ray analysis (EDX) was employed to study the chemical composition of the specimens.

3.4.4 X-ray diffraction (XRD)

X-ray diffraction (XRD) is a very important experimental technique that has long been used to address all issues related to the crystal structure of solids, including lattice constants, identification of unknown materials, orientation of single crystals, and etc. In XRD, a collimated beam of X-rays, with a wavelength typically ranging from 0.7 to 2 Å, is incident on a specimen and is diffracted by the crystalline phases.

The crystallite size, d, can be estimated from the peak width with the Scherrer's formula:

$$d = 0.9\lambda/\beta\cos\theta$$

Where λ is the X-ray wave length, β is the full width of height maximum of a diffraction peak, θ is the diffraction angle, and K is the Scherrer's constant of the order of unity for usual crystal.

In our studies, Siemens (D5000) and D2 XRD have been used to for the orientation of diamond and other materials. The schematic diagram of XRD is shown in Figure 3.7. The Cu K_α characteristic X-ray (wavelength: 1.54Å) is used as X-ray sources for the XRD measurements. Since Cu K_β characteristic (wavelength: 1.39Å) is also radiated from X-ray tube with Cu target, a Ni filter is used to eliminate the XRD peak caused by the K_β X-ray.

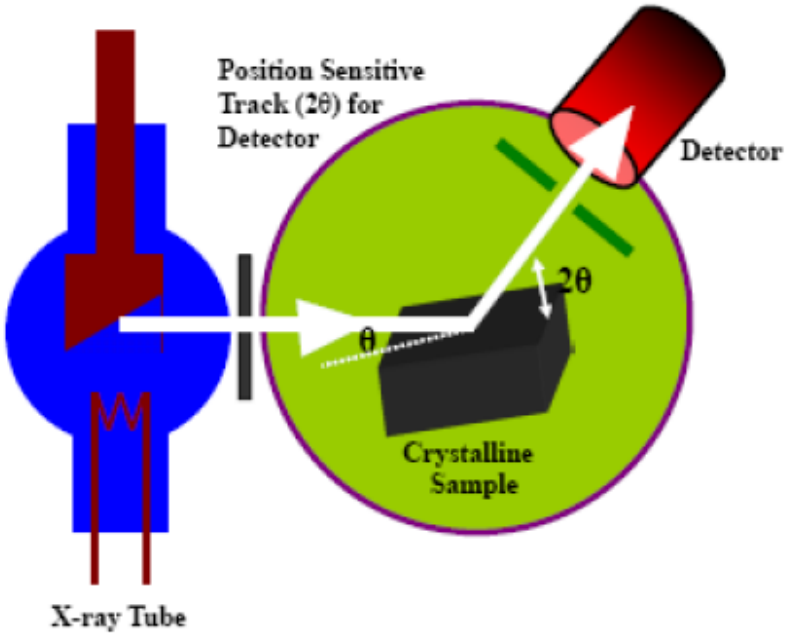

Figure 3.7: Schematic diagram of the X-ray diffractometer.

3.4.5 X-ray photoelectron spectroscopy (XPS)

Surface analysis by X-ray photoelectron spectroscopy (XPS) involves irradiating a solid in vacuum with monoenergetic soft X-rays and analyzing the emitted electrons by energy. The method requires the sample of interest to be bombarded with low energy X-rays, produced from an aluminum or magnesium source, with energy of hv. These X-rays cause electrons to be ejected from either a valence or inner core electron shell. The energy of the electron, E, is given by $E = hv - E_1 - \Phi$, where E_1 is the binding energy of the atom and Φ is the work function of the sample. Thus, it is possible to calculate the binding energy of the ejected electron, and therefore identify the atom (and its chemical state) from which the electron originates. The spectrum is obtained as a plot of the number of detected electrons per energy interval versus their binding energy (or kinetic energy). Since the mean free path of the electrons is very small, the electrons which are detected originate from only the top few atomic layers. Quantitative data can be obtained from peak heights or peak areas, and the identification of chemical states often can be made from exact measurements of peak positions and separations.

In this study, XPS was used to analyze the chemical states of carbon, silicon and

platinum. The schematic diagram of XPS is shown in Figure 3.8. XPS analyses were performed on a VG Microlab 310F system with Mg-K x-ray source. Argon ion with ion energy of 5 keV was used for sputter profiling. Elemental mapping in cross section was performed using a PHI700 scanning Auger nanoprobe (ULVAC-PHI Inc.) at the Department of Materials science and Engineering, National Tsing Hua University, Hsinchu, Taiwan.

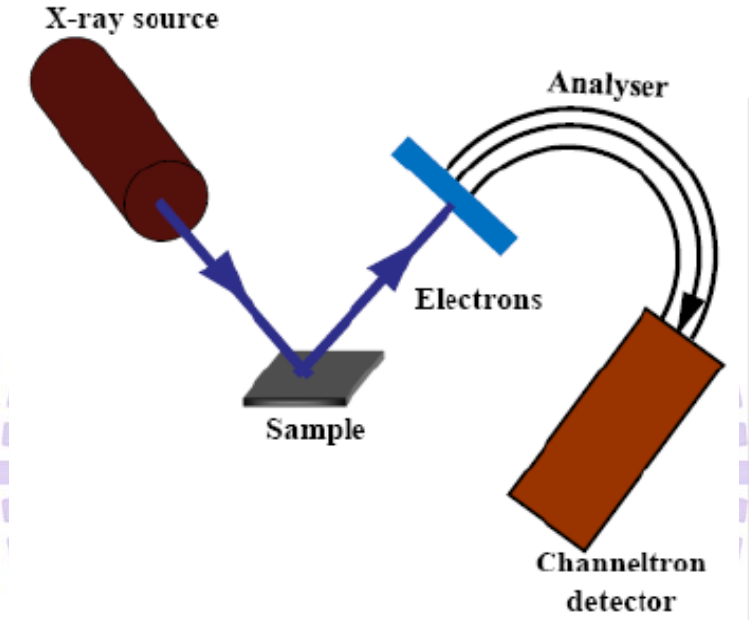

Figure 3.8: Schematic diagram of X-ray photoelectron spectroscopy.

3.4.6 Atomic Force Microscopy (AFM)

Atomic force microscopy (AFM) is common tool for the use of the surface imaging and analytical studies of roughness. Both Contact and Tapping Mode are well suited for topographical imaging of surfaces, with vertical resolution ranging from one micron down to sub nanometer scales. In all techniques (Contact, Tapping, Scanning Tunneling and Lateral force modes) share a common approach where a motor controlling a mechanical tip is placed in a feedback loop as the tip is scanned across a surface. Tapping Mode in D3100 is the most common imaging technique we have used in our work. This mode operates by scanning a tip attached to the end of an oscillating cantilever across the sample surface. The amplitude of oscillation ranges from 20 nm to 100 nm, with the

frequency near the resonant peak of the cantilever. The tip lightly 'taps' the surface, altering the oscillatory motion as the scanner moves across the surface. By adjusting the vertical position of the scanner to maintain a constant RMS signal of oscillation, a surface is imaged. The oscillation is measured by a laser positioned by the user to reflect signal into a photodiode detector. The schematic diagram of AFM is shown in Figure 3.9.

In our studies, we have used Digital Instruments Nanoscope, D-3100 AFM at a scan size of 5 and 2.5 μm^2 and a scan rate of 1 Hz to know surface imaging and roughness of the films. The Si tips that we used for the study of roughness and morphology of our specimen were sharp. Sometimes tips were broken due to the high surface roughness of our specimen.

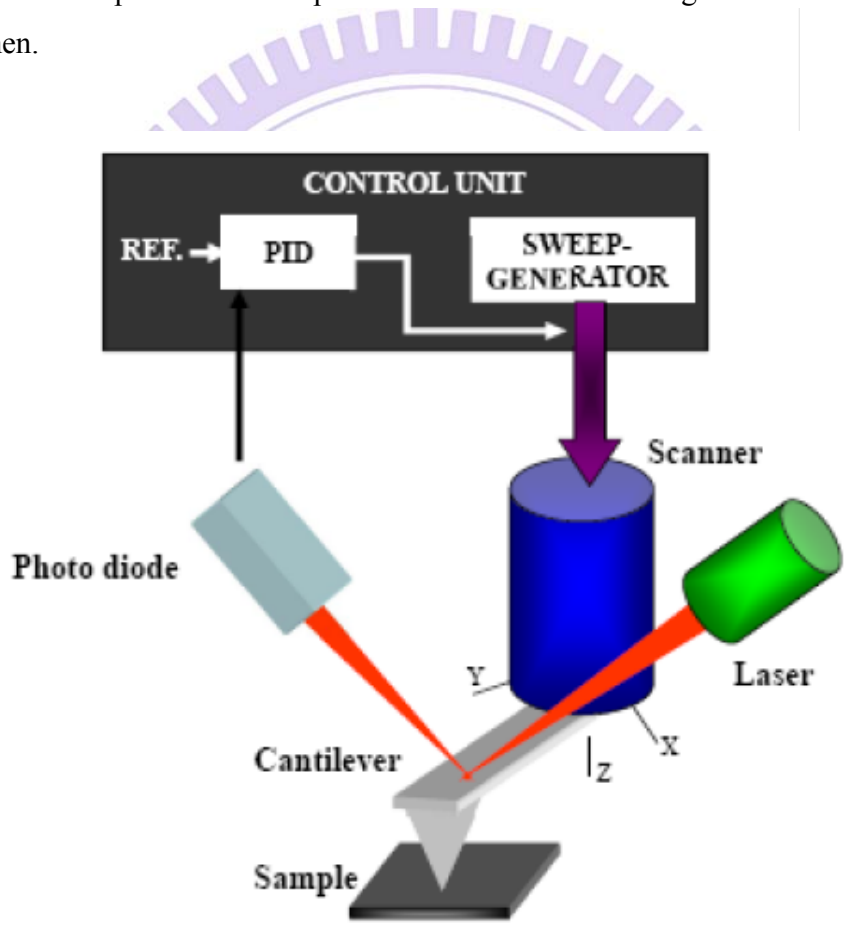

Figure 3.9: Schematic diagram of atomic force microscope

3.5 Electron Field emission measurements

Room temperature electron field emission (EFE) properties were measured with an electrometer (Keithley 237) using a parallel cathode-anode home built setup. Anode was made of circular Mo tip with diameter of 2 mm. Fowler-Nordheim (FN) theory was used to explain the EFE behavior of materials. According to FN theory, $J(E) = AE^2 \exp[(-B\Phi^{3/2})/E]$, where J is current density, E is applied field, A and B are constants, and Φ is the work function of the emitting material. In addition, one can estimate the field enhancement factor (β-value) of emitter materials from the effective work function ($\Phi_{eff} = \Phi^{3/2}/\beta$), which is proportional to the slope of FN plot in the high field segment. The turn-on field is designated as the lowest value of FN plot, which can be extrapolated from the low- and high-field segments in FN plot. The schematic diagram of field emission measurement set up is shown in Figure 3.10.

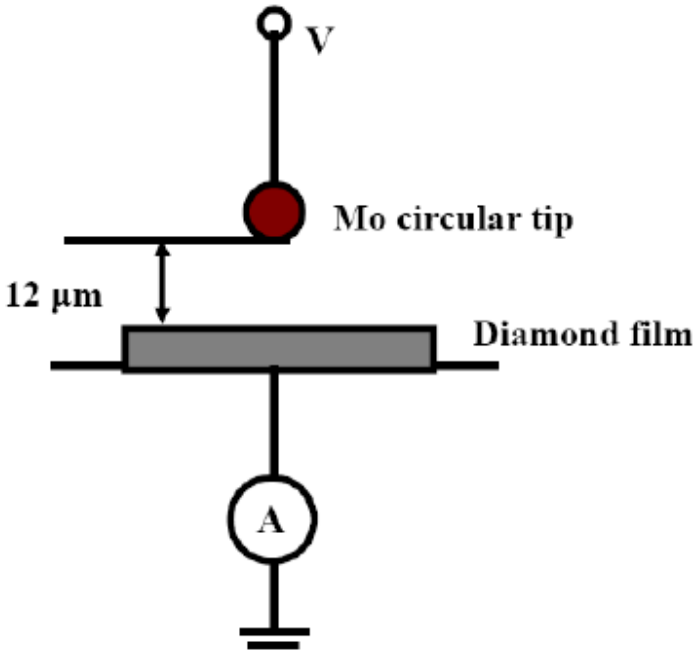

Figure 3.10: Setup of field emission measurement [77].

Chapter 4

The synthesis of diamond films on adamantane-coated Si substrate at low temperatures

4. 1 Introduction

The synthesis of diamond film by chemical vapor deposition (CVD) has been widely demonstrated in the past few decades, due to the combination of its outstanding physical and chemical properties. such as wide band gap, negative electron affinity, chemical inertness, high carrier mobility, excellent biological compatibility, good optical transparency, excellent thermal conductivity, high propagation speed of acoustic wave, and the greatest hardness. The unique properties of diamond make it an ideal material for a wide range of scientific and technological applications such as optics, microelectronics, tribological, thermal management, biomedical, DNA sensor, and so on [78-84].

It is well know that CVD deposition of diamond on non-scratched nondiamond substrates results in a very low nucleation density of the order of 10^{2-3} cm^{-2}**.** Therefore, diamond deposition on the non-diamond substrates is performed by nucleation processing step. Nucleation, correspond to the formation of diamond nuclei, i.e. the smallest thermodynamically stable islands, at the substrate surface. Nucleation procedures have been developed by performing either ex situ treatments on the substrate such as scratching with powders (diamond, carbide, oxides, silicides, nitride carbides, borides, and etc.) or in situ methods before CVD (chemical vapor deposition) growth such as dc or ac voltage bias technique [85-87]. The former process leads to inhomogeneous density of the nuclei as well as deleterious surface, while the later one is limited by the conductivity of the substrate. The deleterious surface and roughening resulting from scratching is not friendly with numerous applications such as optical windows, masks used in photolithography, and so on, while non-scratching method for growing thick diamond film with high nucleation density are particular significance. Currently several groups have used different seeding materials (without scratching) such as graphite fibers, fullerenes clusters, hydrocarbon oil, and thin films of different types of carbon for the diamond deposition [75, 88, 89]. However, despite rapid progress, the growth of diamond

film on the silicon substrate by microwave plasma chemical vapor deposition (MPCVD) still require nucleation step for improvement in terms of yield, quality, purity, and uniformity to synthesis of diamond at relatively low temperature and pressure.

Here we introduce the application of adamantane for diamond synthesis. Adamantane ($C_{10}H_{16}$) is one of a series of carbon structure, very stable crystalline compound, and highly symmetric molecule with point group symmetry, Td. Adamantane is the smallest possible diamondoids (chemical formula $C_{(4n+6)}H_{(4n+12)}$, where n = 0, 1, 2, 3, …), consisting of 10 carbon atoms arranged as a single diamond cage surrounded by 16 hydrogen atoms, as shown in Figure 4.2 (iii). A cage-like structure is formed with six CH_2 and four CH groups giving rise to a molecular structure with four cyclohexane rings in chair form. Its structure has zero strain as all C-C-C bond angles are 109.45° with a corresponding bond length of 1.54 Å and C-H bond length is 1.1 Å. The density of adamantane is 1.07 g/cm³. Adamantane does not melt at ambient pressure but sublimates. Adamantane can sublime easily and has a relatively high vapor pressure. Partial breakdown of adamantane is known to yield carbon clusters (C_nH_x), where n = 3, 5, 6, 7, 8 and 9, of significant abundance [90]. Matsumoto and Matsui in their study of diamond synthesis by chemical vapor deposition two decades ago suggested that hydrocarbon cage molecules such as adamantane are possible embryos for the homogeneous nucleation of diamond [91], there are rarely studies of diamond synthesis related with diamondoids. Previously, LeRoy et al. and Giraud et al. had been used 2, 2-divinyladamantane molecules (adamantane derivative) for diamond nucleation and growth on the silicon (111) substrate at 850°C [75, 85]. Another important issue in particular chemical vapor deposition (CVD) diamond, since early 1980 report is the high deposition temperature (700-900°C) [84, 92,-97], which limits only on thermal stable substrates. Consequently, a major goal in the diamond research has been to lower the substrate temperature required for diamond growth. This will permit the use of a much wider range of substrate materials of industrial importance such as Al, Si, SiC, GaN, GaAs, Ni and steel in different mechanical, electrical, optical and electronic applications. Lowering of substrate temperature during diamond synthesis could be an important step for deposition on low melting materials as well. The deposition of high quality diamond at low temperature is

still challenging even if some studies reported diamond deposition at temperature below 550°C [98-101].

Here we report a simple method for the synthesis of good-quality diamond film on adamantane ($C_{10}H_{16}$)-coated Si surface by the microwave plasma chemical vapor deposition (MPCVD) at relatively low temperature. Silicon is the most widely used substrate material for the deposition of diamond by CVD. Silicon wafers are the most common substrate material not only due to its chemical affinity and adhesion to diamond, inertness under deposition conditions, but also due to its availability and ease of use. Its carbide bond strength is also impressive. Therefore, we used Si substrate for diamond growth. Adamantane-coated Si substrate by hotplate method is shown in Figure 4.1. To the best of our knowledge, this is the first report showing the synthesis of diamond films on the adamantane-coated Si (100) substrate at low temperature. The rate of film growth in 0.6% methane (CH_4) in hydrogen (H_2) was 0.5 $\mu m\, h^{-1}$. A quantitative estimation of minimum temperature for diamond deposition is proposed. Interest, which exists in the development of CVD diamond processes at low temperature, is to deposit high quality diamond film at high growth rate. The advantages for using the adamantane are that it is not much expensive and easily commercially available. The deposited diamond crystallites films are well faceted. Their excellent field emission properties are also reported.

4.2 Experimental process for diamond synthesis

4.2.1 Coating of adamatane on Si substrates by hotplate method

The schematic diagram of adamantane coating on Si substrate by hotplate method is shown in Figure 4.1. The commercial adamantane powders in 99+% purity were obtained from Sigma-Aldrich Chemie GmbH (CAS:281-23-2). The synthesis processes of the diamond films consisted of the following steps: a mirror- polished p-type (100) Si wafer with dimensions of 1 x 1 cm^2 without any mechanical pre-treatment were used as the substrates.

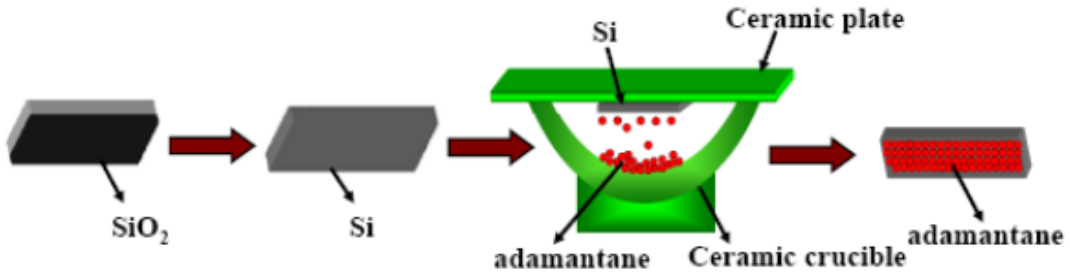

Figure 4.1: Schematic diagram of adamantane deposition on the Si surface by hotplate method.

The Si substrates were ultrasonically cleaned consecutively in acetone and alcohol for 10 min, and dried with N_2 spray. Subsequently, cleaned substrates were dipped in buffered oxide etch solution for 5 min to remove the native oxide layer from the Si substrate surface. Further, the cleaned Si samples were fixed onto a ceramic plate by sellotape and paper. First sellotape was fixed on the ceramics plate and then we used paper to stick on sellotape. The upper side of paper was sticky. And then Si was fixed on that sticky paper. The adamantane powder was kept in a ceramic (Al_2O_3) crucible and covered with fixed Si substrates onto the ceramic plate, and then placed on a hot plate at 250°C (hereafter called hotplate method) for 5 min. At 250°C, adamantane sublimed immediately and thick adamantane layer deposited on the Si substrate. When we used adamantane (2gm) for the deposition on the Si surface at 250°C for 5 min, major fraction of adamantane was deposited on the Si substrate and less fraction of adamantane still left

in a crucible. Manually, we measured the thickness of deposited adamantane by scale, it was approximately ~0.9 mm. The distance between the fixed Si substrates and adamantane powder was ~2 cm, as shown in Figure 4.2.

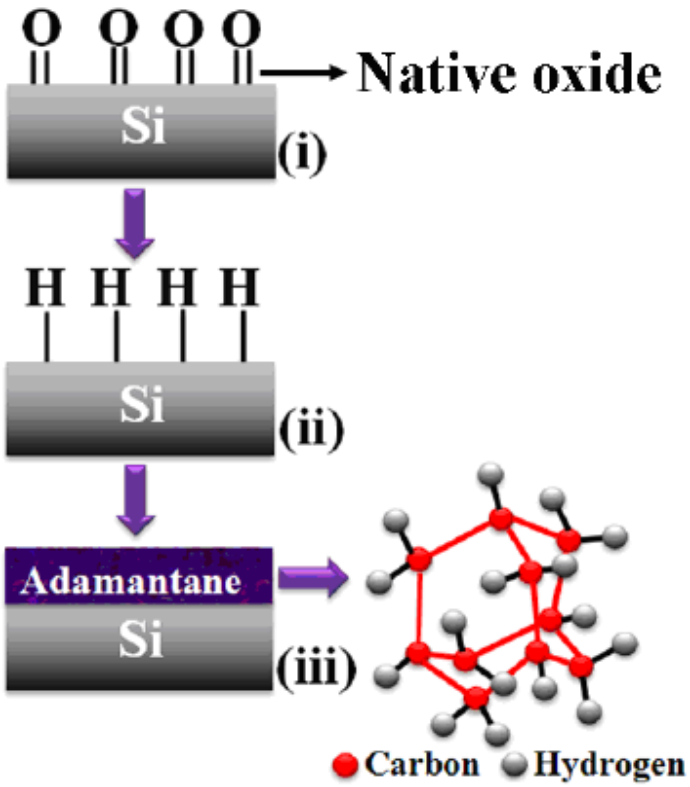

Figure 4.2: Schematic diagram showing adamantane coating on Si in three steps; (i) silicon substrate with native oxide layer, (ii) BOE solution for 5 min to remove native oxide from the Si surface, and (iii) adamantane deposited on silicon surface by hotplate method.

4.2.2 Process for diamond synthesis

The deposited adamantane on Si substrate was then placed on a Mo-disk holder for diamond synthesis. The schematic diagram of diamond synthesis is shown in Figure 4.3. The deposition of diamond was carried out in a 1.5kW AsTeX-type microwave plasma chemical vapor deposition (MPCVD) system. The pressure, total gas flow rate, and deposition time was fixed at 20 torr, 200 sccm, 270 min, respectively, while the

microwave power was varied from 200 to 350W. The temperature was measured by optical pyrometer (We had also qualitatively calibrated the temperature, using an Al foil below Si substrate for 1 hr. The Al foil did not melt silicon substrate. From this result, we were sure the temperature was below < 580°C). The temperature was varied from 400 to 530°C. Finally, the samples were allowed to cool down to ambient temperature in the presence of hydrogen gas (10 torr) to etch the nondiamond phases that remained on the

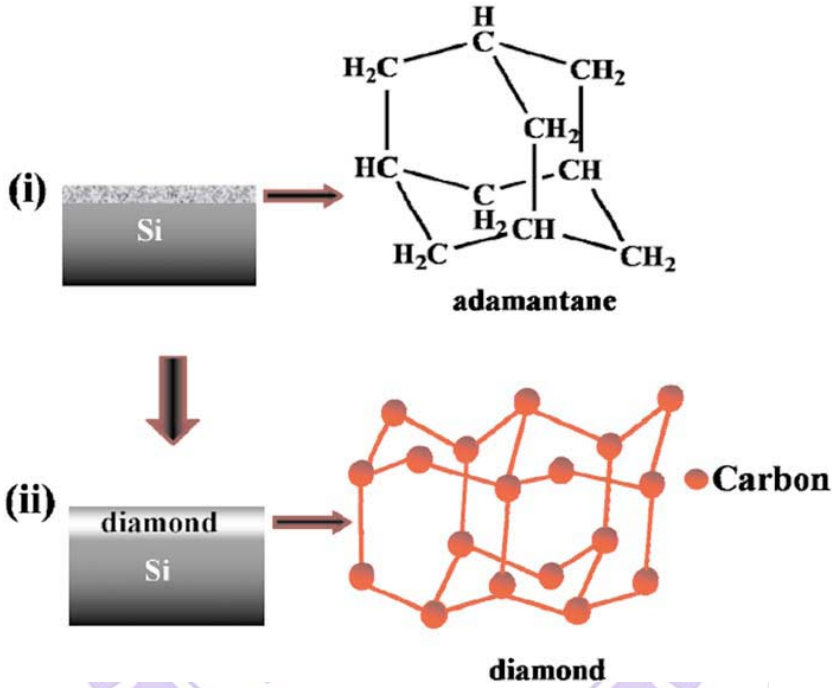

Figure 4.3: Schematic diagram showing diamond synthesis in two steps; (i) adamantane deposited on silicon surface by hotplate method and (ii) diamond growth by MPCVD.

film surface after the diamond growth. To study the role of adamantane in diamond growth, we prepared another sample without adamantane coated (WAC) on Si substrate. The diamond growth conditions were similar to that for adamantane-coated (AC) Si substrate.

4.3 Structural characterization of adamantane

Adamantane is a colorless, solid, and crystalline powder. Photograph of adamantane powder is shown in Figure 4.4.

Figure 4.4: Photograph of solid crystalline adamantane powder.

After coating of adamantane on Si substrate at 250°C by hotplate method, an optical microscope was used to characterize the surface morphology of the adamantane layer. Figure 4.5 (a) shows that a continuous adamantane film has been coated on the Si (100) surface. The inset high-magnification optical image in Figure 4.5 (a) shows the size of adamantane particles are in several micrometers. The large particles of adamantane may be due to the particle agglomeration. The coated adamantane on Si substrate was then analyzed by X-ray diffraction (XRD) method. The XRD pattern in Figure 4.5 (b) presents sharp and well-defined peaks, and the observed diffraction peaks at 2θ = 16.3, 18.8, 26.7, 31.5, 32.9, 41.7, 47.1, 50.3, 54.9, 57.7, 59.1, 71.3, and 72.0 degrees correspond to the interplanar spacings of adamantane {111}, {200}, {220}, {311}, {222}, {331}, {422}, {511}, {440}, {531}, {600}, {551}, and {640}, respectively. The experimental 2θ values are consistent with the standard JCPDS values (JCPDS file number: 22-1529 and 31-1505). The intensity of adamantane peak is shown in Figure 4.6. Further, the adamantane-coated Si substrate was also evaluated using Raman spectroscopy (LABRAM HR800), as shown in Figure 4.5 (c). The Raman spectra were acquired with a micro-mode using an

Ar laser (laser wavelength; 514.5nm) beam which was focused to ~ 1μm diameter. Intense Raman peaks in the range of 600–1800 cm^{-1} are shown in Figure 4.5 (c). We observed the multiple Raman peaks at 635, 758, 949, 970, 1095, 1120, 1220, 1311, 1370, 1432, and 1509 cm^{-1}. These peaks are due to different modes of hydrocarbon (C-H) in adamantane molecule. The Raman peaks at 635, 758, 949, and 970 were due to CCC bend/CC stretch modes while other Raman peaks at 1095, 1120 and 1220, 1311 and 1370 cm^{-1} was due to doubly–degenerated CH wag/CH_2 twist modes. The Raman peaks at 1432 and 1509 cm^{-1} may be due to E CH_2 scissor mode [102]**.** In literature review, we have noticed that the adamantane peaks in Raman spectrum also show the presence of other carbon phase. The sharp Raman peaks at 758 cm^{-1} is attribute to C-C stretching while 1220 cm^{-1} is likely to be caused by the effect of boron on the diamond lattice and its appearance in the spectrum is independent of the presence of the sp^2 carbon phase in the films [103]. The Raman peak at 970 cm^{-1} shows the second order of silicon while 1095 cm^{-1} for C-H or C-O stretch bonding. The Raman peak at 1120 cm^{-1} usually appears for nanocrystals of 1–2 nm in diameter or carbon clusters of sp^3 bonded material as well as 1312 cm^{-1} exhibit A_{1g} mode of hexagonal nanodiamond phase [104-107]. The Raman peak from 1360-1560 cm^{-1} shows the presence of amorphous carbon [108].

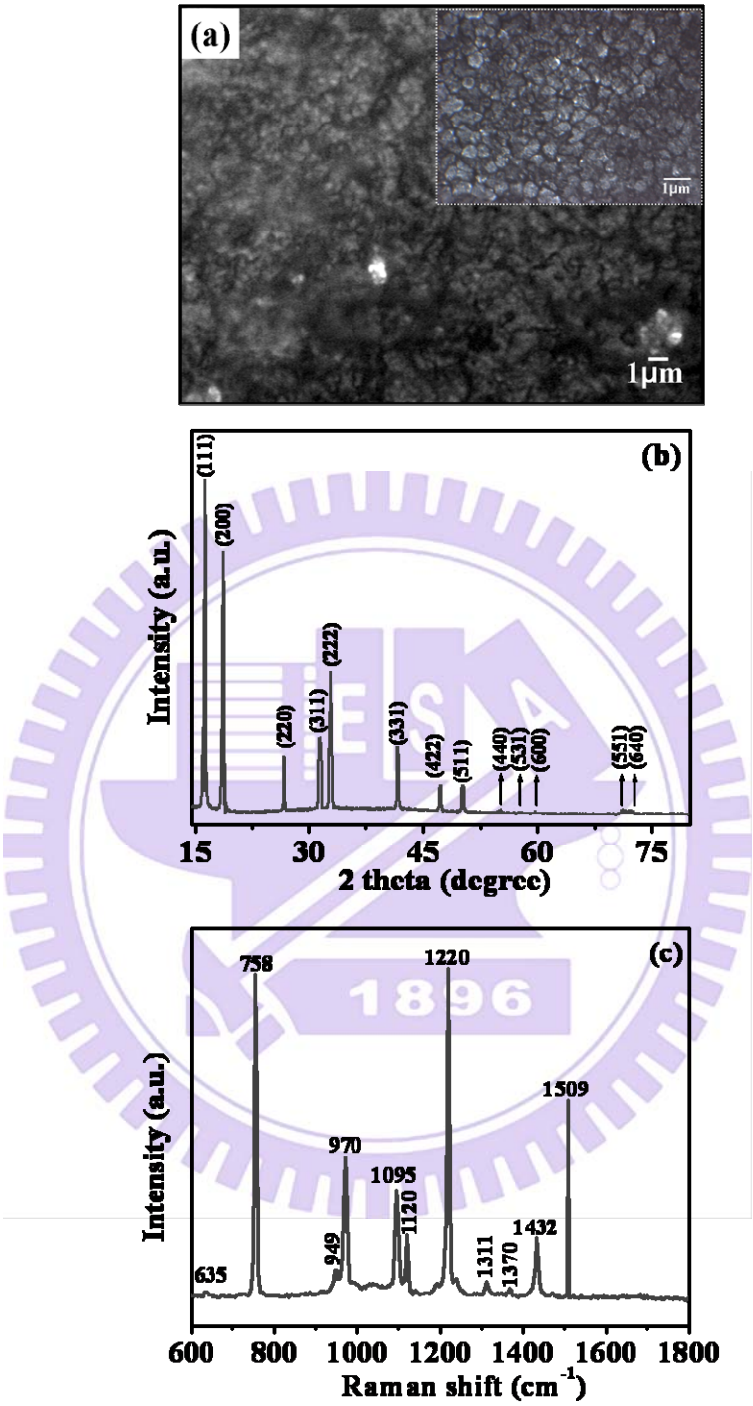

Figure 4.5: (a) Optical image, inset: high-magnification image of the adamantane, (b) XRD pattern of adamantane, and (c) Raman spectrum of the adamantane coating layer on Si (100) substrate.

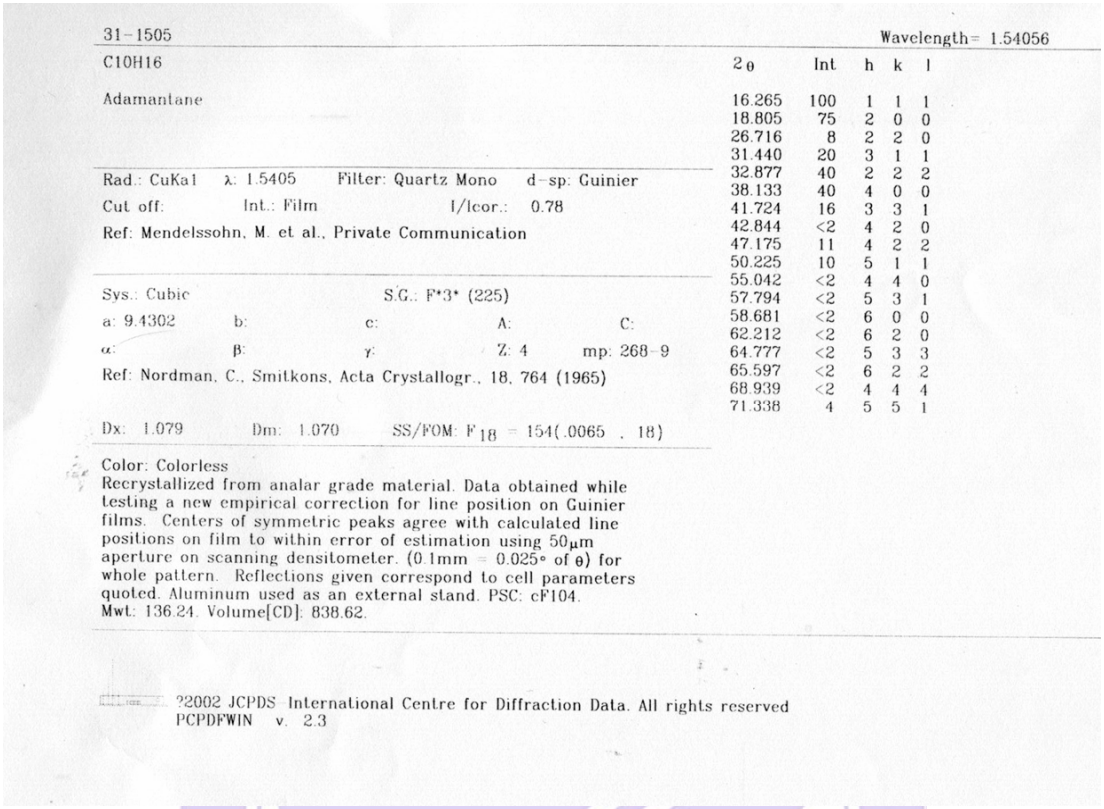

31-1505 Wavelength= 1.54056

C10H16

Adamantane

Rad.: CuKa1 λ: 1.5405 Filter: Quartz Mono d-sp: Guinier

Cut off: Int.: Film I/Icor.: 0.78

Ref: Mendelssohn, M. et al., Private Communication

Sys.: Cubic S.G.: F*3* (225)

a: 9.4302 b: c: A: C:

α: β: γ: Z: 4 mp: 268-9

Ref: Nordman, C., Smitkons, Acta Crystallogr., 18, 764 (1965)

Dx: 1.079 Dm: 1.070 SS/FOM: F_{18} = 154(.0065 , 18)

Color: Colorless

Recrystallized from analar grade material. Data obtained while testing a new empirical correction for line position on Guinier films. Centers of symmetric peaks agree with calculated line positions on film to within error of estimation using 50μm aperture on scanning densitometer. (0.1mm = 0.025° of θ) for whole pattern. Reflections given correspond to cell parameters quoted. Aluminum used as an external stand. PSC: cF104. Mwt: 136.24. Volume[CD]: 838.62.

2θ	Int	h	k	l
16.265	100	1	1	1
18.805	75	2	0	0
26.716	8	2	2	0
31.440	20	3	1	1
32.877	40	2	2	2
38.133	40	4	0	0
41.724	16	3	3	1
42.844	<2	4	2	0
47.175	11	4	2	2
50.225	10	5	1	1
55.042	<2	4	4	0
57.794	<2	5	3	1
58.681	<2	6	0	0
62.212	<2	6	2	0
64.777	<2	5	3	3
65.597	<2	6	2	2
68.939	<2	4	4	4
71.338	4	5	5	1

Figure 4.6: JCPDS file showing the intensity of adamantane peak.

The atomic force microscope (AFM, D3100) was used to evaluate the surface morphology of adamantane-coated Si substrate, as shown in Figure 4.7. Here, we used tapping-mode AFM on a length scale of 2.5 x 2.5μm^2 to determine the surface roughness of the adamantane films. The surface roughness of AC/Si substrates was very high~ 2.92 nm. Therefore, it was not easy to get the surface morphology of adamantane by AFM. However, from the AFM image we can say that the agglomerate [Figure 4.5 (a)] adamantane consisted of several ultra- or nano- size adamantane particles, as shown in Figure 4.6. These ultra- or nano- size adamantane particles bonded together with weak van der Wall's forces.

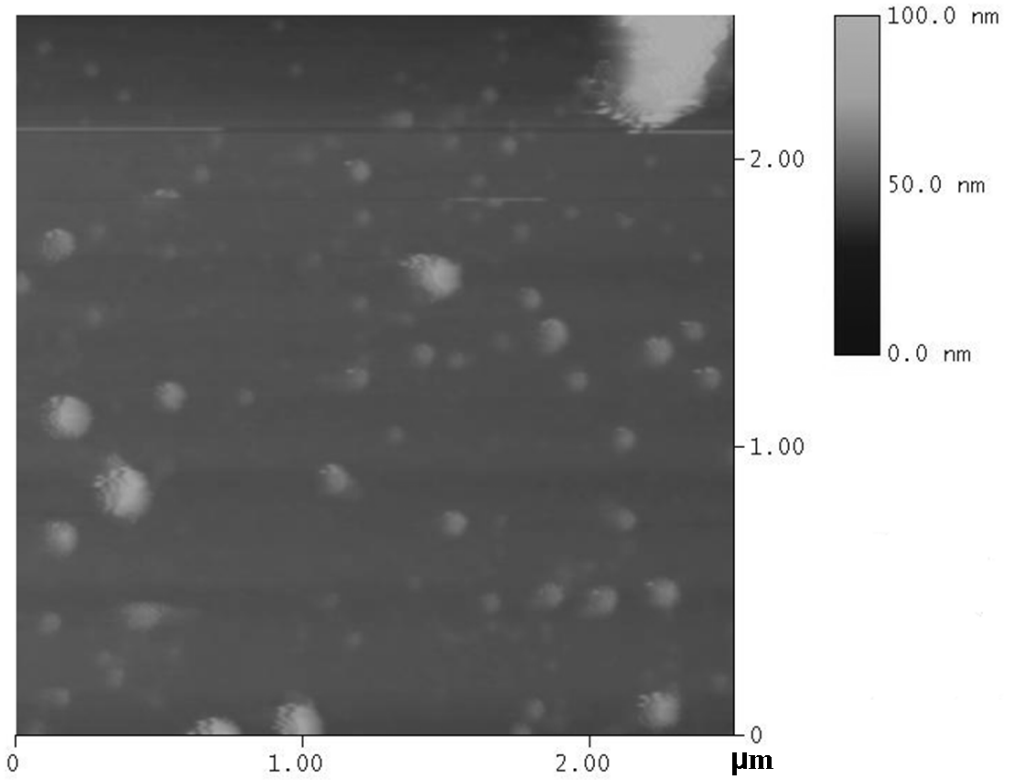

Figure 4.7: Tapping-mode AFM image of adamantane on Si.

The melting point of adamantane is ~ 270°C. The adamantane characteristic is similar to camphor, therefore we noticed that the when the thickness of adamantane was ~ >1 mm it is easy to burn in the CVD reactor at power ~ >400 W, as shown in Figure 4.8.

However, we did not observe b inside the chamber when the power and thickness of adamantane was below 400 W and ~1mm, respectively.

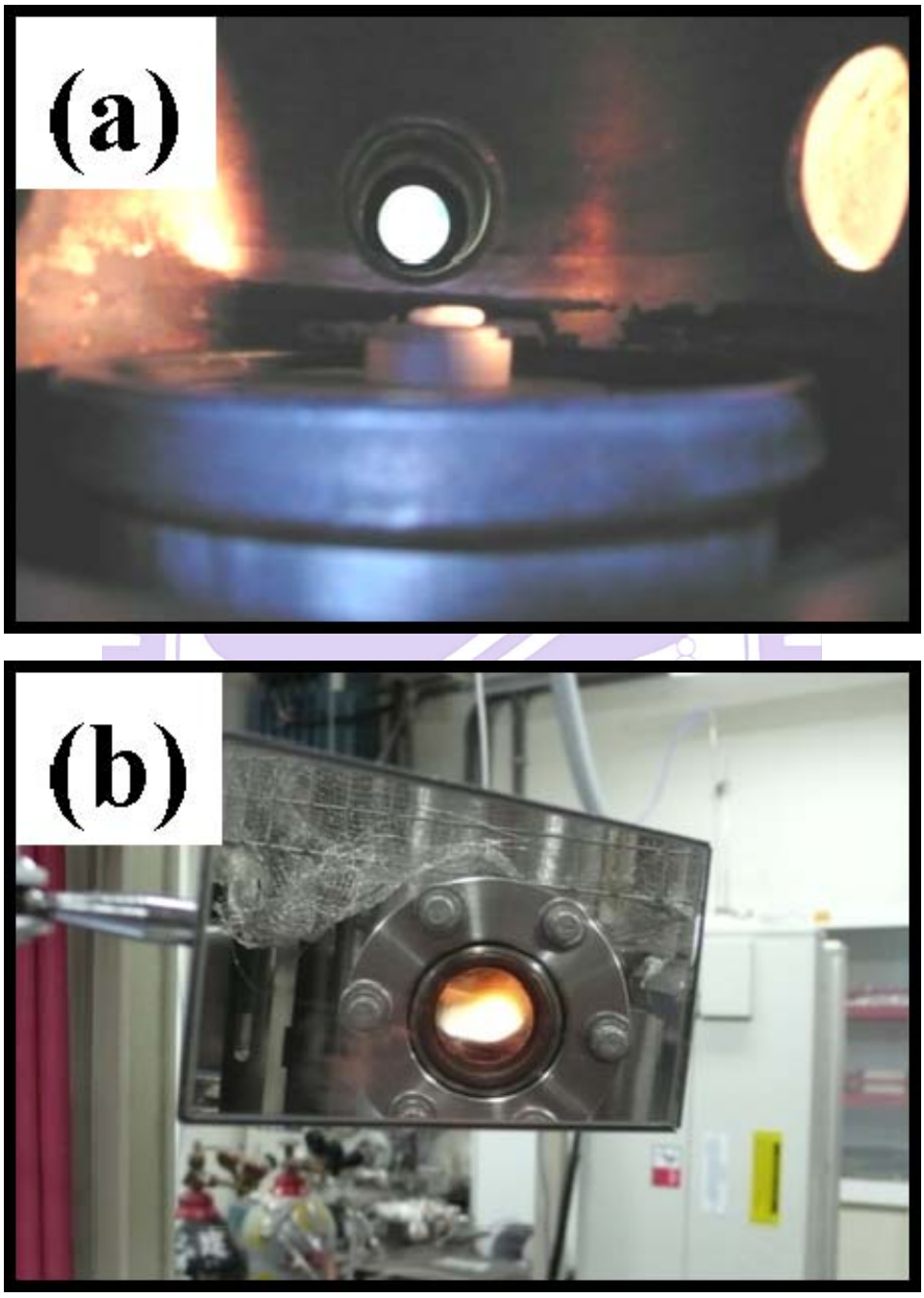

Figure 4.8: Photographs of adamantane at power ~ > 400W at 20 torr.

4.4 Structural characterization of diamond at 200, 250, and 300W

Further the AC/Si substrates were placed in the MPCVD reactor for diamond growth at various microwave power (200 to 350W at fixed pressure of 20 torr). After uploading the AC/Si substrates into the CVD chamber, then gas was flowed (0.6% CH_4 in H_2 plasma) into the chamber. When the pressure reached 10 torr (became constant) then the microwave power was increased to 380W (in general plasma formed between 370 to 400W). When the plasma formed, the power was reduced to 200-350W) while the pressure was maintained at 10 torr. After reducing the microwave power, the pressure was increased up to 20 torr for diamond growth. After diamond growth, the specimen was cooled down at ambient pressure in the presence of hydrogen gas (10 torr). The structure, surface morphology, and size of the synthesized diamond on the Si substrate were examined in a field-emission scanning electron microscope (SEM, JEOL JSM-6700F). Figure 4.9 shows the SEM image of diamond synthesized at 200W. From the SEM image, it is clear that the unusual large crystal sizes ~ 4μm along with a few small (~100nm) particles are formed. The density of small particles is < 10^2 cm^{-2}. The diamond growth on AC/Si substrate at 250W is shown in Figure 4.10 (a), from which the diamond density is ~10^3 cm^{-2}, relatively higher than that at 200W. Figure 4.10 (b) shows the size of diamond is ~ 650nm. It is clearly indicated that not only the diamond density but also their sizes are increased with microwave power. Though the exact substrate temperatures could not be measured at 200 and 250W, the temperature could be below 450°C because the measured temperature at 350W was~ 530°C (qualitatively).

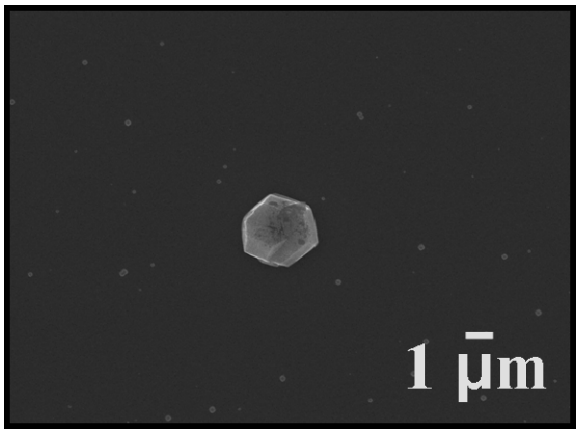

Figure 4.9: SEM image of diamond on AC/Si at 200W after 270 min growth.

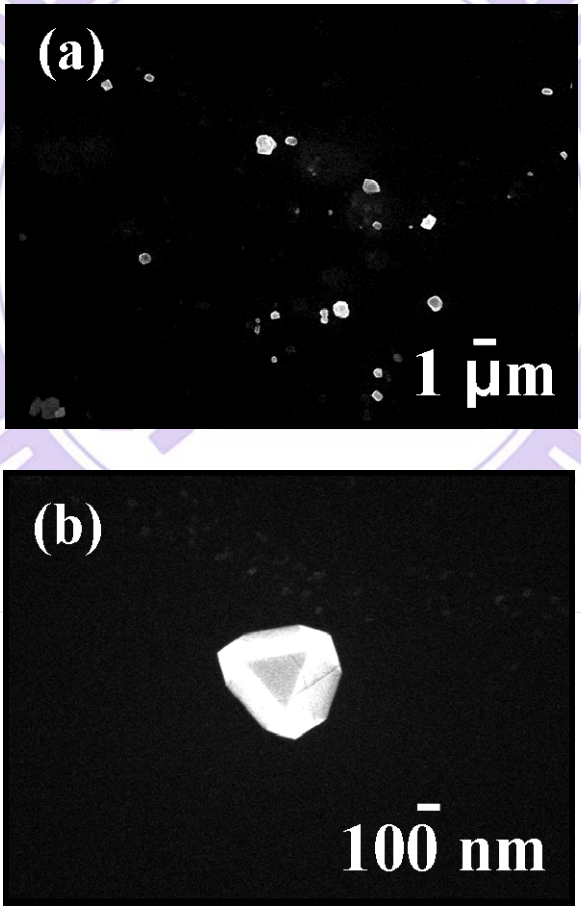

Figure 4.10: (a) low-magnification and (b) high-magnification SEM image of diamond on AC/Si at 250 W after 270 min diamond growth.

Further both Si substrates coated with adamantane and without adamantane were placed side by side in the MPCVD reactor for diamond deposition at 300W for 270 min. Figures 4.11 (a) and (b) show typical plan-view and cross-sectional SEM images of synthesized diamonds on the AC/Si substrate. It is shown that a contnuous diamond film can form on the substrate. The average size and the thickness of synthesized diamond are ~ 2 and ~ 1.8 μm respectively, as shown in Figures 4.11(a) and (b).

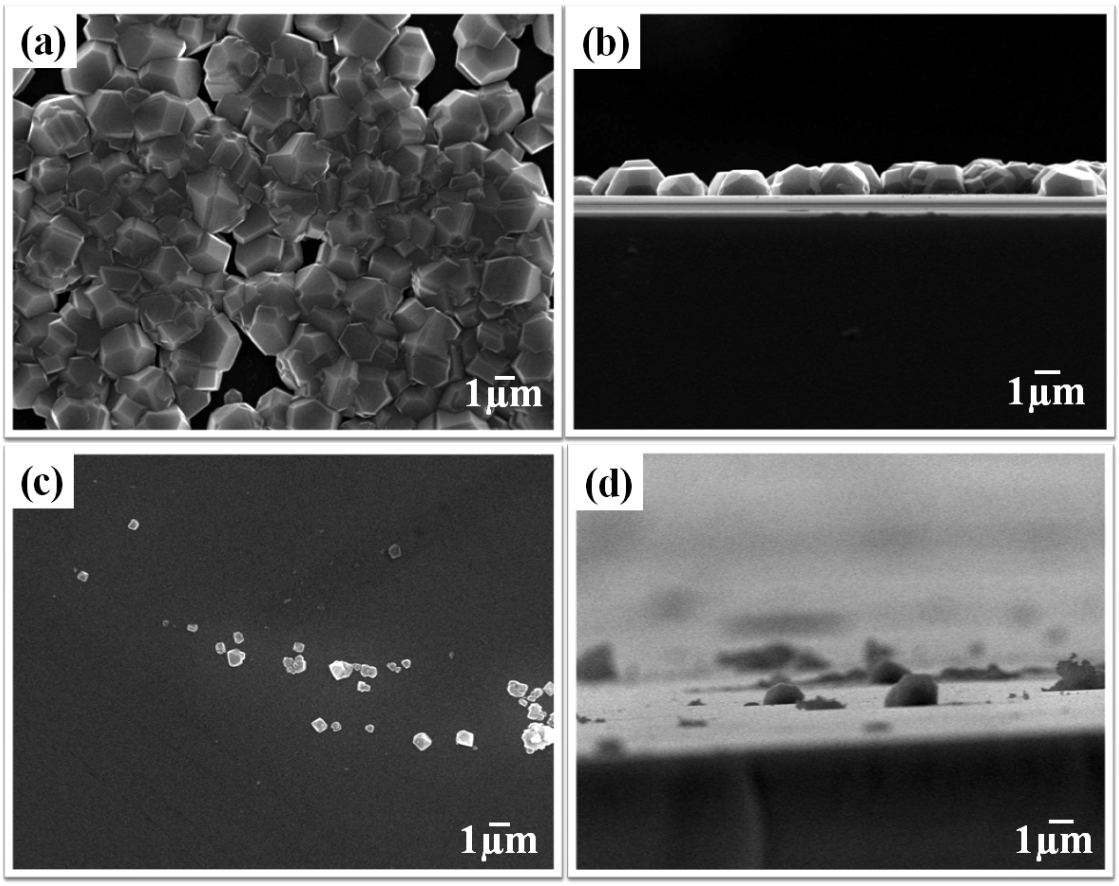

Figure 4.11: SEM images of diamond: (a) plan-view of AC, (b) cross-section view of AC, (c) plan-view of WAC and (d) cross-section view of WAC.

To know the effect of adamantane on diamond nucleation, we have grown the diamond on the WAC/Si substrate under the same experimental condition as AC. The

morphology of synthesized diamonds of WAC is shown in Figures 4.11 (c) and (d). No continous diamond film can be seen on WAC/Si. Figures 4.11 (c) and (d) show a local region where the diamond density is the highest. Most of the areas on WAC are rarely observed diamond particles. The average size of synthesized diamond is ~ 1 μm. In comparison, the density of diamond is ~10^6 and ~10^2 cm^{-2} for AC and WAC respectively, clearly indicating that the density of AC diamond is higher than that of WAC diamond, by four orders. Therefore, it is suggested that the adamantane strongly assists in the nucleation and growth of diamond at low temperature and pressure.

Furthermore, the synthesized diamond films on the AC/Si substrate at 300W were evaluated by Raman spectroscopy, X-ray diffraction, and X-ray photoelectron spectroscopy (XPS, Thermo VG 350, MgKα X-ray source). After diamond growth on AC/Si, all adamantane peaks disappeared and only an extremely sharp Raman peak appeared at the position of 1332 cm^{-1}, as shown in Figure 4.12. The sharp peak at 1332 cm^{-1} in the Raman spectrum is attributable to the first–order phonon mode for diamond, and the width of the peak is 5.6 cm^{-1}. The sharp Raman peak at 1332 cm^{-1} and the absence of graphitic (D and G bands) peaks suggest that the good-quality diamond is obtained. In addition, the XRD pattern is shown in Figure 4.13. In the XRD pattern, the 2θ peak at 28.3° is the Si{111} peak while the sharp peak at 43.9° is diamond{111}. Since Si{100} substrate was used for diamond growth, the appearance of the Si{111} peak may imply that the during the diamond growth the Si might be etched by the hydrogen plasma. The two sharp peaks at 37.8° and 64.38° are identified to be cubic silicon carbide (SiC) {111} and {220}, respectively [109], consistent with the standard JCPDS values (JCPDS file number: 49-1623). The sharp XRD peak of diamond shows that the highly crystalline diamond film has been deposited as supported by our SEM observations in Figure 4.11.

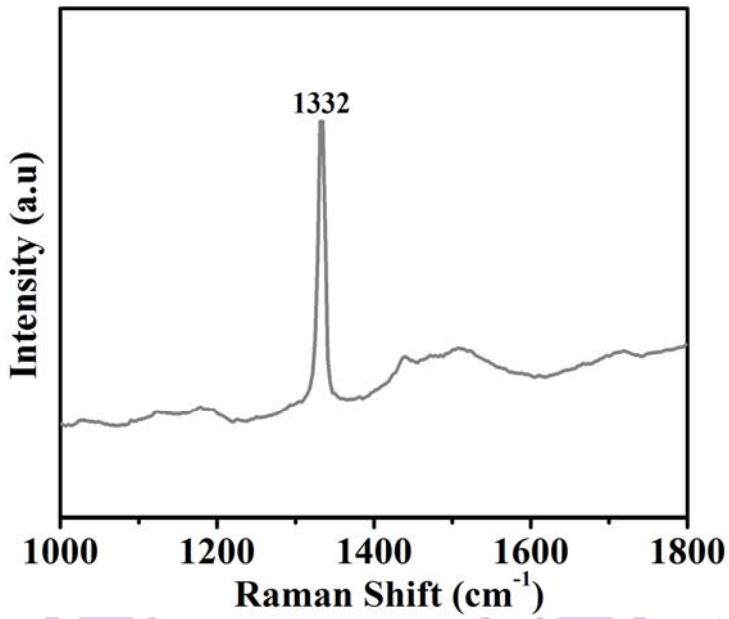

Figure 4.12: Raman spectrum of diamond film on AC/Si at 300W.

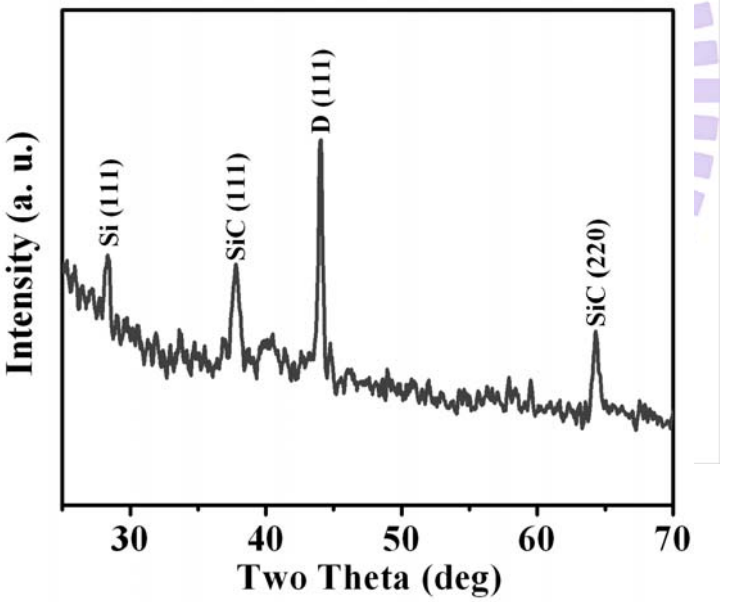

Figure 4.13: XRD pattern of diamond (D) film on AC/Si at 300W. The symbol D in this pattern represents diamond.

Moreover, structural characterization of diamond was done by TEM using a cross-sectional TEM specimen prepared by the focused ion beam (FEI Nova 200 Dual beam FIB) method. For the protection of the TEM specimen against damage from the high-

energy ion beam (30 keV Ga^{+}) in FIB, the specimen was coated with platinum. A cross-sectional bright-field TEM image of diamond/Si is shown in Figure 4.14 (a). The thickness of diamond is ~ 2μm, as shown in Figure 4.14 (a). The interface between Si and diamond is shown in Figure 4.14 (b), and the enlarged-view with the EDX spectrum is shown in Figure 4.14 (c). It is seen that there is an amorphous interlayer between diamond and Si. EDX taken from the interface shows the presence of oxygen, carbon, and Si.

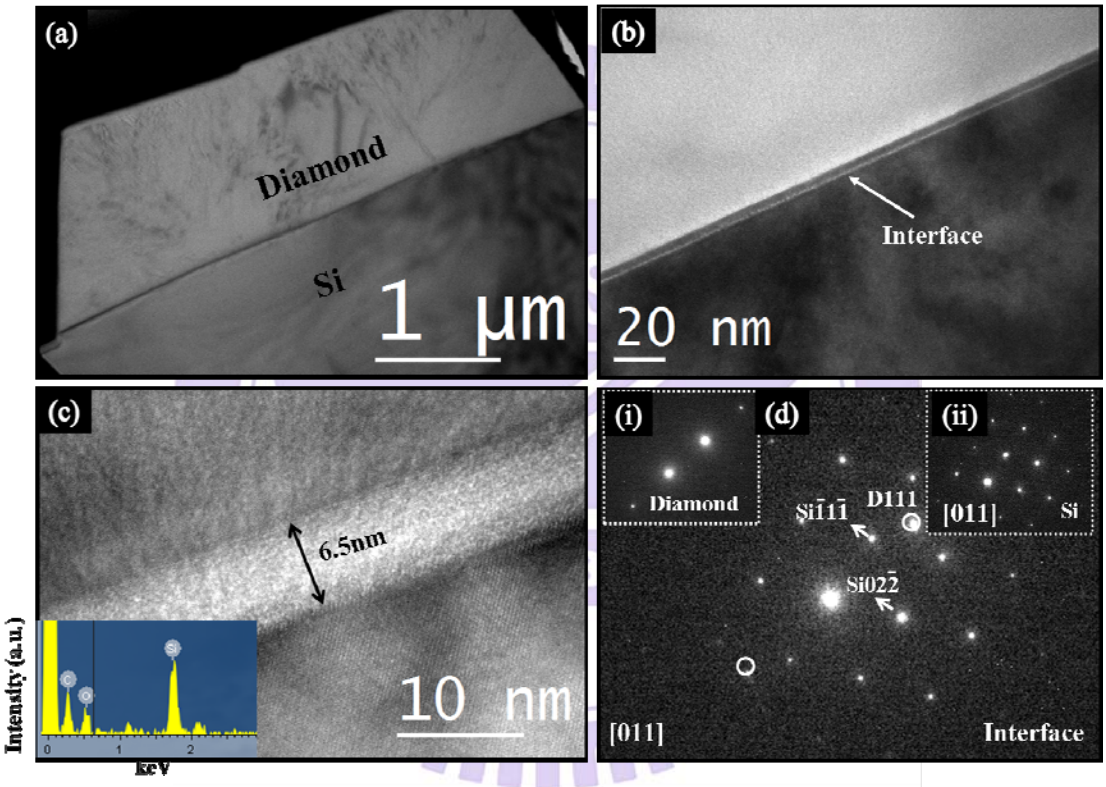

Figure 4.14: (a) Cross-sectional BF-TEM image of diamond/Si, (b) BF-TEM image of interface, (c) enlarged BF image of interface; insert EDX spectrum from interface, and (d) SAED pattern of interfacial region indicating the presence of Si and diamond spots {111} plane along <011> direction; Inset diffraction spots (i) and (ii) showing the of diamond and Si along <011> zone axis.

The Si signal comes from substrate and C from diamond, while the oxygen signal suggests that the presence of native oxide layer on Si substrate. The selected area electron diffraction pattern (SAED) of the interfacial region is shown in Figure 4.14 (d). From the SAED pattern only noticed diffraction spots of Si and diamond as shown in Figure 4.14 (d). Inset images (i) and (ii) in Figure 4.14 (d) shows the diffraction spots of diamond and Si along <011> zone axis. As no SiC diffraction spots can be observed, it might be that the SiC is not a continuous film.

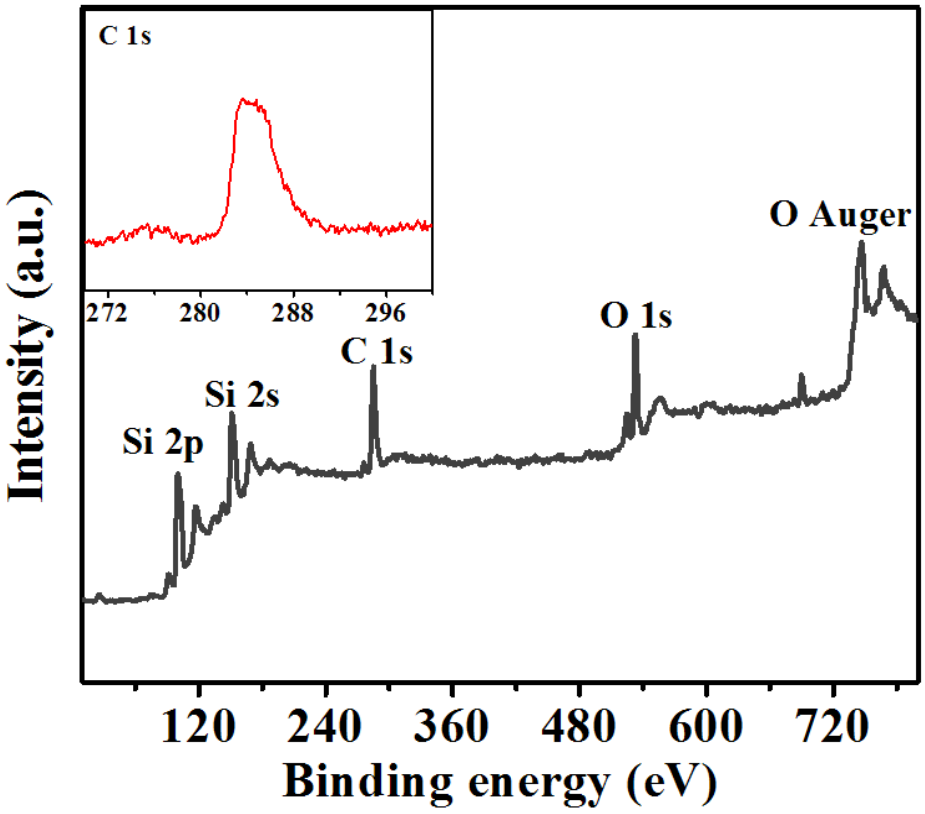

Figure 4.15: The XPS survey spectrum of diamond on AC/Si, insert: high-resolution spectrum of the C 1s region.

In addition, to get a better insight into the above mechanisms we have used XPS to characterize the surface chemical composition of the AC/Si surface after diamond growth. The XPS survey spectrum of the synthesized diamond on the Si substrate is shown in Figure 4.15, which allows measure of the carbon 1s core-level signal considered as an indicator for the quantity of carbon attached to the surface treatment. Apart from the

expected peaks from elements on the diamond surface (C), surface contamination with oxygen containing molecules can be detected. An XPS survey shows strong signals of carbon C 1s at 285.2 eV, attributed to the C-C bond in diamond films. In fact, insert XPS high-resolution spectrum of carbon in Figure 4.15 showed that the C (1s) signal consists of three peaks: the first two peaks at 285.2 and 283.7eV is the characteristics of C-C (sp^3) bonding and the other peak at 283.2eV is the characteristics of Si-C bonding [110]. Many authors have shown that silicon carbide (SiC) forms readily after diamond growth starts [111, 112]. In our case, most fractions of adamantane particles might have been pumped out. However, some embedded hydrocarbon species could react with Si surface and form SiC. Probably, the etched Si (rough) surface would provide more active sites to react with carbon species to form SiC. In general, it is well known that SiC forms at high temperature. However, according to our XPS and XRD results we can say that SiC may form at low temperature. At high temperature, hydrocarbon species come from the plasma and react with Si to form SiC interlayer between diamond and Si. In our case, we have used adamantane therefore either adamantane or other carbon species assist to the formation of SiC. The distribution of carbon species is not homogeneous. The oxygen signal at 532.7 eV is associated with oxide formation with Si surface during the thermal reaction, which can attribute to the O-Si bond in SiO_2 [94, 95]. It seems that the adamantane compact density is low, allowing for high diffusion of oxygen. Therefore, during adamantane coating by hotplate method the oxygen atoms may have diffused through adamantane to Si surface to form native oxide layer. It is also possible that after diamond growth, when we have taken out specimens from the CVD chamber the oxygen would have reacted with Si surface which was uncovered with diamond.

4.5 Hydrogen plasma on AC/Si substrates

Hydrogen abstraction from AC/Si substrates is one of the highly possible mechanisms for the diamond formation. Therefore, it is of interest to study the surface conditions of the AC/Si substrates after the treatment of pure hydrogen plasma without CH_4 for different times (1, 2, 5, 10 and 15 min) in a similar plasma experimental condition. After treatment for various times, the SEM images are shown in Figure 4.16**.** In the first minute deposition, most of adamantane particles have been evaporated and a

few particles are still left on the Si surface, as shown in Figures 4.16 (a) and (b). After 2 min [Figure 4.16 (c)] treatment, not many particles can be seen on the surface. However, a few micro-sized particles are occasionally observed on the Si surface, as shown in Figure 4.16 (d). After 5 and 10 min treatments, SEM images are shown in Figure 4.16 (e)-(j). It is well known that the pure hydrogen plasma also etches (remove) the carbon phase as well as surface. Therefore, some particles in a size of the order of 100 nm are seen, suggesting that most of adamantine particles are either etched or evaporated from the Si surface in the CVD chamber and insignificant amount of hydrocarbon is left on the surface. The size of particles on the Si surface is varied due to hydrogen plasma treatment. Because of insignificant amount of hydrocarbon left on the Si surface, therefore we did not get unambiguous data from micro-Raman spectroscopy. The Raman spectra of these samples are shown in Figure 4.17. In a Raman spectrum of adamantane as shown in Figure 4.5(c), strong peaks are observed at 758 and 1220 cm^{-1} which correspond to the C-C stretch (C-C phase) and doubly-degenerate CH_2 twist mode (C-H phase), respectively. However, after short time (1 min) treatment, such peaks were not observed. Our perception is that in CVD major fraction of adamantane particles have been removed from the Si surface (Figure 4.16) and some adamantane molecules may be left on the Si surface

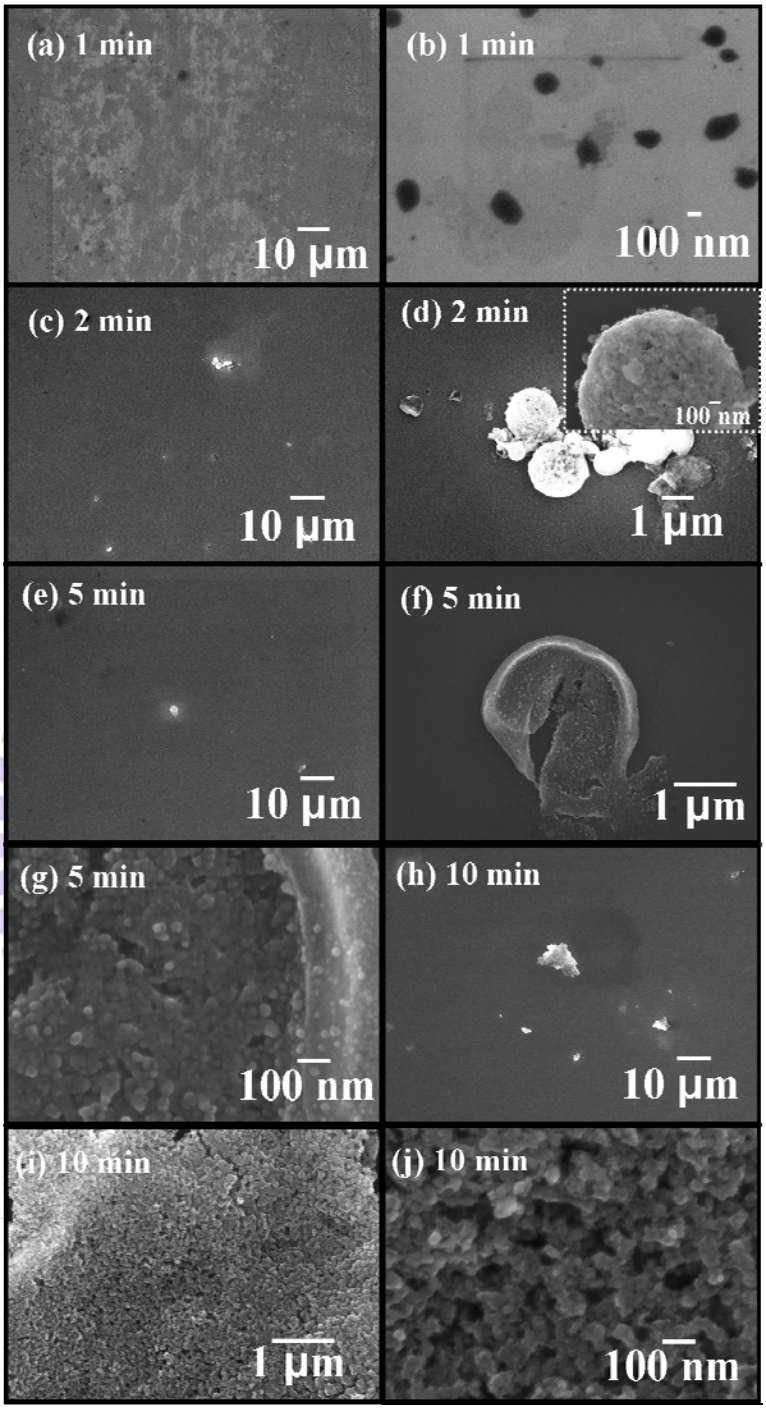

Figure 4.16: SEM images of AC/Si substrates treated with 1, 2, 5, and 10 min by pure hydrogen plasma at 300W.

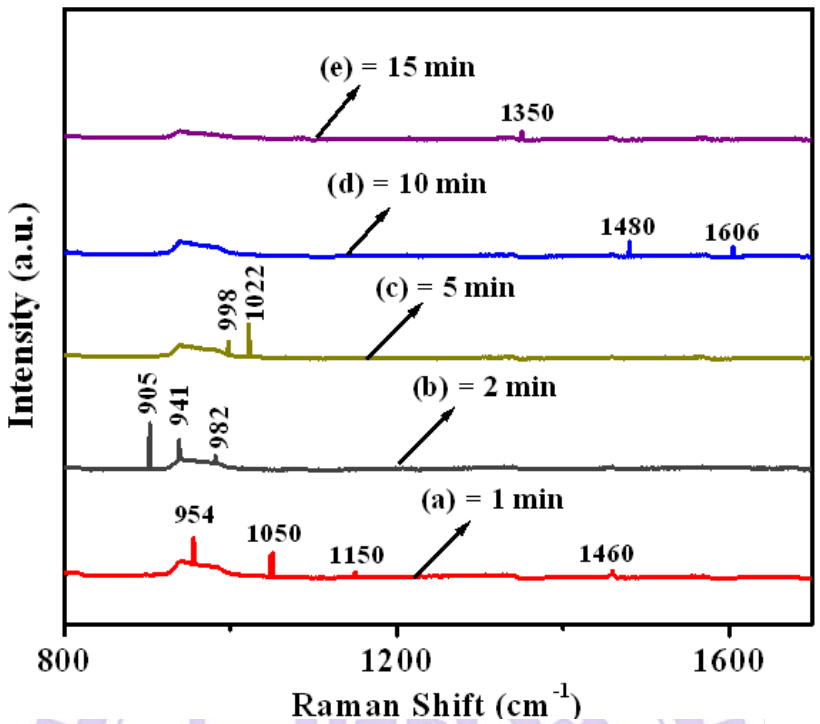

Figure 4.17: Raman spectra of AC/Si sapmles treated with pure hydrogen plasma at different times (1, 2, 5, 10 and 15 min).

would have decomposed either in the form of small molecules [(C_nH_x), where n = 3, 5, 6, 7, 8 and 9] or nanodiamond phase (1150, 1460, and 1480 cm^{-1}) along with other hydrocarbon species. Therefore, there are multi Raman peaks (954, 1050, 1150, 1460, 905, 941, 982, 998, 1022, 1480, 1606, and 1350 cm^{-1}) for different treating times (1, 2, 5, 10, and 15 min). We can observe nanodiamond signals at 1150 and 1460 cm^{-1} after 1 min treatment with pure hydrogen plasma. A number of authors have found either the 1150 cm^{-1} or 1460 cm^{-1} peak and they have shown that whenever the 1150 cm^{-1} peak is observed, the nanodiamond phase can be observed in both XRD pattern and TEM data [113-116]. The peak at 1480 cm^{-1} is also from nanodiamond phase. Marcus et al. and Zhang et al. have shown that the peak at 1480 cm^{-1} can be attributed to a tetrahedrally bonded carbon phase [117, 118]. While other peaks at 1606 cm^{-1} and 1350 cm^{-1} are observed in 10 and 15 min, respectively, which are the D and G modes attributed to disordered graphitic phases. It seems that after 15 min treatment, most of hydrocarbon species have been etched out as the Raman signal intensity is low. From Raman studies it

is clear that adamantane may be decompose into hydrocarbon species, which act as individual diamond nuclei at low temperature. Study of the mechanism behind the origin of diamond nuclei from adamantane molecule is still underway.

4.6 Structural characterization of diamond at 350W

4.6.1 Diamond nucleation

We did not observe the formation of continuous diamond film on AC/Si substrates at 300W. Therefore, we have tried to grow continuous diamond films by increasing the power to 350W with the same experimental condition for gas flow rate and pressure, (0.6% CH_4 in H_2 and 20 torr). In this section we have studied the diamond nucleation and growth of continuous diamond films on the AC/Si. As shown in Figure 4.18 is the surface morphology of the synthesized particles on AC/Si substrates for various deposition times (15 to 45 min). Figure 4.18 (a) shows that tiny particles are formed in a short time (15 min) deposition. The inset high-magnification SEM image in Figure 4.18 (a) shows that the tiny particles are surrounded by several hundred nanometer-sized particles. The micro-Raman spectrum from these particles in Figure 4.18 (d) shows that the major peaks at 1120 and 1603 cm^{-1} are observed, implying that adamantane has been decomposed during 15 min deposition. The Raman peak at 1603 cm^{-1} is the G band of sp^2 carbon bonding, while the Raman peak at 1120 cm^{-1} is not well understood about the bonding characteristics but it is often observed in Raman spectra of nanocrystalline diamond films [105-107]. Previous studies have shown that the Raman peak at 1120 cm^{-1} usually appears for nanocrystals 1–2 nm in diameter or carbon clusters of sp^3 bonded material. It is widely believed that the peak at 1120 cm^{-1} is originated from the presence of confined phonon modes in diamond [119, 120]. After having been decomposed, the surrounded nanosized particles were formed clusters of micrometer-sized carbon particles (after 30 min deposition), as shown in Figure 4.18 (b). The high-magnification SEM image [inset in Figure 4.18 (b)] shows that the particles have bright contrast along with dark contrast. The Raman spectrum from these particles is shown in Figure 4.18 (e). Raman peaks at 1120 cm^{-1}, along with 1361 and 1601 cm^{-1} (D and G bands) are also observed, which are due to nanocrystal diamond, disorder carbon of sp^2 bonding, and graphitic particles.

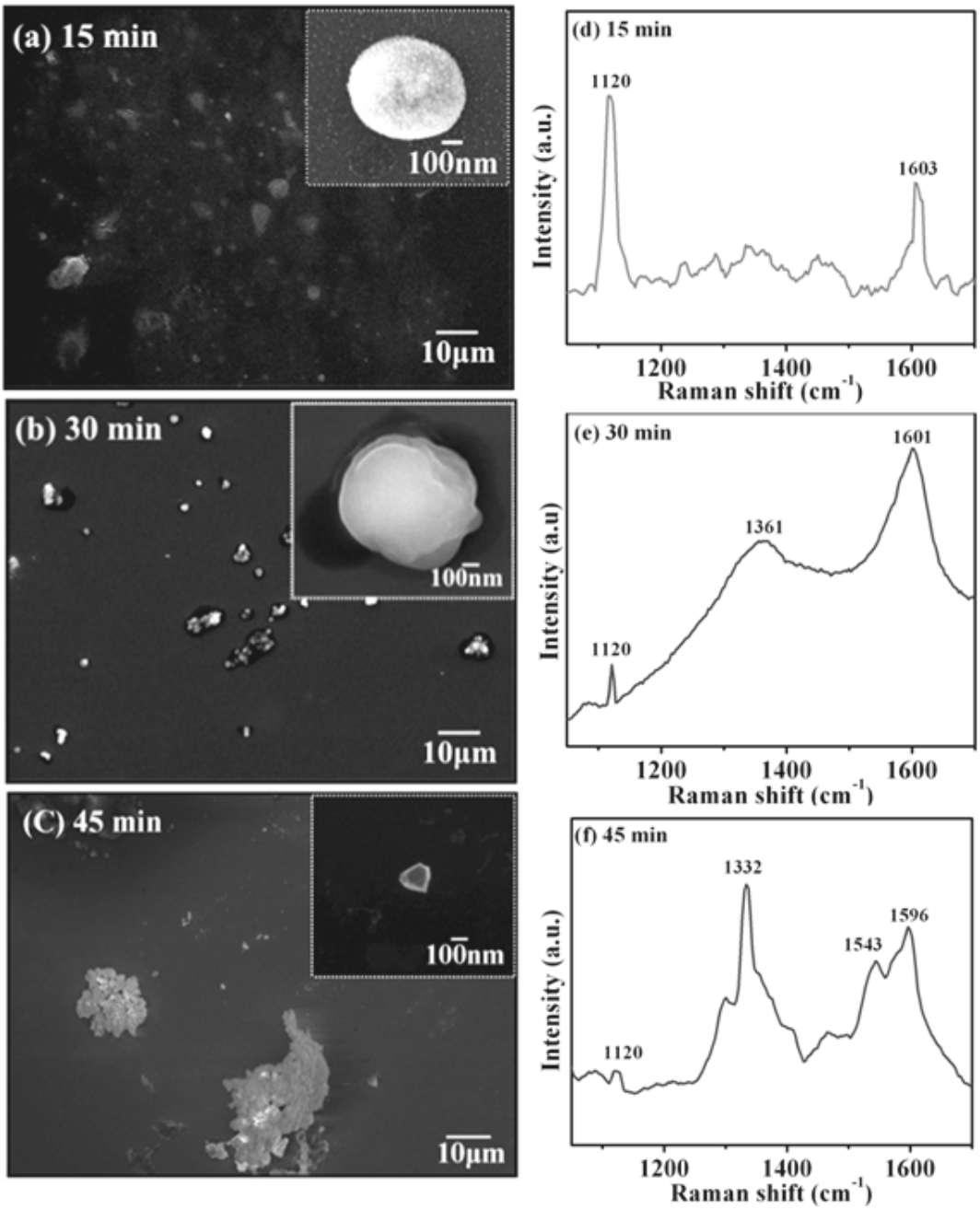

Figure 4.18: Plan-view SEM images and micro-Raman spectra after growth at 350W for deposition times of (a) and (c) 15 min, (b) and (d) 30 min, and (c) and (f) 45 min.

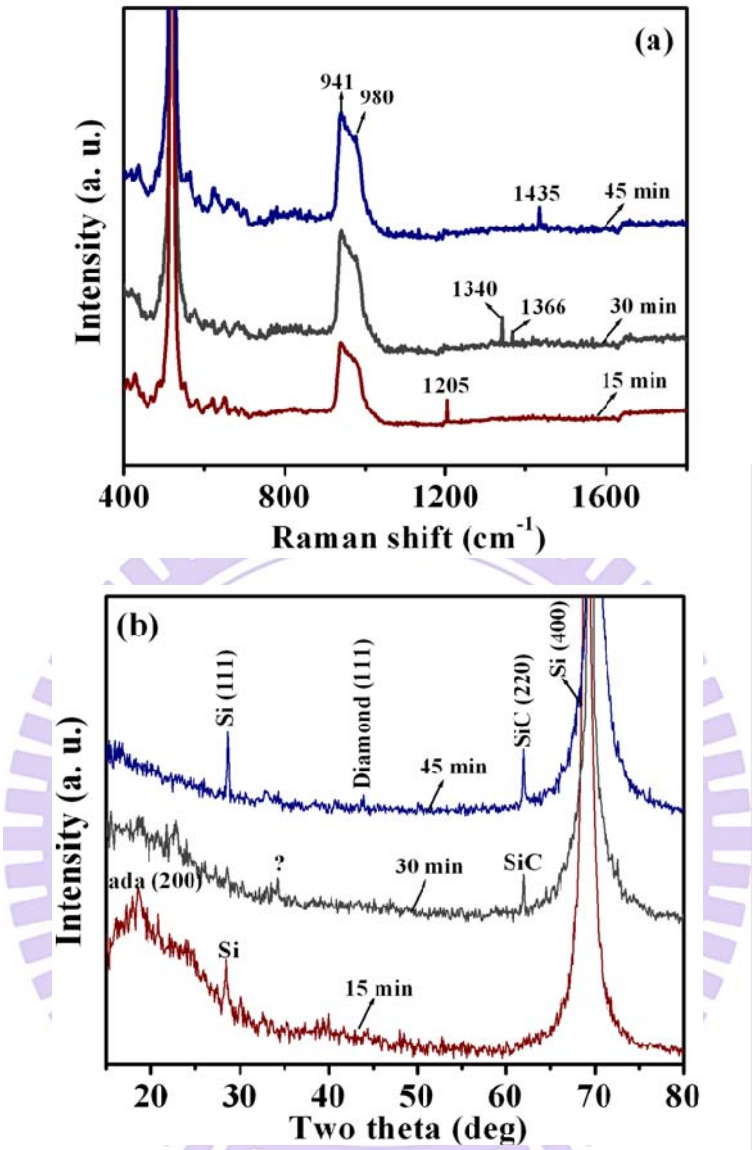

Figure 4.19: (a) Raman spectra from plane regions and (b) XRD patterns of adamantane-coated Si substrates after 15, 30, and 270 min deposition at 350W.

Furthermore, after 45 min, only clusters of carbon particles along with a few nano-sized particles are observed on the Si substrate. The high–magnification SEM image of nanoparticles in Figure 4.18 (c) shows the crystalline facets, suggesting that diamond particles are formed. The existence of Raman peaks at 1120 and 1332 cm^{-1} in the Raman spectrum from these particles in Figure 4.18 (f), supports that the diamond formation has occurred after 45 min deposition. In addition, the hydrogenated amorphous carbon (a-

C:H) peak is seen at 1543 cm^{-1}, and the graphitic phase at 1596 cm^{-1}. For the Si surface region uncovered with particles, the Raman spectra after 15, 30, and 45 min depositions in Figure 4.19 (a) show no adamantane peaks. Instead, there are two strong peaks at approximately 941 and 978 cm^{-1} in all cases. The Raman peaks at 941 and 978 cm^{-1} actually correspond to SiC [121, 122]. The weak Raman peak at 1205 cm^{-1} corresponds to a mixed bond arising between sp^2 and sp^3 bonded carbon. For the 30 min deposition the D band peaks at 1344 and 1366 cm^{-1} are observed, while the Raman peak at 1435 cm^{-1} corresponds to amorphous carbon peak for the 45 min deposition.

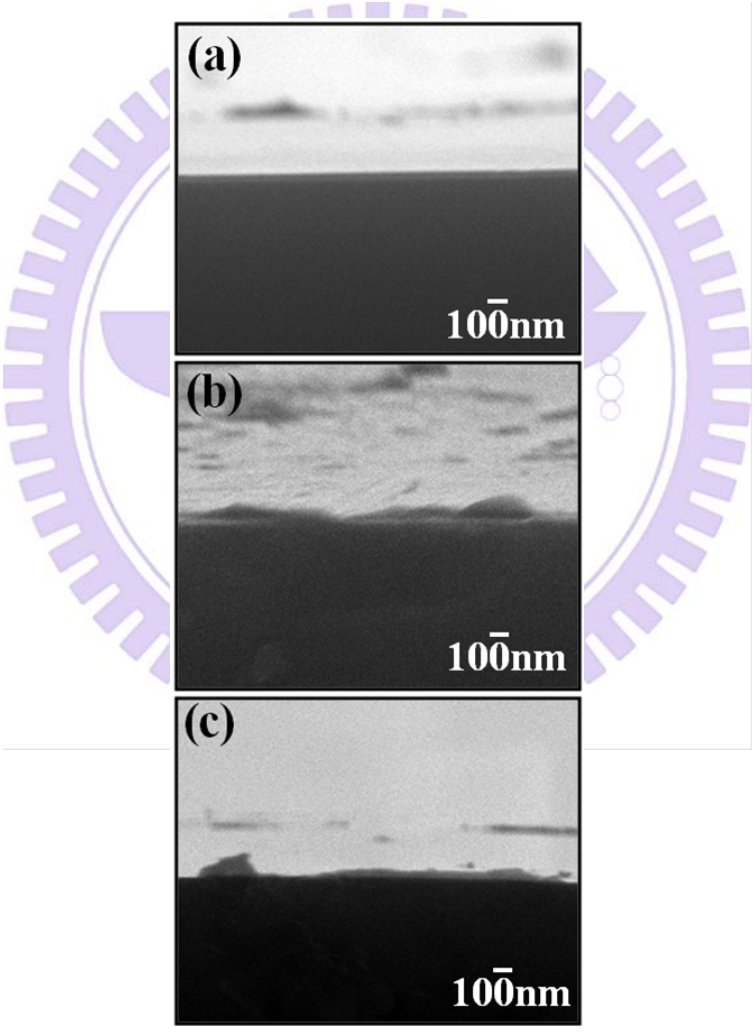

Figure 4.20: Cross-sectional SEM images of adamantane-coated Si substrates treated with various times: (a) 15 min, (b) 30 min, and (c) 45 min at 350W.

This shows that significant amount of non-diamond phase is also formed in the early stage of deposition. Further, the XRD pattern of these samples (after 15, 30 and 45 min depositions) is shown in Figure 4.19 (b). In short time (15 min) deposition minor fraction of adamantane particles were left on the Si surface as shown by the small adamantane {200} peak in Figure 4.19 (b). The average thickness of hydrocarbon particles on the Si surface is ~ 90nm, as shown in Figure 4.20 (a). However for the AC/Si substrate treated with pure hydrogen plasma at 300W for 15 min, no any adamantane signals can be found (Figure 4.17). It seems that the adamantane particles were either evaporated or etched by pure hydrogen plasma. In the presence of methane (0.6% in H_2) we still observed the adamantane existence on the Si surface after 15 min deposition [Figure 4.19 (b)]. Probably, methane would have reduced the evaporation or etching rate of adamantane. After long deposition time (30 min) we observed a sharp 3C-SiC {220} peak at 2θ=61.7 degree [123] along with a weak signal at 34.22 degree in XRD. The weak signal at 34.22 degree is still unknown. It seems that the weak signal would be from sp^2 phase. However, we did not notice the adamantane signal after 30 min deposition. For 45 min deposition, the peak at 43.9° is characteristic of crystalline diamond {111} along with 3C-SiC {220} at 61.7°, consistent with SEM and Raman data. It is also clear that the SiC forms first, followed by diamond formation. As shown in Figure 4.20, the average film thickness after 30 and 45 min depositions are ~ 110, and 130 nm, respectively, indicating that thickness increases with increasing the deposition times. In addition, XPS was used to identify of chemical composition on Si surface after 15, 30, and 45 min deposition, as shown in Figure 4.21. We used Ar ions for 20 sec to clean the contaminations on the Si surface. XPS signals in the survey spectrum [Figure 4.21 (a)] shows the presence of elements such as C, Si. Ar, and oxygen. In addition to carbon and Si, the unwanted peaks are appeared of oxygen. The high-resolution spectrum of carbon is shown in Figures 4.21(b), (c) and (d). The fitting components were assigned as follows: sp^3 carbon with C–C bonds (C–C sp^3 carbon, 283.7 eV), sp^2 carbon with C–C bonds (C–C sp^2 carbon, 284.4 eV), sp^2 carbon with H–C bonds (H–C sp^2 carbon, 284.8 eV), sp^3 carbon with H–C bonds(H–C sp^3 carbon, 285.2 eV), and 283.2eV corresponds to SiC [110, 124]. We have already discussed about the Si-C peak at 283.2eV [XPS result of diamond at 300W]. For

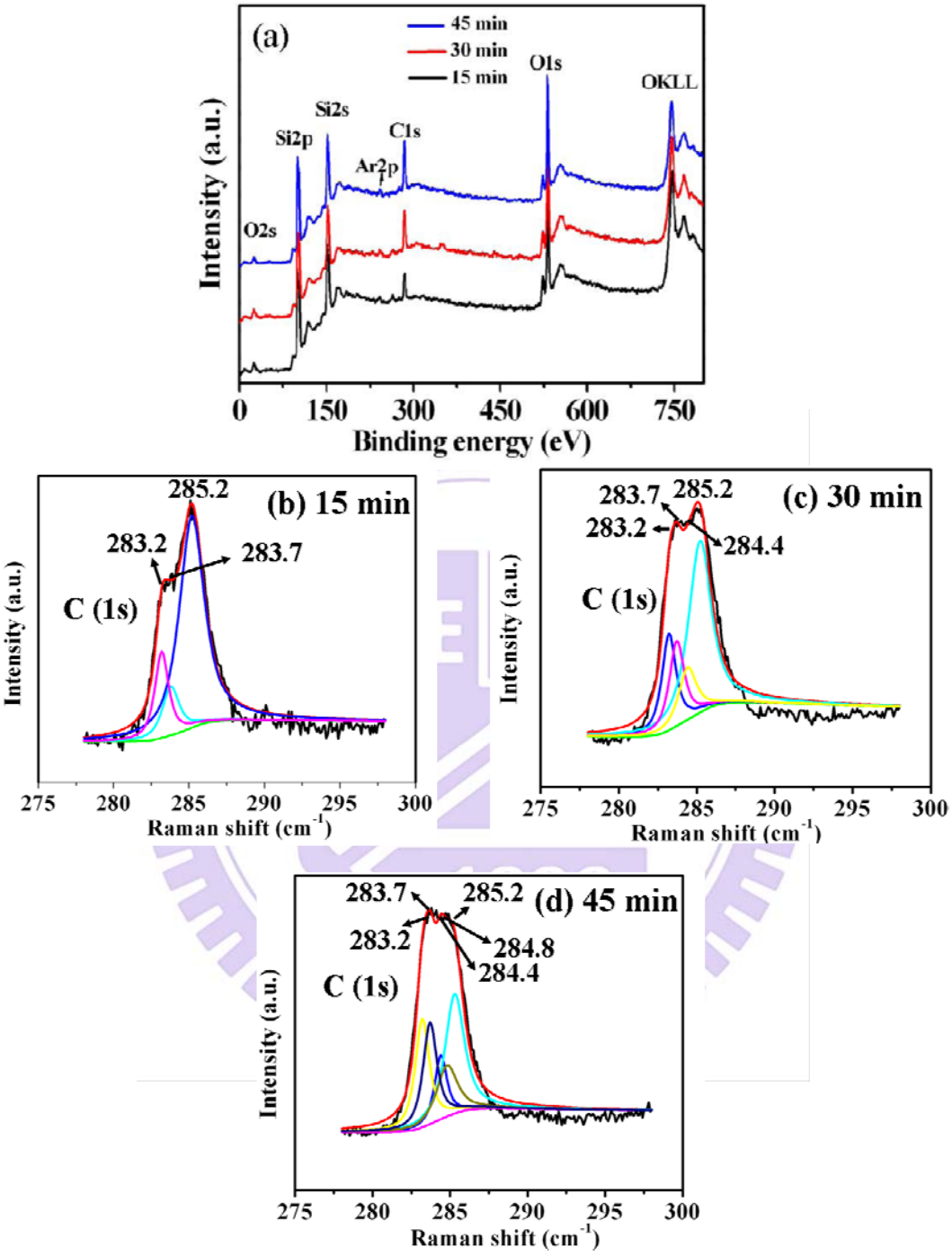

Figure 4.21: (a) XPS survey spectrum, (b), (c), and (d) high resolution spectrum of the C(1s) region after 15, 30 and 45 min deposition.

the 15 min deposition, the peak at 283.2 eV is seen with lower intensity, while this peak intensity increases for 30 and 45 min deposition. From this result it is clear that SiC has already formed after 15 min deposition. The strong signal of silicon at Si(2p) and Si(2s) at 99 and 151 eV, respectively, and oxygen signal at 532.7 eV attributed to the O–Si bond in SiO_2, show that there are regions on the Si surface not covered by the deposits. This is consistent of our SEM result.

The photographs of CVD plasma (during diamond growth) are shown in Figure 4.22. When we placed adamantane (thickness in ~0.9mm)-coated Si samples in the reactor, the adamantane molecules were evaporating from the Si surface and mixed with the gaseous plasma (plasma color changed within 1 min), as shown in Figure 4.22 (a). After 1 min, major fraction of adamantane molecules were removed and minor fraction of adamantane molecules might be re-deposited back to the Si surface. After 5 min, the plasma became stable, as shown in Figure 4.22 (b).

In general, adamantane can evaporate at room temperature. In summer season, the average ambient temperature of our lab was ~300K. The evaporation rate of adamantane can be determined from the measured total mass loss of adamantane divided by the total evaporation time. Table 4.1 shows the evaporation rate of adamantane at various temperatures [evaporation rate of adamantane depends upon seasons. In summer season we observed high evaporation rate while less in winter season]. In our experiments, we have found that the evaporation rate is accelerated by temperature.

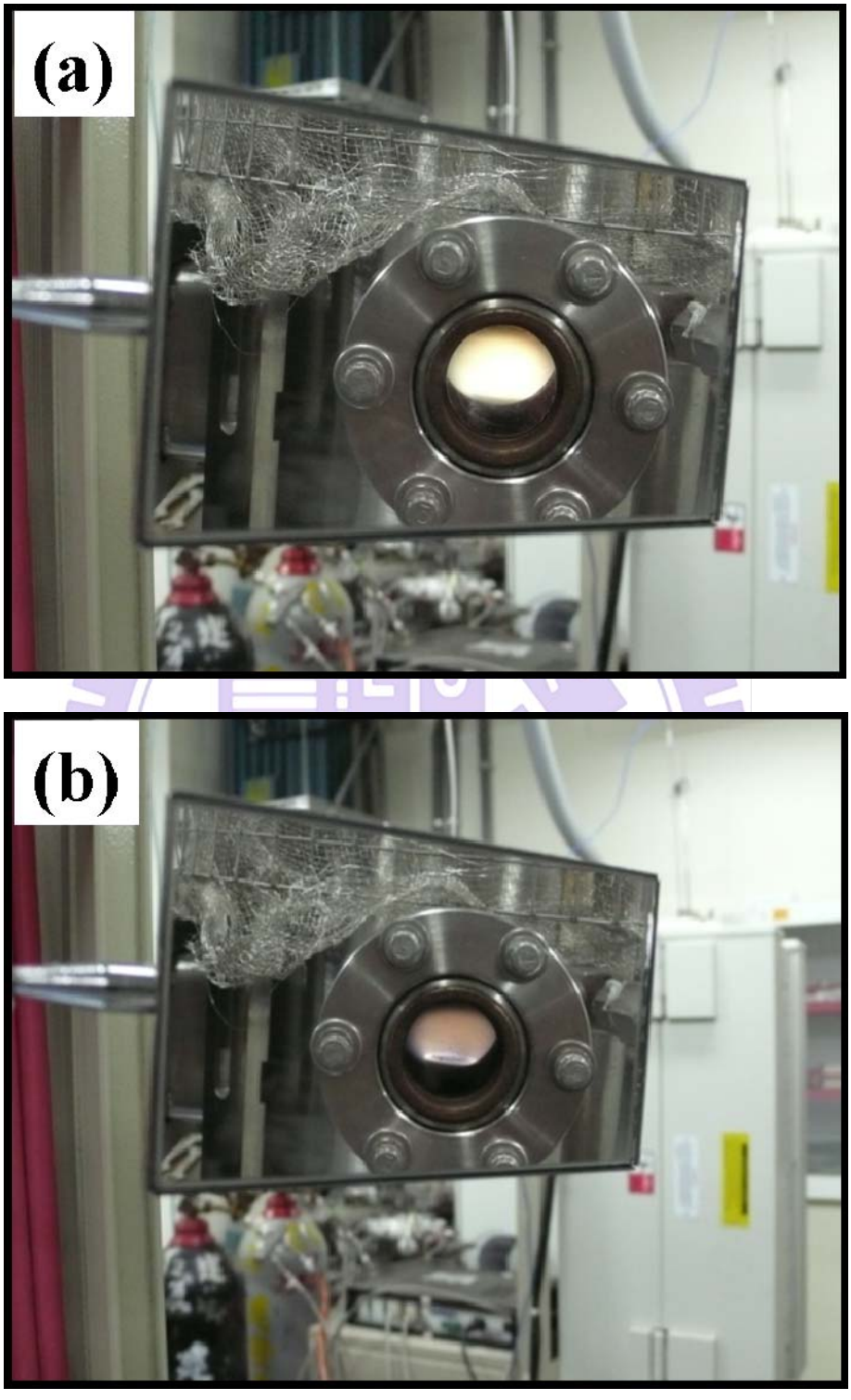

Figure 4.22: Photographs of CVD plasma (a) at120 and (b) at 300 sec.

Table 4.1: Experimentally measured evaporation rate of adamantane at various temperatures in summer season.

Temperature (°C)	Evaporation rate of adamantane (mg/sec)
200	0.55
250	0.63
300	0.70
350	0.82
400	0.91
450	1.1

4.6.2 Growth of continuous diamond film

The structure, surface morphology, and size of the synthesized diamond on the Si substrate with and without adamantane coating are shown in Figures 4.23, 4.24, and 4.25 for 270 min deposition. It is well known that the growth of diamond on WAC/Si is difficult. Figure 4.23 shows the SEM image and Raman spectrum from a sample deposited on WAC/Si for 30 min. It can be seen that the density of particles is very low, and no diamond peak at 1132 cm^{-1} can be found. Raman peaks appear at 1120 and 1477 cm^{-1}, which can attribute to nanocrystals in 1–2 nm in diameter or carbon clusters of sp^3 bonded material and amorphous carbon as mentioned above. For further extended deposition of 270 min, the SEM images in Figure 4.24 show a similar low density (~10^3 cm^{-2}) but with bigger size of a few micrometers. We did not observe G-band signal in the Raman spectrum (Figure 4.23) after 30 min deposition on WAC/Si, while we observed G-band signals from AC/Si substrates (Figure 4.18). It seems that some of adamantane molecules might change into the graphitic states (Figure 4.18) in the plasma. Whether it may assist to diamond nucleation remains unresolved issue in the present case, though previous studies have shown that the graphite seeding can enhance diamond nucleation [125, 126].

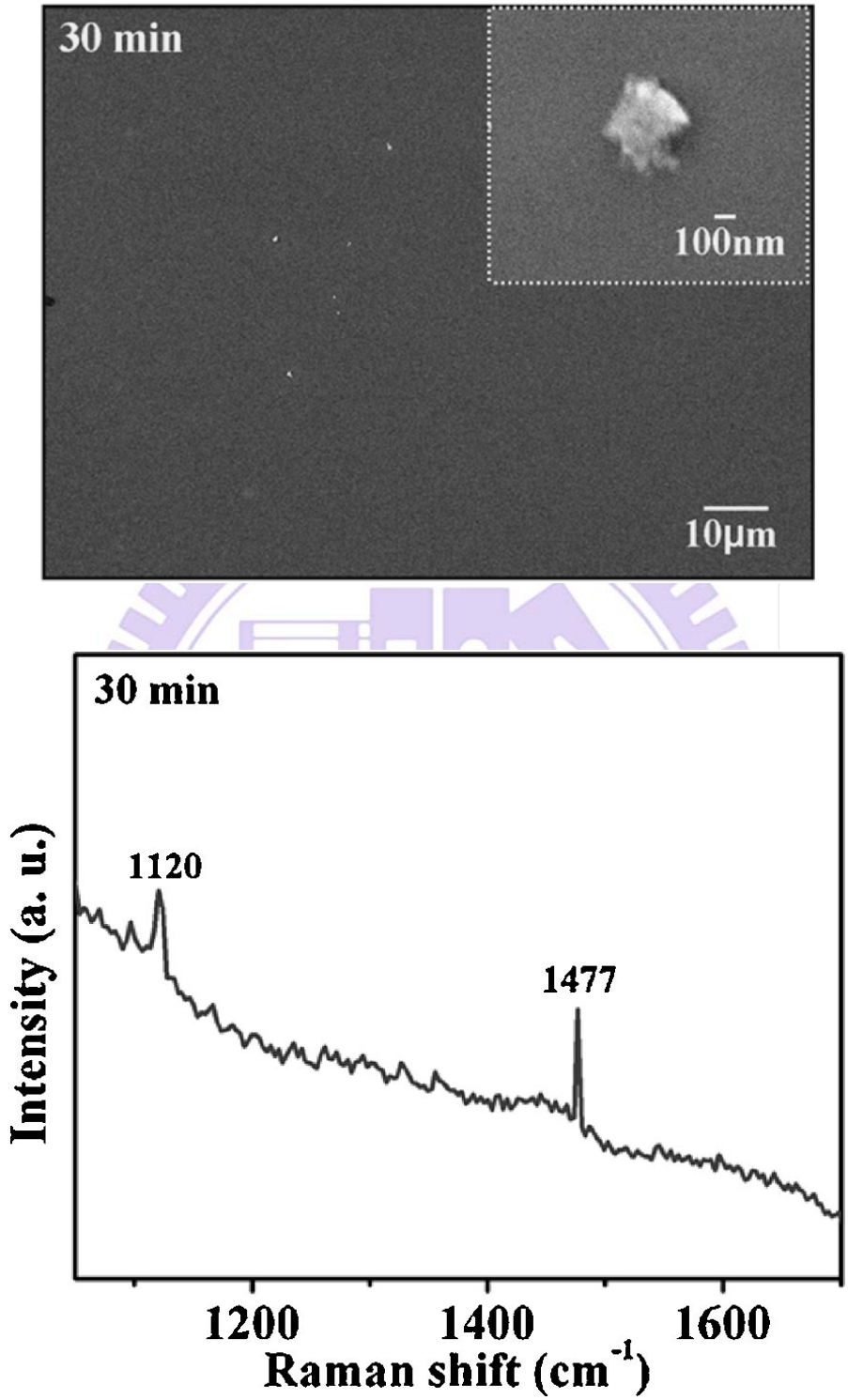

Figure 4.23: SEM image and Raman spectrum after 30 min growth on WAC/Si.

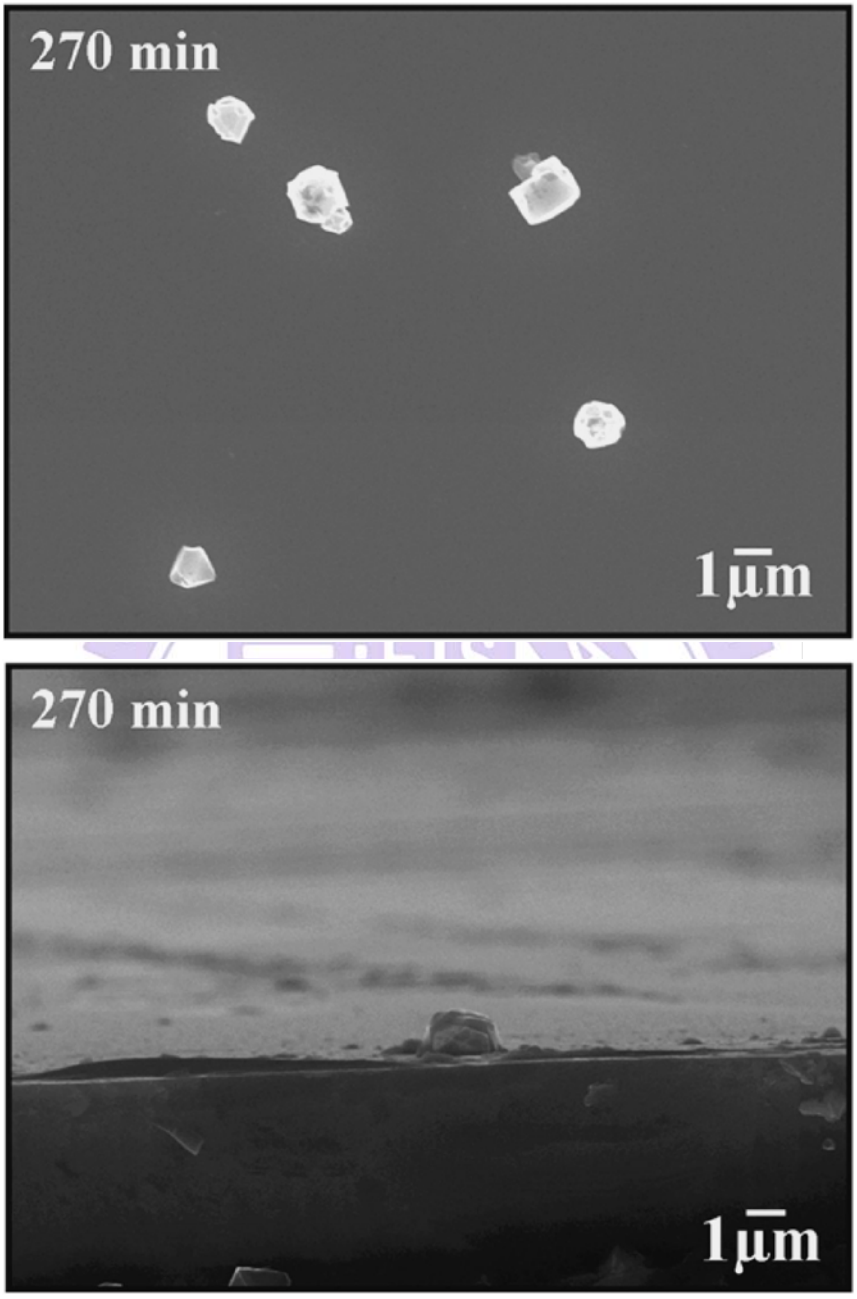

Figure 4.24: Plan-view and cross-sectional SEM images of diamond after 270 min growth on WAC/Si substrate.

Figure 4.25 shows plan-view and cross-sectional SEM images of synthesized diamond on AC/Si substrate after 270 min deposition. The average size and thickness of well-faceted diamond are ~ 1.6 and ~ 2 μm, respectively, as shown in Figures 4.25 (a) and (b). The growth rate of diamond is estimated to be ~ 0.5μm/hr, and the density of diamond is ~ 10^8 cm^{-2} on the AC/Si substrates. However, it is seen in Figure 4.25(a) that not all the Si surface is covered with diamond crystallites. The inset SEM image in Figure 4.25 (b) shows that a ~50 nm thick layer may form on such uncovered Si surface areas. From the XPS and Raman results shown below, it may be a SiC film. In our previous section, we have shown that the adamantane precursor not only increases the quality, cystallinity, and growth rate, but also enhances the yield than that without adamantane [127]. Further, the XRD pattern in Figure 4.26 (a) also supports formation of the microcrystalline diamond film. In addition to Si peaks, the XRD pattern presents sharp and well-defined peaks, and the observed diffraction peaks at 2θ = 43.9 and 61.7 degrees correspond to diamond {111} and crystalline 3C-SiC{220}, respectively. The micro-Raman spectrum of the diamond film is shown in Figure 4.26 (b). The sharp Raman peak at 1332 cm^{-1} suggests that high-quality microdiamonds have been synthesized on the Si surface. The XRD and Raman results show that the high-crystalline quality diamond film has been synthesized at 530°C.

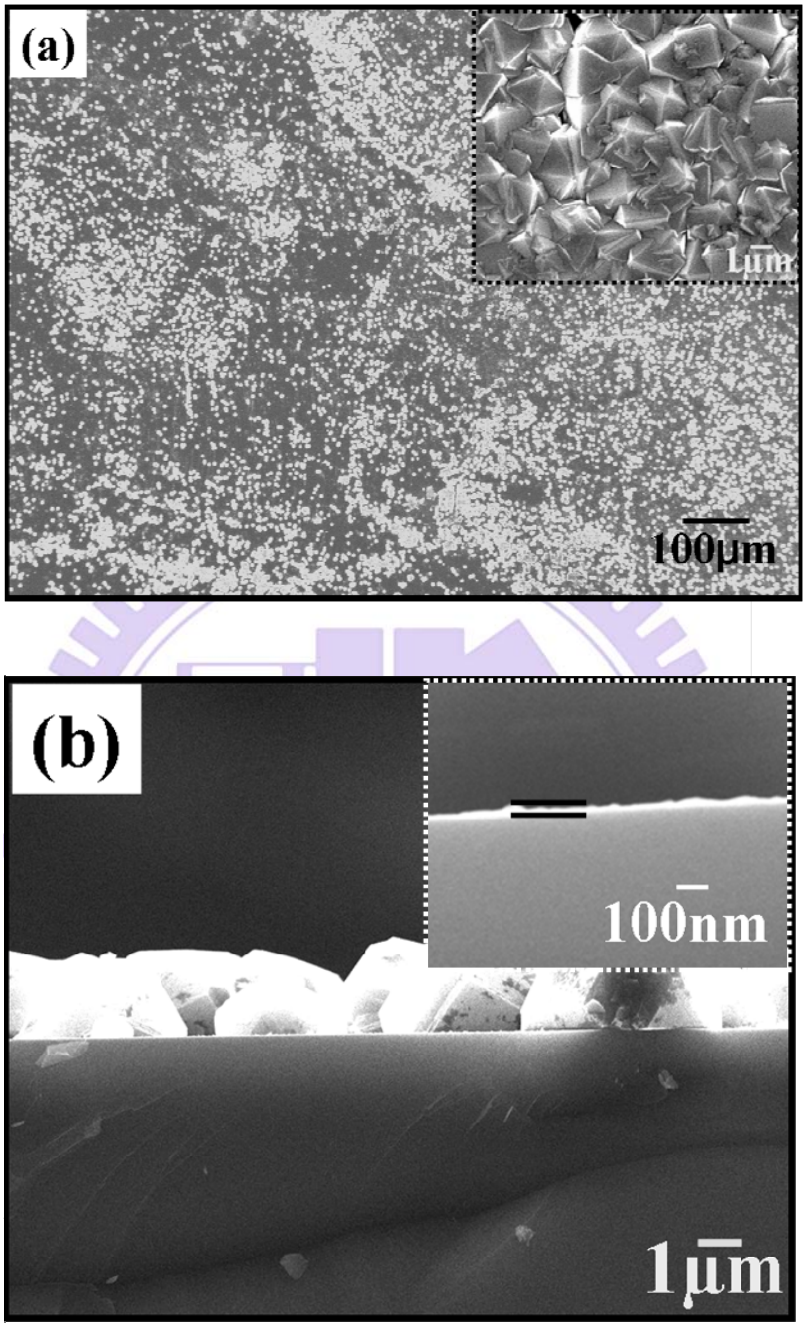

Figure 4.25: SEM images of deposited diamond in (a) plan–view: inset high magnification of diamond and (b) cross-sectional view, inset: high-magnification image of interlayer after synthesized diamond (growth time 270 min) on AC/Si at 350W.

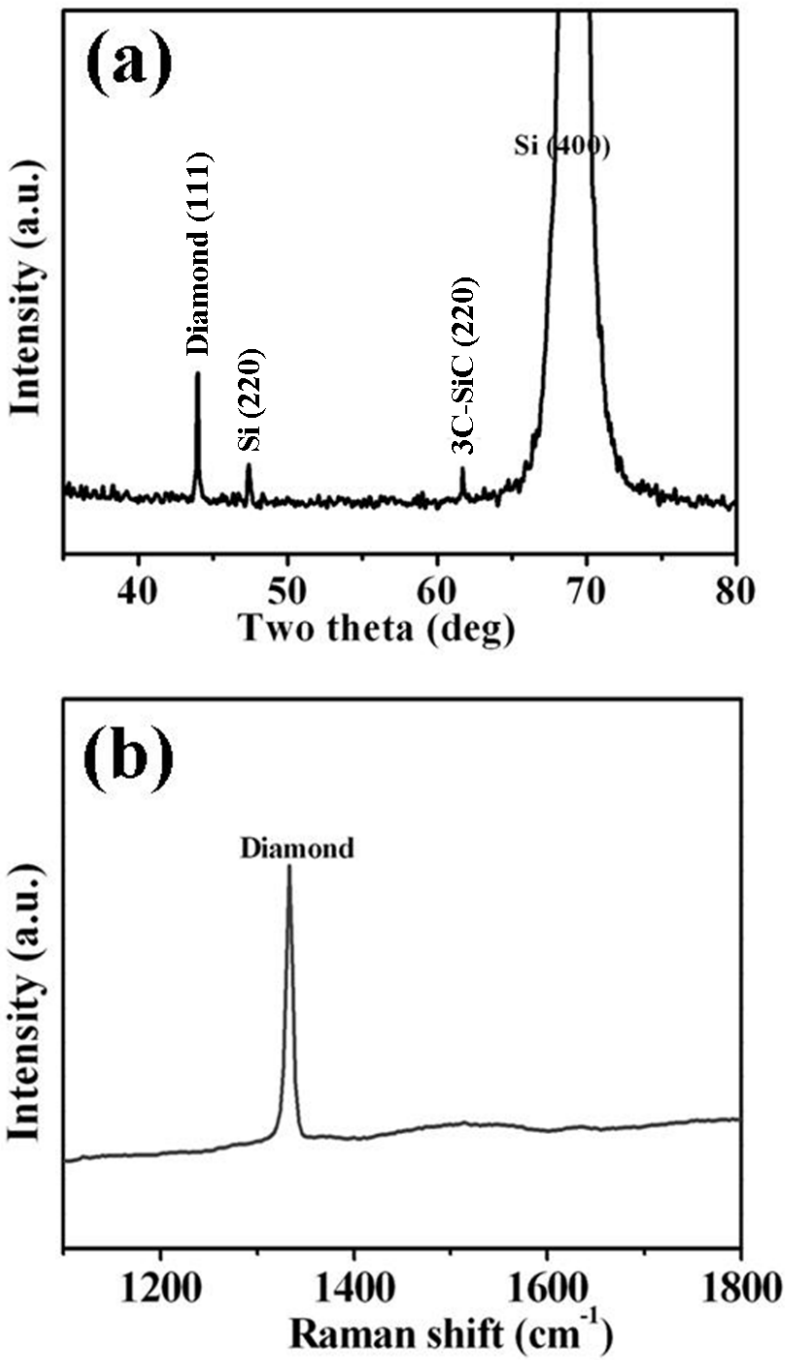

Figure 4.26: (a) XRD and (b) Raman spectrum of diamond after 270 min growth at 350W.

The uncovered regions on Si surface were characterized by atomic force microscopy (AFM) and Raman spectroscopy, as shown in Figure 4.27. Figure 4.27 (a) shows that the nanoparticles have also been formed on the AC/Si surface after 270 min growth at 350W. Raman spectrum of these nanoparticles in Figure 4.27 (b) shows two sharp Raman

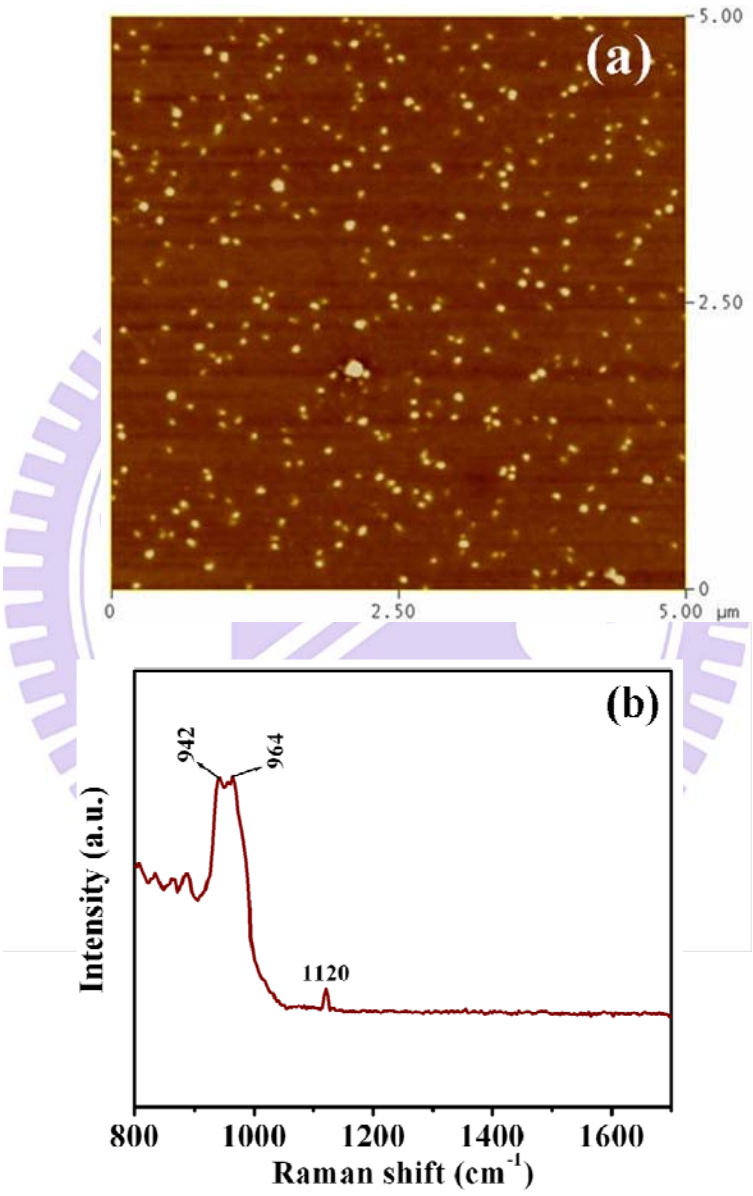

Figure 4.27: (a) AFM and (b) corresponding Raman spectrum of plane region where we did not observe microdiamond film after 270 min diamond growth.

signals at 941 and 964 cm^{-1} and one weak signal at 1120 cm^{-1}. These two sharp peaks at 941 and 964 cm^{-1} are from SiC particles [128] while the peak at 1120cm^{-1} from nanodiamond (described above).

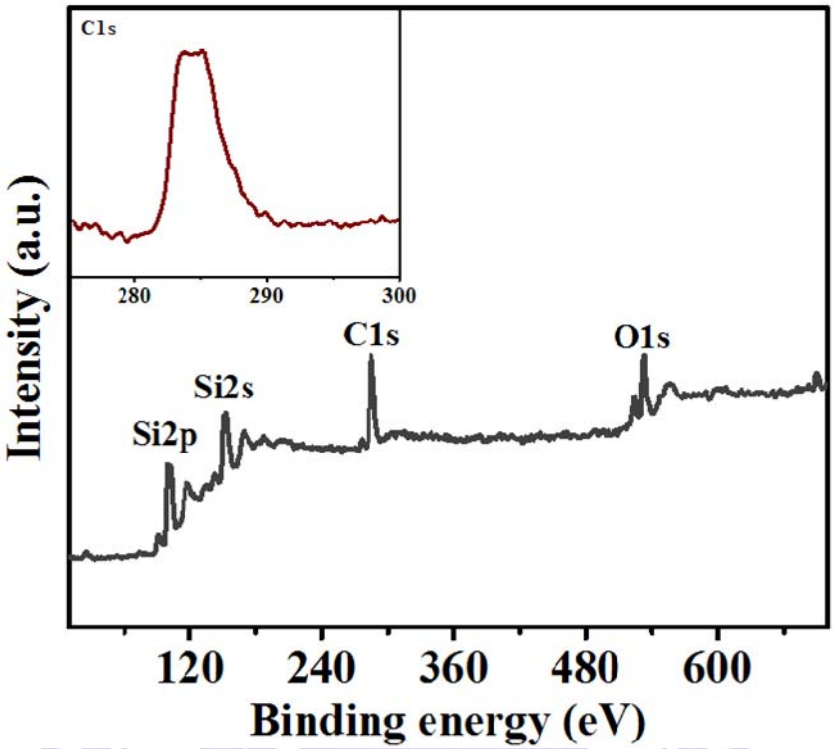

Figure 4.28: The XPS survey spectrum of diamond/Si, inset: high resolution spectrum of the C 1*s* region.

. The XPS survey spectrum of diamond growth on AC/Si at 350W is shown in Figure 4.28. The features are similar to those in Figure 4.21. The strong signals of carbon C 1s at 283.7 and 285.2 eV can attribute to the C-C bond in diamond films, and the peak at 283.2 eV is the characteristics of C–Si bonding. On the basis of XPS results, we confirm the existence of diamond as well as SiC. This is the consistent of our SEM, XRD, and Raman results.

Furthermore, a cross-sectional bright-field TEM image of diamond/Si is shown in Figure 4.29 (a). It is clear that the thickness of diamond particle is ~2μm. This is consistent of our SEM results. The SAED taken from the interface is shown in Figure 4.29 (b). In the SAED pattern only Si{111} and diamond{111} and {311} diffraction

spots are observed without SiC diffraction spots. Thus, it is likely that the SiC may not be uniformly distributed on the Si surface. The SAED pattern from the diamond particle [Figure 4.29 (c)] shows the single crystalline characteristics along <110> direction. The measured interplanar spacing from the HRTEM image of diamond [Figure 4.29 (d)] is ~2.04 Å, which corresponds to the set of {111} diamond lattice plane.

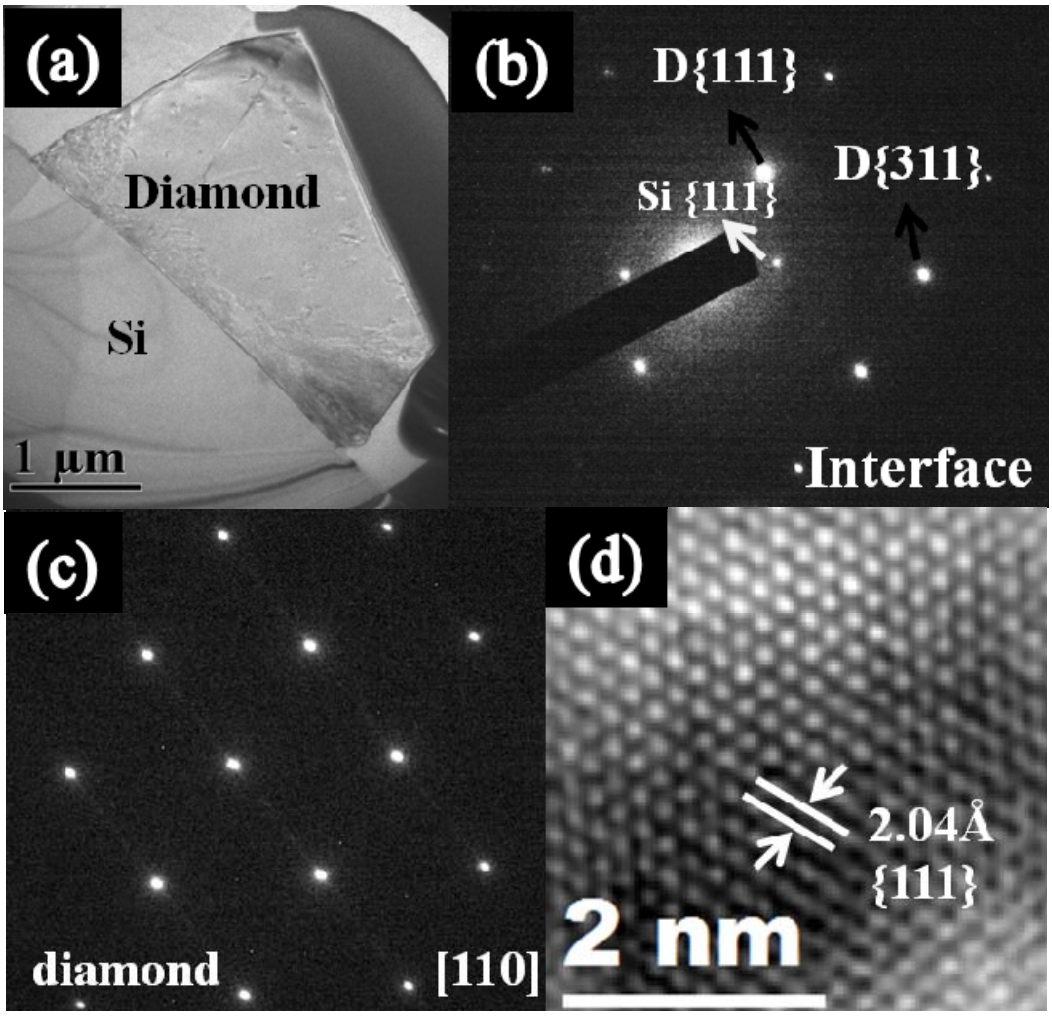

Figure 4.29: (a) Cross-sectional BF-TEM image of diamond/Si, (b) SAED pattern of interface between Si and diamond, (c) SAED pattern of diamond {111} plane along <110> direction, (d) High-resolution TEM lattice image of diamond; the d-spacing between the fringes is ~ 2.04 Å of {111} diamond lattice plane.

4.7 Field emission measurement

The field emission measurements were carried out in a vacuum chamber with a base pressure of 10^{-6} torr at room temperature by using a parallel cathode-anode setup [129] with a 2 mm diameter molybdenum tip as anode. The distance between the anode tip and the cathode was set at 12 μm by a digital micrometer controller and an optical microscope. The current-voltage characteristics of the films were acquired using a Keithley 237 electron source unit and were modeled with the Fowler- Nordheim theory [130].

After diamond growth at 350W for 270 min, field emission properties were investigated. Figure 4.30 shows the relation of emission current density as a function of applied electrical field on diamond. The field emission characteristic of the sample has been carried out by defining a threshold field corresponding to current density of 10 $\mu A/cm^2$. The inset in Figure 4.30 is the corresponding Fowler-Nordheim (F-N) plot, $\ln(J/E^2)$ versus 1/E, of the corresponding field emission (FE) data, indicating that the field electron emission of well-faceted diamond [Figure 4.25 (a) and (b)] follows the classic field emission mechanism. The turn-on field of diamond film at the current density of 0.0011 mA/cm^2 is approximately 55 V/μm. This value is better than previously reported values for various field emitting materials including micro diamond films, but worse than that of oriented nano-, submicro-, and micro-diamond film [81, 131, 132]**.** The SEM images in Figure 4.25 (a) and (b) show the well-faceted microdiamond films (thickness: ~2 μm) have been deposited on the Si surface. Probably, the diamond edges can be acted as electron emitters, resulting in high current density 1.6 mA/cm^2 for an applied field of 96 V/μm. The low turn-on field and high current density of diamond film on the Si surface could be assigned following factors: Firstly, the well-faceted edges [Figure 4.25 (a) and (b)] may enhance the field emission properties [81]. Another reason may be that well-faceted diamond films act like separated emitting edge, which not only could have a large field enhancement factor, but could also effectively depress the screen effect.

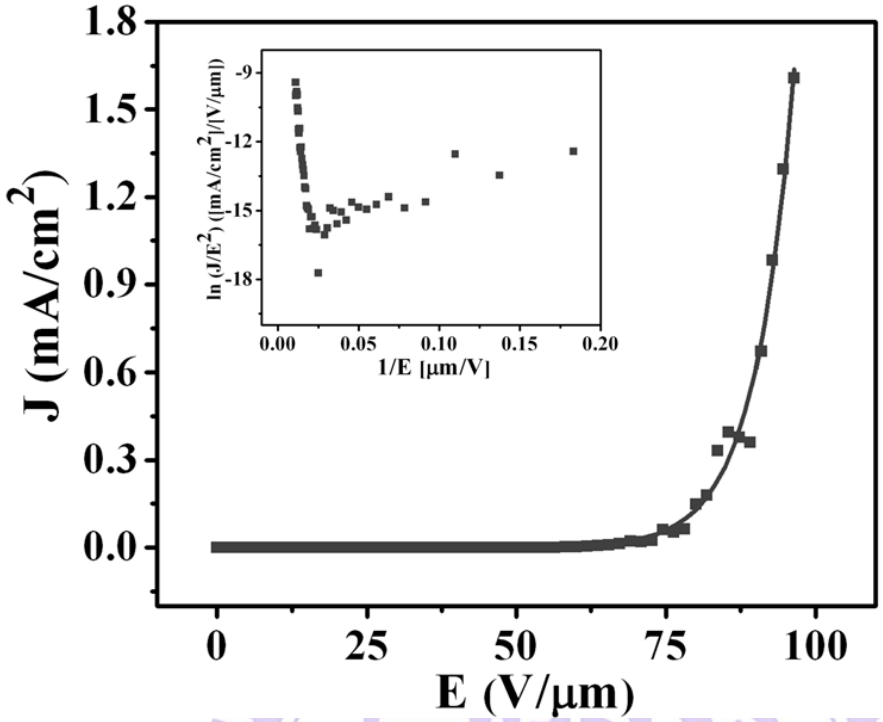

Figure 4.30: Emission current density as a function of applied electrical field for diamond plates and inset corresponding F–N plot.

4.8 Possible mechanisms for adamantane assisted diamond nucleation and growth

In this study, microcrystalline diamond films have been synthesized on AC/Si substrates by MPCVD at relatively low temperature. The synthesized diamond on AC/Si substrate may provide some essential information to understand growth mechanisms. Adamantane is the smallest unit of diamondoids (recent discovery of previously inaccessible quantities of nanometer-sized hydrogen-terminated diamond clusters, also known as diamondoids) [133, 134]. It is also speculated that the adamantane may serve as embryos for nucleation of diamond in the gas phase. Here, it is worthwhile to briefly discuss the possible mechanisms for diamond nucleation and growth from adamantane.

As a result, when the AC/Si substrates exposed to CVD diamond growth environment, adamantane molecules are desorbed from the Si surface and mix with gaseous (0.6% CH_4 in H_2) plasma. It gives the crucial information about nucleation of crystalline diamond. Probably, one possibility is that during the evaporation and mixing

with gaseous plasma, the adamantane might decompose into individual molecules which can either remain in the gas or be removed from its surrounded hydrogen by hydrogen abstraction. The hydrogen abstraction is one of the highly possible mechanisms for diamond nucleation in the gas phase as adamantane can be considered as diamond nucleus covered with hydrogen atoms and then methane gas species in hydrogen plasma may facilitate the growth of three dimensionally individual nuclei. Alternatively, the high evaporation rate of adamantane molecules would increase the concentration of carbon in the plasma which favors to form the nucleation from supersaturation. The deposited crystallized particles can act as nuclei for the subsequent growth of diamond on the Si substrate. Finally, probably the residue of adamantane molecules would behave as nuclei or embryos for diamond formation, and then carbon radicals from methane species in the plasma enhance the diamond growth.

In the intermediate growth stages, as shown in Figure 4.18, the adamantane might change into graphite phase intermixed with amorphous carbon, which can also enhance the diamond growth. A similar observation (graphite transformation into diamond) of diamond deposition on the Si substrate has been reported previously [135, 136]. Previously, Kompoulos et al. and Feng et al. have observed formation of diamond films on thin amorphous carbon coated Si substrates, while Barnes et al. had noticed that the high density of diamond nucleation on the Si substrate which was first scratched with diamond paste and then deposited with a nondiamond amorphous carbon film.

In microwave plasma, the mixture of gases (methane/hydrogen) can produce hydrogen and. methyl radicals (CH_3^*) as shown in the following reaction

$CH_4 + H^* = CH_3^* + H_2$

Methane gas species favor individual nuclei to grow three dimensionally by a vapor-solid growth. The hydrogen atom (H-atom) abstraction from the CH_4 molecules (shown in reaction) will form methyl radicals (CH_3^-) or other active hydrocarbons. The growth of microcrystalline diamond film may proceed through surface chemical reactions such as the formation and migration of hydrocarbon in the vicinity of surface, hydrogen abstraction, dehydrogenation of absorbed complexes, recombination of hydrogen atoms, and so on., which can be more than 99% sp^3 bonded carbon, and do possess many of the properties of natural diamond. Often some degree of non-diamond carbon is incorporated

during nucleation and growth. Atomic hydrogen and ions can generally prevent the formation of nondiamond carbon impurity on the surface or etch the graphitic state and favor to diamond growth. From the SEM views, it is clear that the after forming stable crystalline particles, deposition with low concentration of methane results in formation of (111) diamond facets, as shown in Figure 4.25 (b). The study of the exact mechanism of diamond nucleation and growth from adamantane is still underway.

4.9 Summary

In summary, we demonstrated a new, simple and efficient way to synthesize the high-quality crystalline diamond films on adamantane-coated Si substrate by microwave plasma chemical vapor deposition. The results show that the presence of the adamantane molecules is found indispensable in promoting an efficient nucleation of diamond with a high density at low temperature. Thus, the adamantane molecules may have a better potential application for diamond nucleation and growth at low temperature. The charactirization of synthesized products revealed that the adamantane first results in the formation of some sp^3 and other sp^2 bonding carbon species and then diamond films in the later stage of deposition. SEM shows that well-faceted diamonds (thickness in ~ 2μm) with ~50nm SiC interlayer have been formed after 270 min with 350W. XRD and XPS show diamonds deposited with the SiC as well. Low-temperature deposition of diamond can make it undesirable for use in critical applications. The deposited diamond exhibit good field emission characteristics of reasonably low threshold voltage and high current density.

Chapter 5

Enhanced diamond nucleation on adamantane-coated Pt/Si substrates

5.1 Introduction

Recently, platinum (Pt) is used for high-pressure high temperature diamond synthesis as a catalytic solvent [137]. It is also known that Pt is a strong catalyst for hydrogen and hydrocarbons. Therefore, there was certain interest in studying effects of diamond growth on Pt. The lattice constant of diamond and platinum (fcc) is 3.56 and 3.92Å, respectively. Therefore, the lattice difference between diamond and Pt is approximately ~ 10% [138]. Tachibana et al. have studied diamond growth on Pt substrate by bias-enhanced nucleation method. They had noticed that the density of diamond nucleation was enhanced with bias time [139]. Most recently, the growth of diamond films on Pt layer was realized by microwave plasma chemical vapor deposition (MPCVD) without bias treatment. In this technique, they used diamond seeding particles to enhance the diamond nucleation [140]. Although diamond films on Pt/non-Si substrate, for example, single crystal $SrTiO_3$ (111) or sapphire substrates have been studied [141, 142]. However, a very few study of diamond growth on Pt/Si substrate has been reported. The prevention of silicidation is the key to grow high-quality diamond on Pt/Si.

In this chapter, we report, for the first time, microwave plasma chemical vapor deposition of diamond films on $Pt/SiO_2/Si$ by using adamantane (discussed in chapter 4 in details) as a seeding layer to enhance the diamond nucleation. Adamantane is easy dissolved in organic solvents. Therefore, in this study we used hexane (C_6H_{14}) as a solvent. The evaporation of hexane is high. After adamantane seeded on the Si surface by ultrasonication, the hexane will be evaporated from the Si surface and only pure adamantane left on the Si surface. The Pt interlayer on Si substrate adsorbs the hydrocarbons from carbon source materials (adamantane), which can play a major role in diamond nucleation and growth. The nucleation and growth of diamond on the Pt/Si substrate will be discussed. The rate of film growth in MPCVD with 1% methane (CH_4) in hydrogen (H_2) was 0.45 μm h^{-1}.

5.2 Experimental process for diamond growth

The schematic diagram for the deposition of diamond on $Pt/SiO_2/Si$ is shown in Figure 1. The synthesis processes of the diamond films on $Pt/SiO_2/Si$ are described as follows:

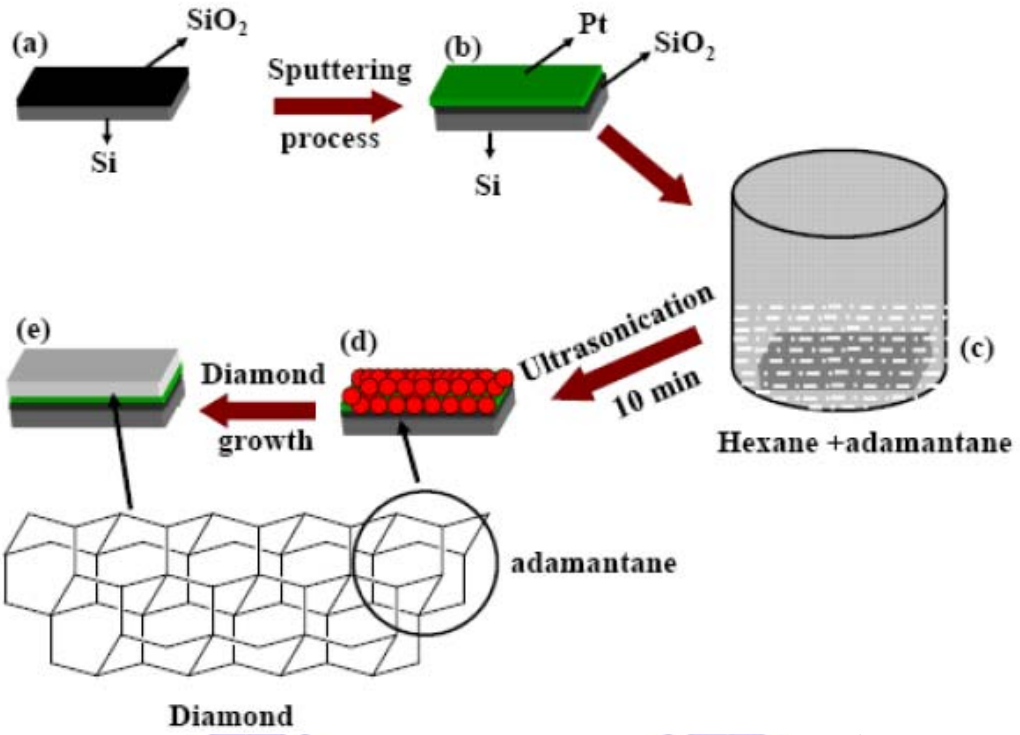

Figure 5.1: Schematic diagram showing diamond synthesis in five steps; (a) silicon substrate with native oxide layer, (b) Pt coated on SiO_2/Si substrate by sputtering process, (c) $Pt/SiO_2/Si$ immersed into the solution of hexane and adamantane, (d) adamantane deposited on $Pt/SiO_2/Si$ surface by ultrasonication, and (e) diamond growth by MPCVD.

Mirror-polished p-type (100) silicon wafers with dimensions of 1 x 1 cm^2 without any mechanical pre-treatment were used as substrates. The substrates were ultrasonically cleaned with acetone and alcohol for 10 min respectively, and then dried

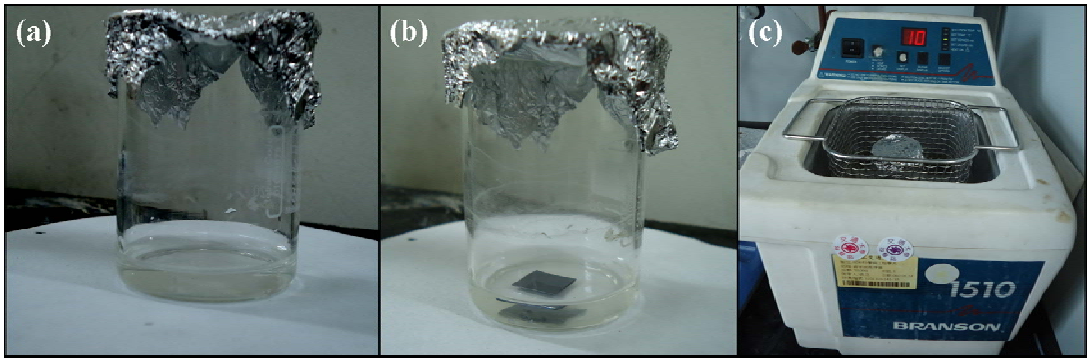

Figure 5.2: Photographs of (a) adamantane (100mg) + (5ml) hexane solution, (b) $Pt/SiO_2/Si$ dipped into solution, and (c) ultrasonication process for adamantane deposition.

with high pressure nitrogen gas to remove any contamination particles left on the surface. As the oxide layer on Si can prevent silicidation between Pt and Si, we did not use BOE solution to remove the native oxide (SiO_2) from the Si surface. Further, the platinum particles/film were coated on SiO_2/Si substrates by a sputtering process at room temperature for 210 second (used from SEM specimen coating) and then again cleaned with acetone and alcohol for 10 min, respectively. A 20 mA current was used during the Pt coating on SiO_2/Si. The average thickness/size of Pt particles is~ 50nm. Further, adamantane was seeded on cleaned $Pt/SiO_2/Si$ samples by ultrasonic method. In this method, the solution was prepared by using (100mg) adamantane + (5 ml) hexane and stirred for 1 min [the commercial adamantane powders in 99+% purity were obtained from Sigma-Aldrich Chemie GmbH (CAS:281-23-2)]. After 60 sec manually stirring at room temperature, the adamantane was fully dissolved into hexane solvent and became a colorless solution, as shown in Figure 5.2 (a). Then, $Pt/SiO_2/Si$ samples were immersed into the solution for 10 min ultrasonication [Figure 5.2 (b) and (c)]. After ultrasonication the adamantane was seeded on the $Pt/SiO_2/Si$ surface. We did not use any kind of process to dry the sample. Because the evaporation property of hexane is very high therefore hexane evaporated from the sample and adamantane left on the $Pt/SiO_2/Si$ surface. Hexane is a colorless liquid, mainly obtained by the refining of crude oil and it has considerable vapor pressure at room temperature. Hexane is relatively safe, largely

unreactive, and easily evaporated. Finally, the adamantane-seeded $Pt/SiO_2/Si$ substrates were then placed on a Mo-disk holder for diamond growth in a 1.5 AsTeX-type MPCVD system. The detailed processing parameters for MPCVD are as follows: the total pressure was 20 torr, the microwave power was 600 W, the total flow rate was 200 sccm (1%CH_4 in H_2), and deposition time was varied from 2 to 120 min. Finally, the samples were allowed to cool down to ambient temperature in the presence of hydrogen gas at 10 torr. To know the role of Pt, we also prepared Si substrates without Pt coating and treated with the same experimental condition.

5.3 Structural characterization of adamantane

After adamantane seeding on $Pt/SiO_2/Si$ surface by the ultrasonic treatment, the surface morphology was characterized by scanning electron microscopy (SEM). The plan-view SEM image is shown in Figure 5.3 (a). From the SEM image it is clear that the adamantane particles are homogeneously dispersed on the $Pt/SiO_2/Si$ surface by ultrasonic treatment. The inset high-magnification SEM image in Figure 5.3 (a) shows that the adamantane particle sizes are varied from 10 nm to 1.5 μm. The cross-sectional SEM image in Figure 5.3 (b) shows the thickness of adamantane particles in ~100nm thickness on $Pt/SiO_2/Si$ surface after 10 min ultrasonic process. Further, the bonding characteristics of the adamanatne film were identified by Fourier-transform infrared spectroscopy (FT-IR) and Raman spectroscopy, as shown in Figures 5.3 (c) and (d). There are several weak and strong peaks in Figure 5.3 (c). The peak at 1037 cm^{-1} can be assigned CC stretch/CH bend while the band at around 1107- 1375 cm^{-1} can be attributed to sp^2 (C-H) group. In the FTIR spectrum the peak due to CH_2 deformation appears as a strong absorption band at 1455 cm^{-1}. The strong band at 2572, 2665, 2860, 2883, and 2921 cm^{-1} can be attributed to CH stretching [143, 144]. In addition, the adamantane-seeded on $Pt/SiO_2/Si$ substrate was evaluated using Raman spectroscopy (LABRAM HR800). Intense Raman peaks in the range of 600–1800 cm^{-1} are shown in Figure 5.3 (d). All the multiple Raman peaks at 635, 758, 949, 970, 1095, 1220, 1240, 1311, 1432, and 1472, cm^{-1} are the typical characteristics of adamantane molecules [102]. We observed that the hydrocarbon signals from adamantane/$Pt/SiO_2/Si$ are partially similar in FTIR and Raman spectra, as shown in Figures 5.3 (c) and (d). In previous chapter (Chapter 4),

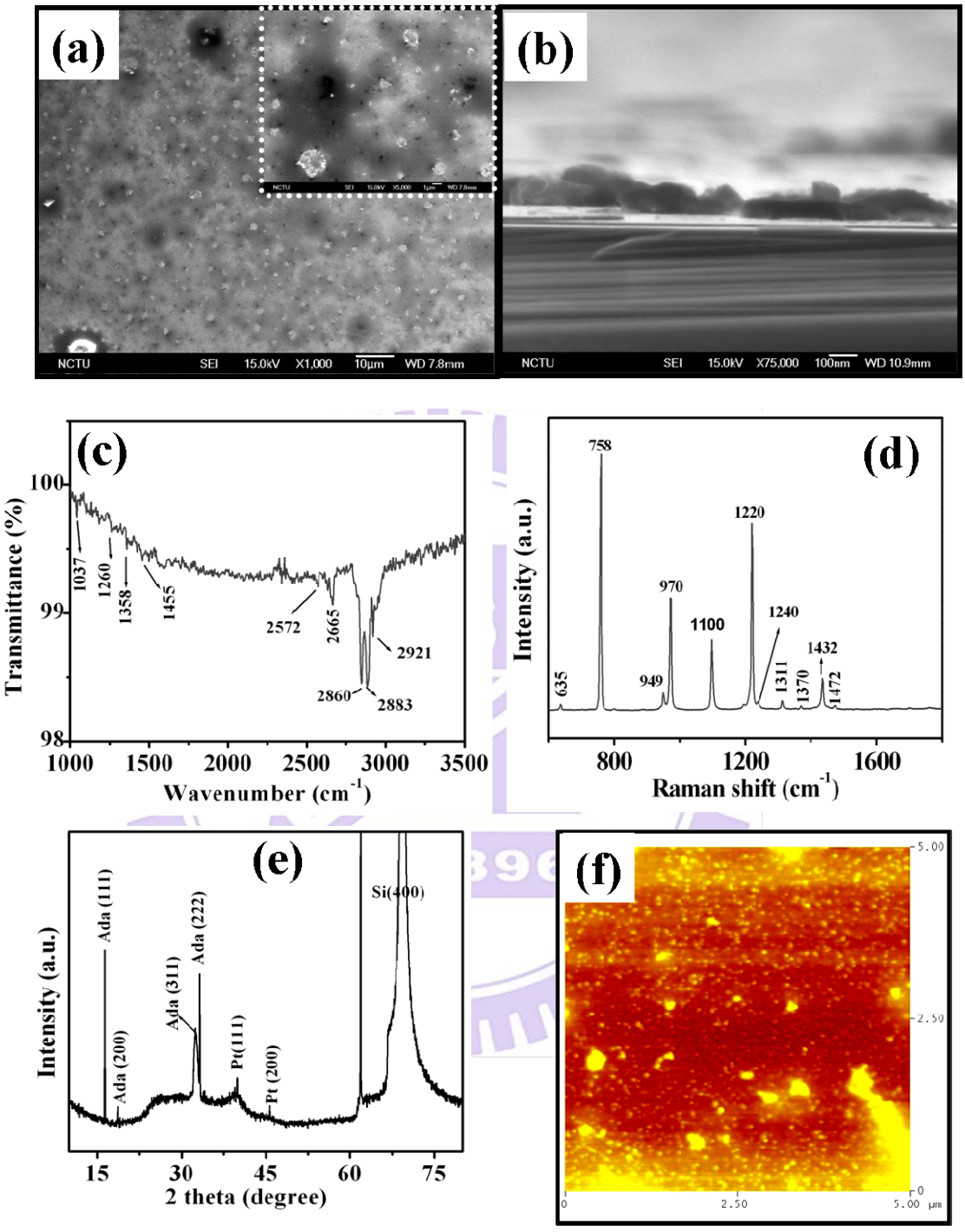

Figure 5.3: (a) plan-view SEM image; insert high magnification image, (b) cross-section view, (c) FTIR spectrum, (d) Raman spectrum, (e) x-ray diffraction pattern, and (f) AFM image of adamantane on the $Pt/SiO_2/Si$ after ultrasonic process.

we have discussed the Raman spectra of adamantane which was deposited on Si substrate by hotplate method. Here, we used ultrasonic process for the deposition of adamantane on $Pt/SiO_2/Si$ substrates. Most of the Raman peaks of adamantane (hotplate method) appear after the ultrasonic process. We also notice that there do not have any kind of bond formation between adamantane and hexane. It is clear that the hexane has been evaporated and only adamantane left on the $Pt/SiO_2/Si$ surface for diamond growth. In addition, we used D2 XRD to evaluate the adamantane/$Pt/SiO_2/Si$ substrate. The XRD pattern in Figure 5.3(e) shows the diffraction peaks at 2θ = 16.3, 18.8, 31.5, and 32.9 degrees corresponding to the interplanar spacings of adamantane {111}, {200}, {220}, {222}, and {640}, respectively. In addition to Si peaks, the diffraction peaks of Pt {111} and Pt {200} are seen at 39.8 and 46.3 degrees, respectively [145], indicating that Pt on SiO_2/Si substrate has survived after the solution treatment of hexane and adamantane with ultasonication. Further, the tapping-mode atomic force microscope (AFM, D3100) was used to evaluate the surface morphology and roughness of the adamantane/$Pt/SiO_2/Si$, as shown in Figure 5.3 (f). Here, we used AFM on a length scale of $5x5\mu m^2$ to determine the surface roughness and morphology. The roughness of the film surface was ~ 1.43nm.

5.4 The early stage of deposition

After adamantane seeding on $Pt/SiO_2/Si$, we placed the sample in the MPCVD reactor for diamond growth. We used 1% CH_4 in H_2 for diamond growth. The growth time was varied from 2 to 15 min in the presence of 1% CH_4 in H_2. Figures 5.4 and 5.5 show the SEM images after different growth time. Plan-view SEM images in Figure 5.4 (a) show that there is a homogeneously distributed film on the $Pt/SiO_2/Si$ surface. The high magnification SEM images in Figure 5.4 (b) and (c) shows that the film consists of networking islands. In general, similar morphology has been observed for diamond nucleation and growth with carburization process [146]. After 5 min deposition the shape of particles are changed, as shown in Figures 5.4 (d), (e), and (f), into the disconnected clusters with a density of $\sim 10^{11\sim12}$ cm^{-2}. After 10 min deposition, the SEM images in Figures 5.5 (a), (b), and (c) show that most of particles are formed in the spherical shape

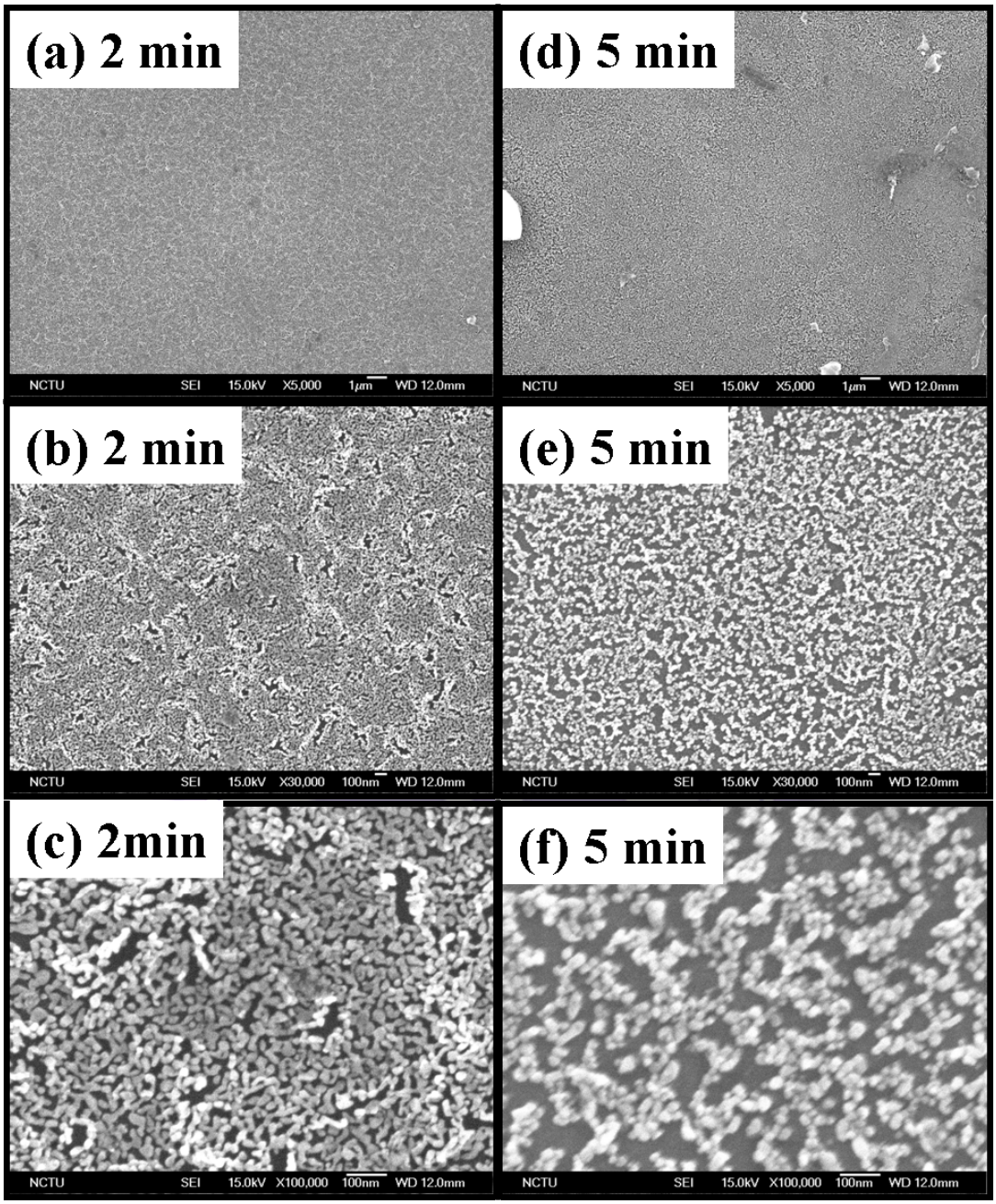

Figure 5.4: Top-view SEM images of (a), (b), (c) after 2 min and (d), (e), (f) after 5 min growth on adamantane/Pt/SiO_2/Si.

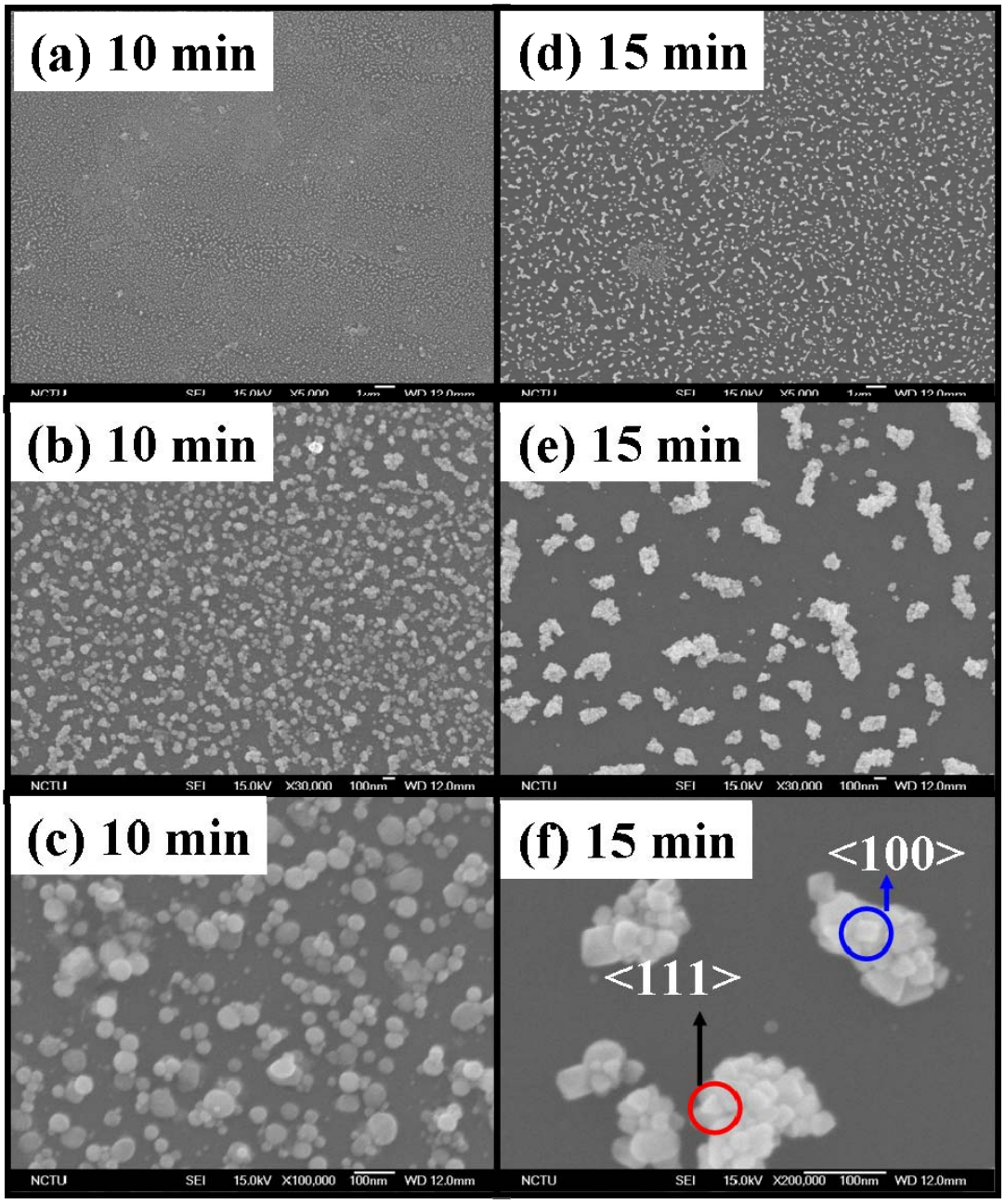

Figure 5.5: Top-view SEM images of (a), (b), (c) after 10 min and (d), (e), (f) after 15 min growth on adamantane/ Pt/SiO_2/Si

with an average size less than 100 nm. The SEM image in Figure 5.5 (f) shows that some oriented carbon particles in square and triangle facets have been formed after 15 min growth. The density of carbon particles is ~ $10^{7\sim8}$ cm^{-2}.

Further, the cross-sectional SEM images after 2, 5, 10 and 15 min deposition are shown in Figure 5.6. After 2 min deposition, the film thickness is ~100 nm similar to that of the adamantane seeding film, suggesting that most of adamantane molecules may have undergone a transformation into other forms of carbon species in MPCVD as no adamantane evidence can be obtained from Raman data shown later. After 5 and 10 min deposition, the average particle height is ~ 115 and 130 nm, while it is ~ 150 nm after 15 min. It is clear that the height increases with the deposition time.

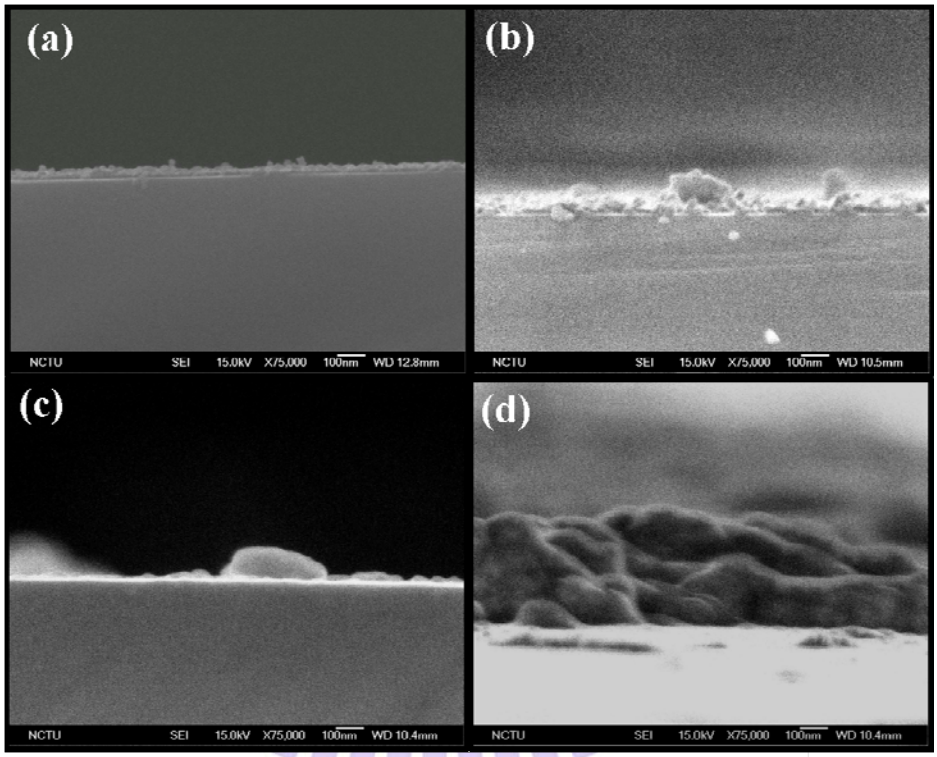

Figure 5.6: Cross-sectional view SEM images of (a) after 2min, (b) after 5 min, (c) after 10 min, and (d) after 15 min growth on adamantane/Pt/SiO_2/Si

In addition, we used Auger electron mapping in cross-section to identify the presence of elements and their distribution on the surface after 2 min treatment. The elemental mapping in cross section was performed in a PHI 700 Scanning AugerNanoprobe (ULVAC-PHI Inc.). The cross-sectional specimen was prepared simply by cleavage. Figure 5.7 (a) shows a SEM micrograph in cross-sectional view with the corresponding

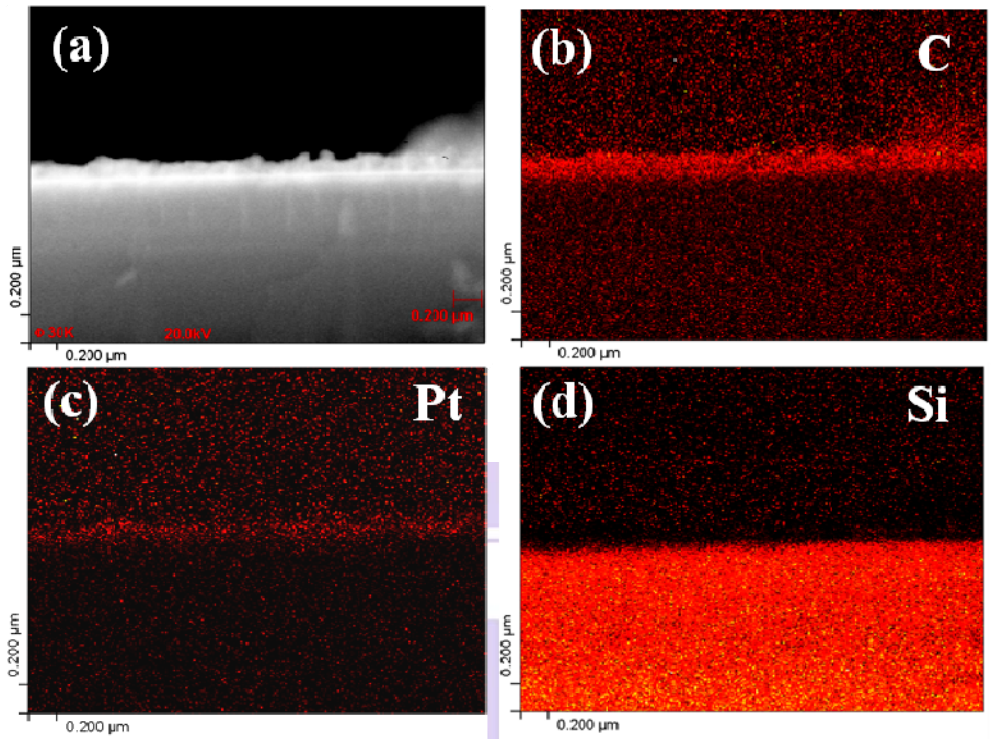

Figure 5.7 (a) Cross-sectional SEM of deposited adamantane/Pt/Si with the corresponding nanobeam Auger electron mapping of (b) Carbon, (c) Platinum, and (d) Silicon.

maps of C, Pt, and Si in Figures 5.7 (b)-(d). From the image contrast in SEM and the elemental maps, it can clearly identify two regions which correspond to carbon and Si phases, while the Pt interlayer shows low contrast. There have two possibilities to show low contrast; (i) the platinum particles were not uniformly distributed on the surface and (ii) the Pt may overlap with hydrocarbons. Moreover, to understand the role of Pt interlayer in diamond deposition, we prepared adamantane-coated samples on SiO_2/Si substrates without Pt coating under the same experimental condition. After 2 min deposition, we can see that the carbon film is not uniformly distributed on the Si surface, as shown in Figure 5.8 (a). It is likely that most of adamantane are either etched by hydrogen plasma or evaporated. The high-magnification SEM image [Figure 5.8 (b)] shows that the particles are several nanometer sizes. After 5, 10, and 15 min deposition, particles are uniformly distributed. The size of carbon particles are changed with deposition time. In comparison, the density of particles became less in the absence of Pt

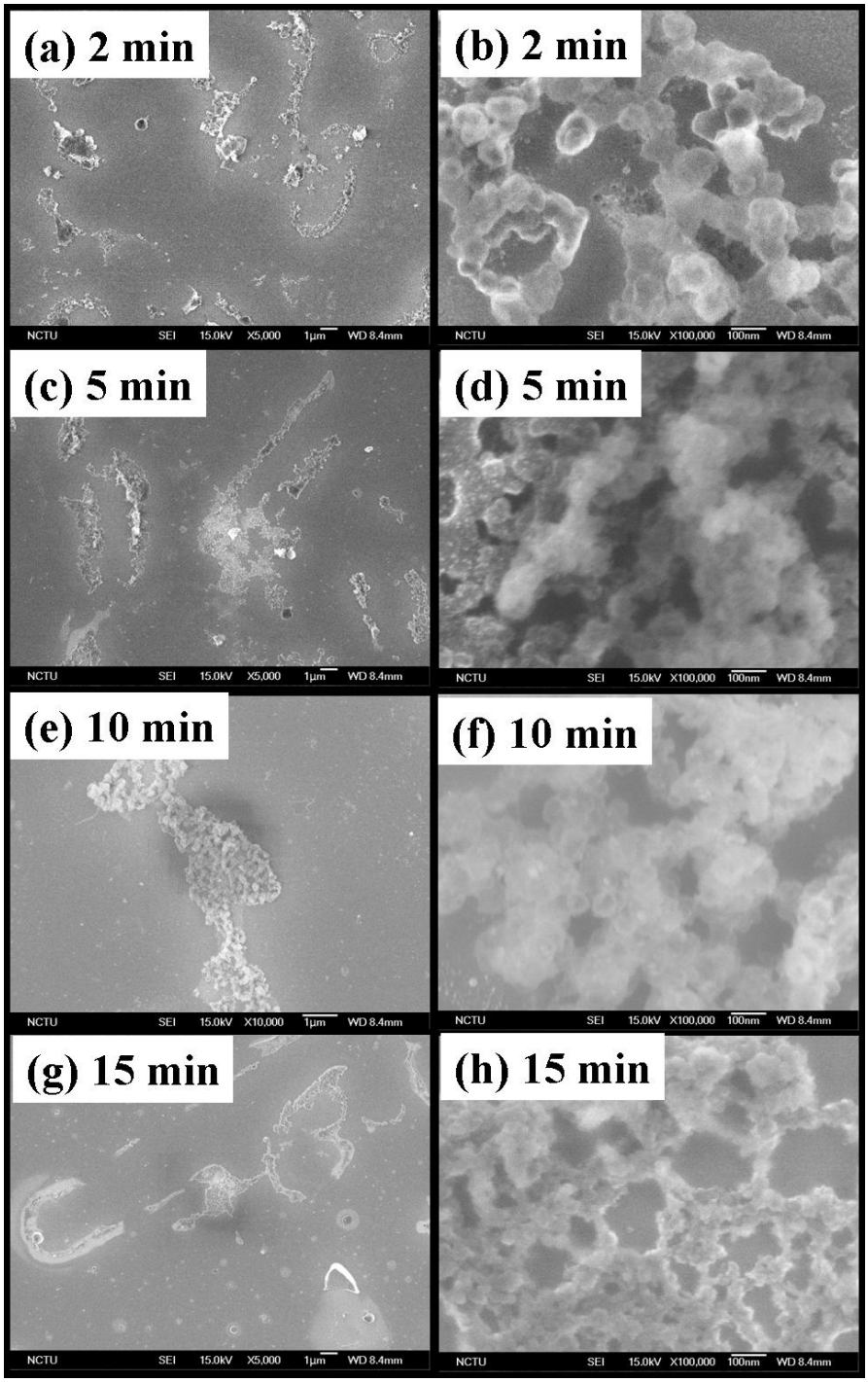

Figure 5.8: Plan-view SEM images of (a) and (b) after 2 min, (c) and (d) after 5 min, (e) and (f) after 10 min, (g) and (h) after 15 min growth on adamantane/SiO_2/Si (without Pt).

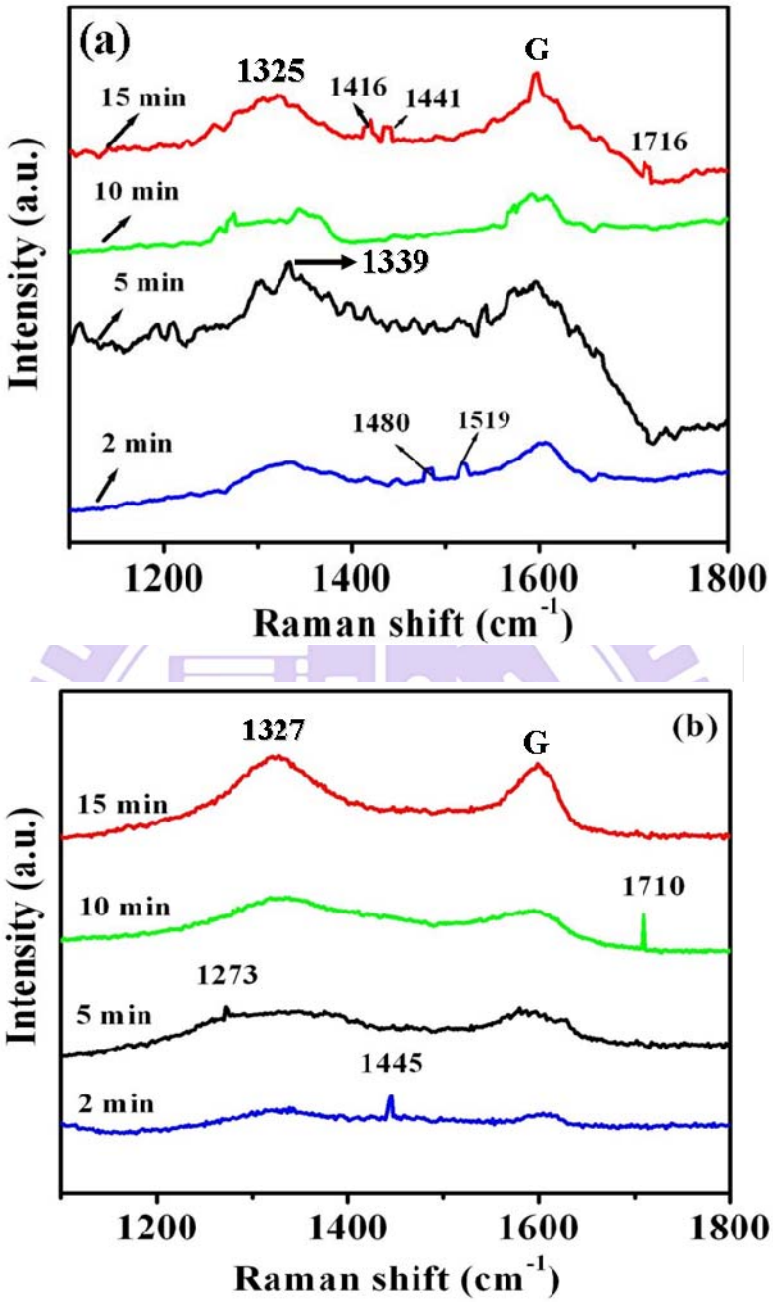

Figure 5.9: Raman spectra of (a) adamantane seeded $Pt/SiO_2/Si$ (with Pt) and (b) adamantane seeded/SiO_2/Si (without Pt) after 2, 5, 10, and 15 min treated with 1% CH_4 in H_2 at same experimental conditions.

interlayer. Furthermore, the samples after deposition on adamantane seeded on $Pt/SiO_2/Si$ and without Pt (adamantane seeded/Si) were characterized by Raman spectroscopy, as

shown in Figure 5.9. In both cases, similar features are observed [broad range (1250-1370 cm^{-1}) and G band]. The broad range peak (1250-1370 cm^{-1}) shows the presence of sp^2/sp^3. In the broad peak range (1250-1370 cm^{-1}), we observed the high intensity peaks at 1325 and 1327 cm^{-1} along with G band in both cases (after 15 min deposition) as shown in Figure 5.9 (a) and (b). Previous studies have shown that these peaks (1325 and 1327 cm^{-1} in both cases) show the presence of nanodiamond phase and the peak shifting due to the effect of nanodiamond size [147]. On the other hand, the second-order G-band does not require an elastic defect-related scattering process, and has been shown for defect-free sp^2 carbons [148]. Figure 5.9 shows the intensity of peaks is increasing with times. If the bands (D and G) have similar intensity, this may imply a high quantity of structural defects [148, 149]. Up to 10 min, the intensity of Raman signals is almost similar in both cases. However, we noticed that the one additional peak (presence of Pt) at 1339 cm^{-1} may correspond to diamond defect. After 15 min in Figure 5.9 (a) shows a sharp Raman peak at 1598 cm^{-1}, while no any such kind of peaks are seen in case of no Pt coating [Figure 5.9 (b)]. Therefore, it is likely that more graphite particles or other sp^2 phases along with nanodiamond (sp^3) phase are formed in the presence of Pt interlayer than that of without Pt. The weak Raman signals at 1480, 1519, 1416, 1441, and 1716 cm^{-1} may come from different carbon phases. In Chapter 4, we have discussed that the peak at 1480 cm^{-1} may come from nanodiamond. Therefore, it is possible that in short time deposition (2 min) some nanodiamond (sp^3) may form on Pt and further deposition results in the change of the sp^3 phase to other carbon phases.

It is well know that pure hydrogen plasma can etch the hydrocarbon layer. Therefore, to evaluate the adsorption of hydrocarbon by Pt, we prepared two adamantane seeded on $Pt/SiO_2/Si$ samples which were treated with pure hydrogen gas plasma for 5 and 15 min, as shown in Figure 5.11. The SEM image in Figure 5.10 (a) shows that the carbon film (after 5 min etching) is uniformly distributed on the $Pt/SiO_2/Si$ surface. The high-magnification SEM image in Figure 5.10 (b) shows the surface morphology of carbon film in network structure after 5 min treatment. While after 15 min treatment, the carbon network is broken by hydrogen plasma [Figure 5.10 (d)]. However, when we treated adamantane/Si (without Pt) by pure hydrogen plasma at the same experimental condition, most of the film disappeared and few particles left on Si surface. Therefore, it

strongly suggests that the Pt particles/interlayer can effectively adsorb the hydrocarbons and significantly reduce the evaporation rate of adamantane (hydrocarbon) from the surface [150] which then might transform into other forms of carbon phases.

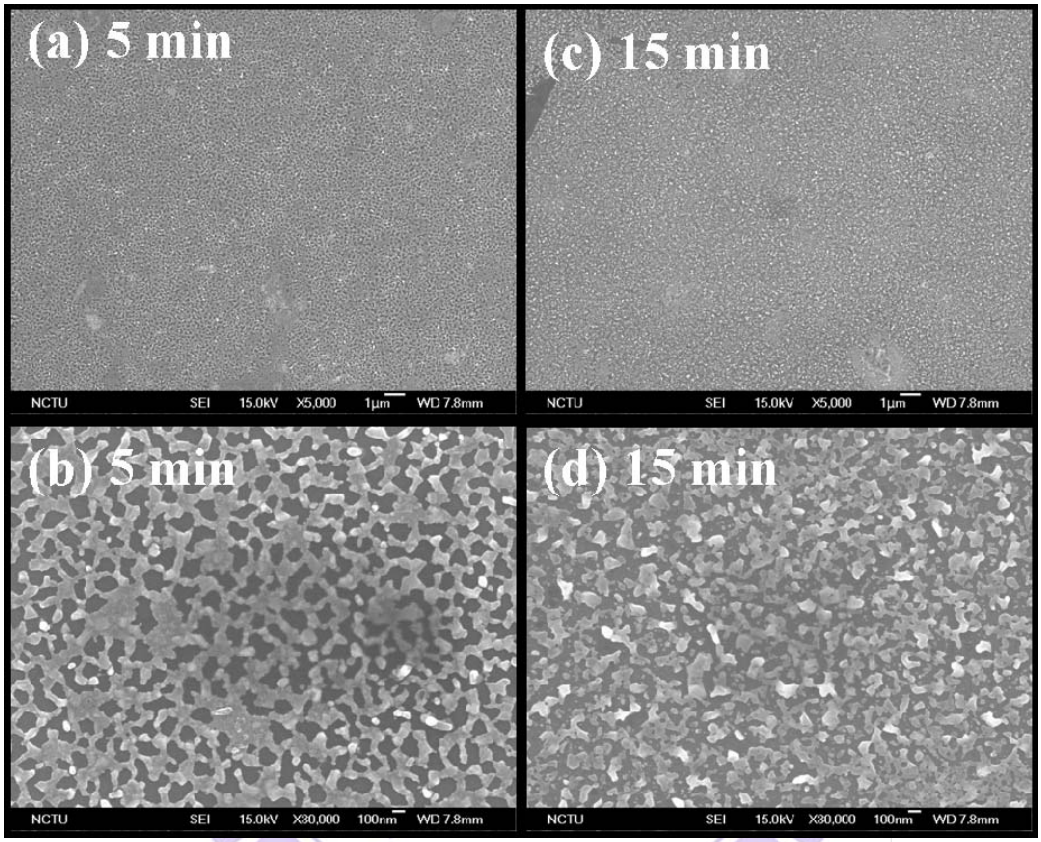

Figure 5.10: Plan-view SEM images of (a) and (b) after 5 min, (c) and (d) after 15 min, treated with pure hydrogen plasma on adamantane/Pt/SiO_2/Si.

In addition, XPS was used to identify the presence of chemical compositions on Pt/SiO_2/Si surface after 2, 5, 10, and 15 min depositions. Figure 5.11 (a) shows the survey spectra of the adamantane-seeded Pt/SiO_2/Si samples treated with 1% CH_4 in H_2 for various times (2, 5, 10, and 15 min), while Figure 5.12 (a) shows a survey spectrum of adamantane-seeded Pt/SiO_2/Si treated (5 min) with pure hydrogen (200sccm). In addition to XPS signals due to Pt particles/film and the carbon overlayer, the XPS analysis also

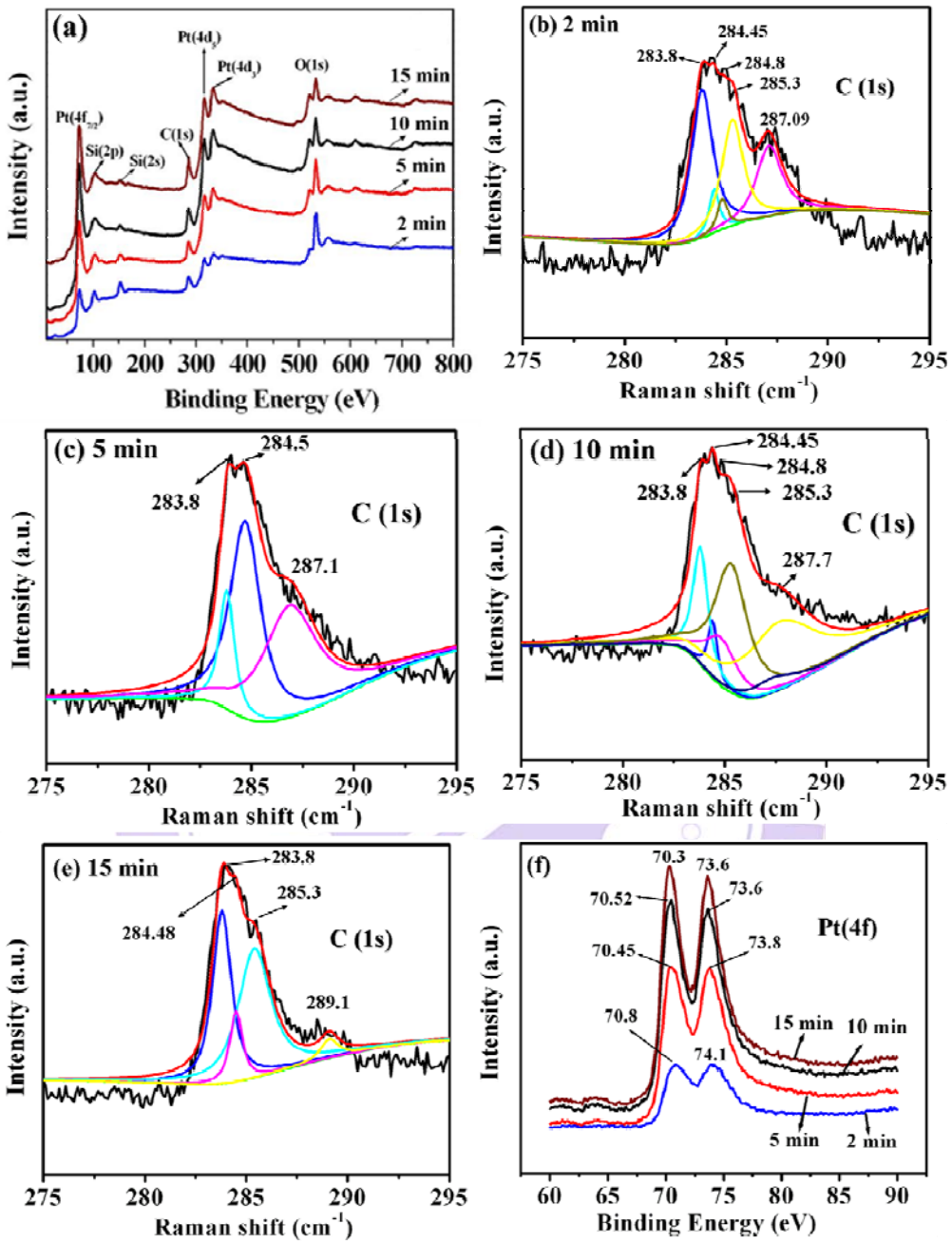

Figure 5.11: (a) XPS survey spectrum of adamantane/Pt/SiO_2/Si (b), (c), (d), and (e) high-resolution spectrum of the C (1s), and (f) high-resolution spectrum of the Pt (4f) region after various time treatments.

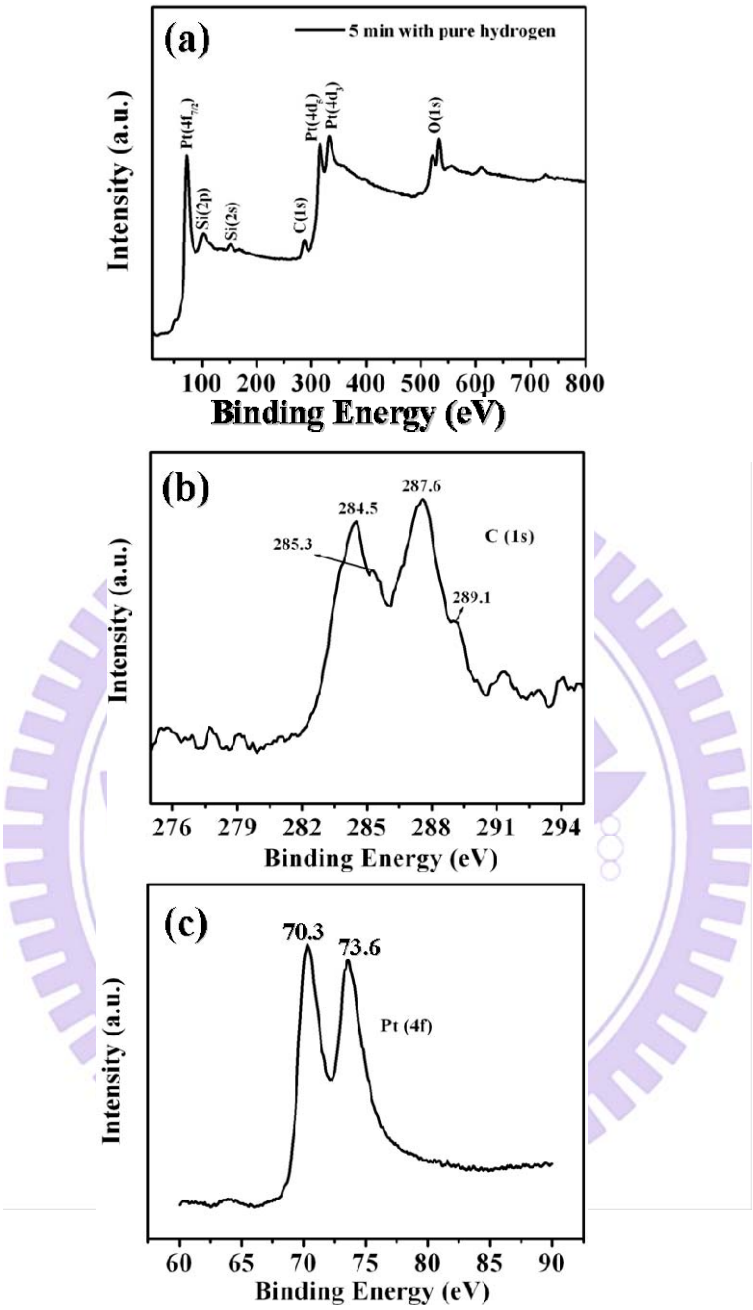

Figure 5.12: (a) XPS survey spectrum of adamantane/Pt/SiO_2/Si, (b) high-resolution spectrum of the C (1s), and (c) high-resolution spectrum of the Pt (4f) region after 5 min treatment with pure hydrogen plasma.

detects O(1s), Si(2p) and Si(2s) photoelectrons in both cases [Figures 5.11 (a) and 5.12 (d)]. The XPS high-resolution spectra of carbon (C1s) are shown in Figures 5.11 (b) (c)

(d) and (e). It is reasonable to expect that the adamantane decomposes into CH_x species after various time treatments (2, 5, 10, and 15 min). Each of the fitting components is almost similar in all cases. The carbon (C1s) can be assigned as follows: sp^3 carbon with C–C bonds (C–C sp^3 carbon, 283.7-283-8 eV), sp^2 carbon with C–C bonds (C–C sp^2 carbon, 284.4-284.45 eV), sp^2 carbon with H–C bonds (H–C sp^2 carbon, 284.8 eV), sp^3 carbon with H–C bonds (H–C sp^3 carbon, 285.2-285.3 eV) and CO at ~ 287.1 and 287.7eV [124, 151, 152], as we have already discussed in Chapter 4. Interestingly, the carbon signals from pure hydrogen treated sample (after 5 min) in Figure 5.12 (b) shows the doublet peaks of carbon at 284.5 and 287.6 eV. The peak is approximately ~ at 284.5eV which is the typical characteristics of graphitic sp^2 bonding [153,154]. The signal at 284.5 eV shows the presence of graphite phase while 287.6 eV from carbonyl or C-O groups [152]. The XPS carbon signal at 289.1 eV also corresponds to carbonyl or C-O groups [155]. It is most likely that carbon bonded with native layer oxygen (SiO_2). Similar observations are seen in the spectra for the cases of deposition with CH_4, as shown in Figures 5.11 (b), (c), (d), and (e). Figure 5.11 (f) shows the intensity of the carbon peak is increased with times. Therefore, the surface concentration of carbon (sp^2) phase may increase with deposition time. Nevertheless, the sp^3 carbon might be always present on the surface in all cases. The Pt(4f) XPS spectrum shown in Figures 5.11 (f) and 5.12 (c) exhibited a broad doublet peak with the Pt($4f_{7/2}$) peak maximum at 70.3 eV, which negatively shifted from that for bulk Pt by~0.9 eV. We ascribe the negative binding energy shift of the Pt(4f) doublet peak due to the size effect of Pt particles. The oxygen signal at 532.7 eV is associated with native oxide on Si surface. The oxygen peak at 532.7 eV attributed to the O-Si bond in SiO_2 [94, 95]. The signals of silicon Si(2p) and Si(2s) at 99 and 151 eV, indicates that the substrate surface is uncovered by Pt and carbon films [156].

5.5 Diamond formation after 120 min deposition time

Further, diamond growth for 120 min was carried out on adamantane-seeded Pt/SiO_2/Si substrates and adamantane-seeded SiO_2/Si substrates without Pt over-coating. The structure and surface morphology of synthesized diamond and their characteristics

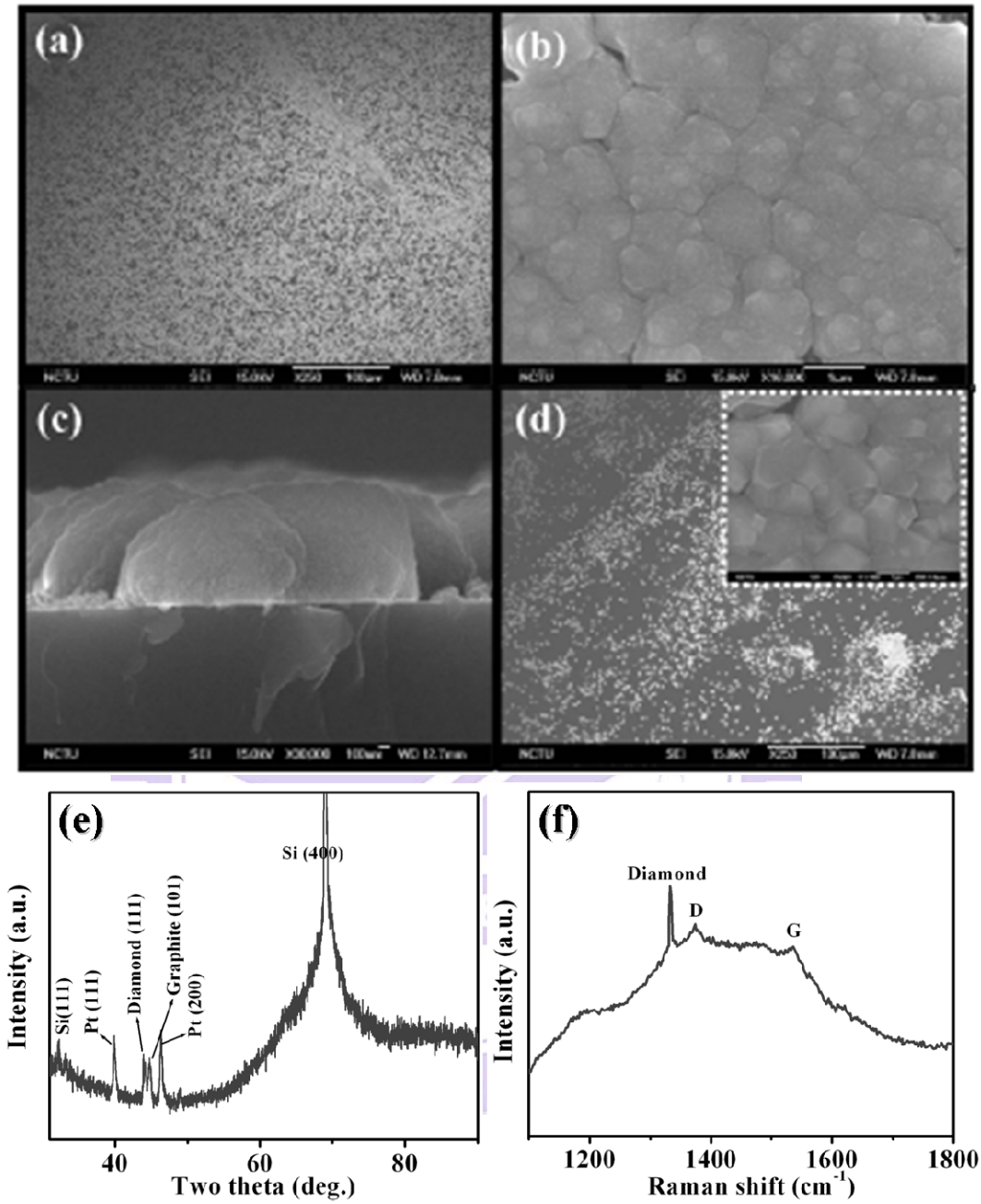

Figure 5.13: (a) Plan-view SEM, (b) high-magnification SEM image, (c) cross-sectional SEM image, (e) XRD pattern, and (f) Raman spectra of diamond (growth time 2 hr) on Pt/SiO_2/Si. (d) Plan-view; insert high magnification image of diamond on substrate without Pt.

are shown in Figure 5.13. Figures 5.13 (a)-(c) show the SEM images of the deposits on $Pt/SiO_2/Si$, revealing that the diamonds has been synthesized uniformly on $Pt/SiO_2/Si$ substrate in cauliflower shape with the appearance of some {100} diamond facets. For the sample without Pt interlayer, the synthesized diamonds in {100} facet are clearly seen in Figure 5.13 (d). However, the density of diamond in the sample with Pt interlayer is ~ 10^8 cm^{-2} much higher than 10^6 cm^{-2} on that without Pt interlayer, as shown in Figures 5.13 (a) and (d). Thus, it is clear that the coating of adamantane on the Pt interlayer can enhance the diamond density. The thickness of diamond on Pt/Si is ~ 900nm, as shown in Figure 5.13 (c), giving the growth rate of diamond in ~ 0.45μm/hr. In addition, the XRD pattern supports the formation of the microcrystalline diamond film on $Pt/SiO_2/Si$, as shown in Figure 5.13(e). In addition to Si peaks, the XRD pattern in Figure 5.13 (e) presents sharp and well-defined peaks at 2θ = 39.8, 43.9, 44.6, and 46.39 degrees corresponding to the interplanar spacings of Pt {111}, diamond {111}, graphite {101}, and Pt {200}, respectively. Moreover, the micro-Raman spectrum of the diamond film on $Pt/SiO_2/Si$ is shown in Figure 5.13(f). The characteristic feature of diamond at 1332 cm^{-1} is clearly observed, the full width at half- maximum of the peak is determined to be 7.2 cm^{-1}. The film also contains disordered graphitic carbon components or amorphous carbon as indicated by D and G bands. We also used XPS to characterize the diamond $Pt/SiO_2/Si$ as shown in the survey spectrum of Figure 5.14 (a). Apart from the expected peaks from elements of diamond (C) and Pt, the oxygen signal has also been detected. Figure 5.14(b) shows the XPS C(1s) spectrum of the diamond sample. The deconvolution of the spectrum has shown that the C 1s peaks are composed of three peaks at ~283.7 ~ 284.4, 284.8 eV, 285.3 eV, and 287.1 eV corresponding to C-C (sp^3), C-C and C-H (sp^2) and C-O bondings [157, 158, 159]. The negative binding energy (0.5eV) shift as shown in high-resolution spectrum of Pt (4f) [Figure 5.14 (c)] is due to size effect of Pt particles. However, the Pt (4f) peak at 73.4eV corresponds to Pt-C bonding [160].

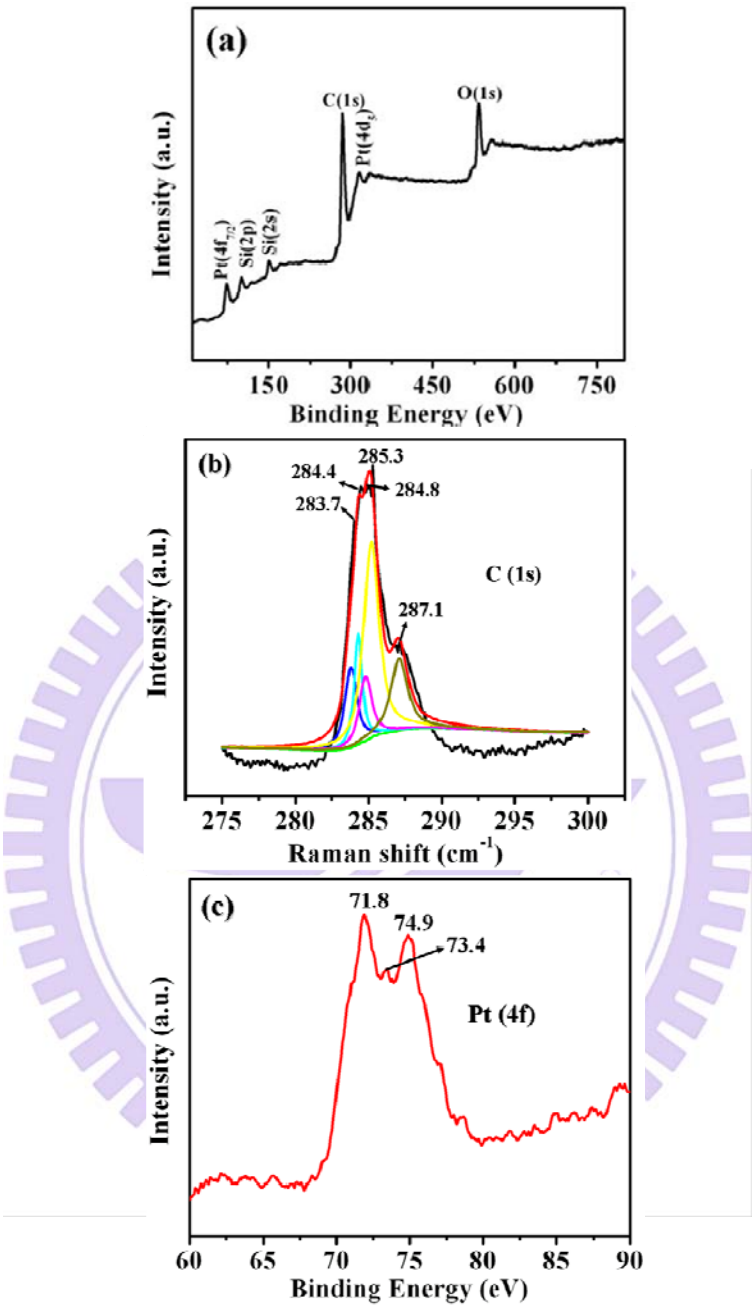

Figure 5.14: The XPS spectra (a) survey spectrum, (b) high-resolution spectrum of the C (1s), and (c) high-resolution spectrum of the Pt (4f) region of diamond on adamantane/Pt/SiO_2/Si.

Furthermore, the cross-sectional TEM specimen of a sample (admantane seeded on Pt/SiO_2/Si) deposited for 2 hr was prepared by focused ion beam (FEI Nova 200 Dual

beam FIB). For the protection of the TEM specimen against damage from the high-energy ion beam (30 keV Ga^+) in FIB, the specimen was coated with platinum. A cross-sectional bright-field TEM image of diamond/Pt/SiO_2/Si is shown in Figure 5.15 (a). From Figure 5.15 (a), the dark contrast regions are actually corresponding Pt particles (as shown in the following EDX) with a size of ~5 to ~50 nm. Clearly, the Pt is not a continuous interlayer. Also, it is seen that the thickness of diamond particle is ~ 900nm. The HRTEM image in Figure 5.15 (b) is obtained from an interfacial region without the Pt particles, showing diamond and Si lattice fringes. The inset Fast Fourier transform (FFT) of lattice image of Si and diamond shows the diffraction characteristics from which the measured interplanar spacing of ~2.06 Å can be identified to be diamond {111} one [Figure 5.15 (b)]. Between diamond and Si, it shows amorphous SiO_2 in a thickness of ~ 4 nm. The SAD pattern obtained from around the marked region of the particle [Figure 5.15 (a)] shows the single crystalline diamond characteristics in <110> zone axis. To further identify the Pt phase at the interface, we acquired EDX from different regions, as shown numerical mark in Figure 5.15 (a). In Figure 5.16, the EDX spectrum from region 1 [Figure 5.15 (a)] where we can see some particles (in black contrast) at the interface, shows Pt, Si, and O peaks, whereas at region 2 on interface (where no black particles exist) it shows Si, O, as well as Cu peaks. Therefore, it is clear that the Pt signal comes from black particles while O and Si signals are from SiO_2 on Si substrate. The Cu signal comes from the Cu grid. The EDX from region 3 (from Si substrate) shows the Si and O and from region 4 (diamond particles) shows the high concentration of carbon. It is also clear that the SiO_2 layer between Pt and Si prevents the silicidation. Hayashi et al have observed high crystalline (111) oriented diamond on Pt/TiO_2/SiO_x/Si. The oxide layers prevent not only the silicidation formation between Pt and Si, and it may also prevent the formation of SiC.

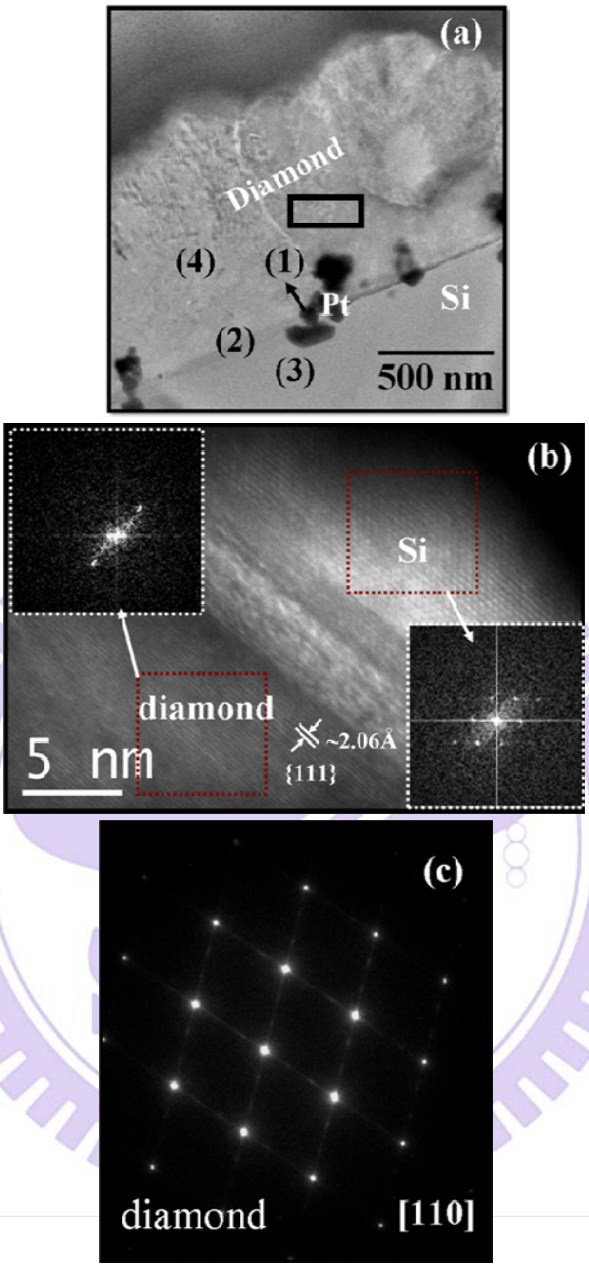

Figure 5.15: (a) Cross-sectional BF-TEM image of diamond/Pt/Si (b) HRTEM image of diamond/Si; the d-spacing between the fringes was ~ 2.06 Å of diamond {111} plane; the inset showing FFT patterns from of Si and diamond lattice images (indicated by arrow), and (c) SAED from marked (rectangle) region of diamond along <110> direction.

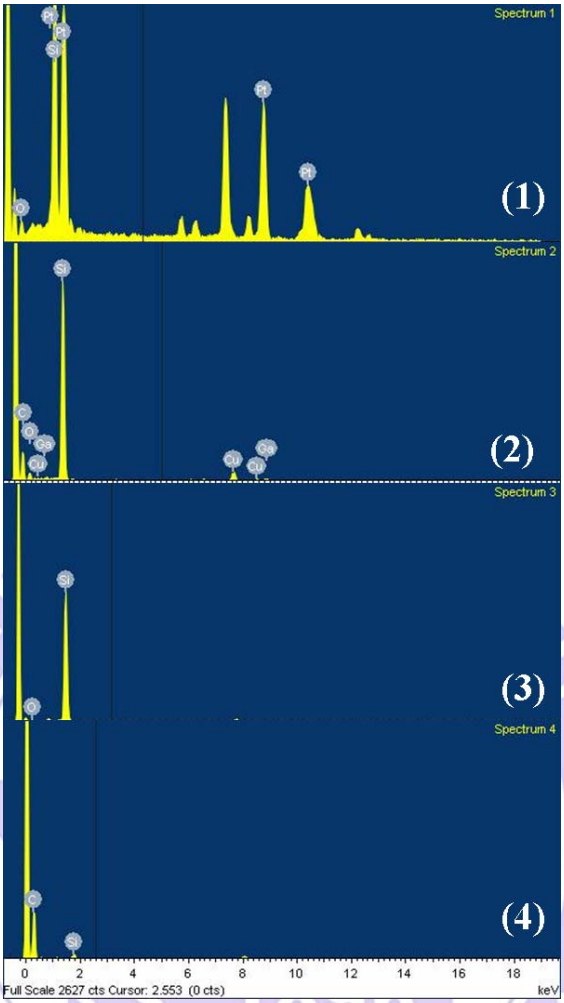

Figure 5.16: EDX spectra of inset mark in B.F image in Figure 5.15 (1) From Pt interface particles, (2) without Pt particles in the interfacial region, (3) Si substrate, and (d) from diamond particles.

The schematic diagram of the growth of diamond film on $Pt/SiO_2/Si$ substrate is shown Figure 5.17. Since Pt has catalytic properties, it can dissolve appreciable amounts of hydrogen and chemically adsorb hydrocarbons [161]. The bonding characteristics depend on their structure such as saturated hydrocarbons which are weakly adsorbed. Methane can desorb intact from Pt (111) surface by heating [162]. Unsaturated hydrocarbons can make covalent bond with Pt surface. Jacob et al. have shown adsorption of various CH_x and C_2H_y hydrocarbons with Pt surface. They noticed that in

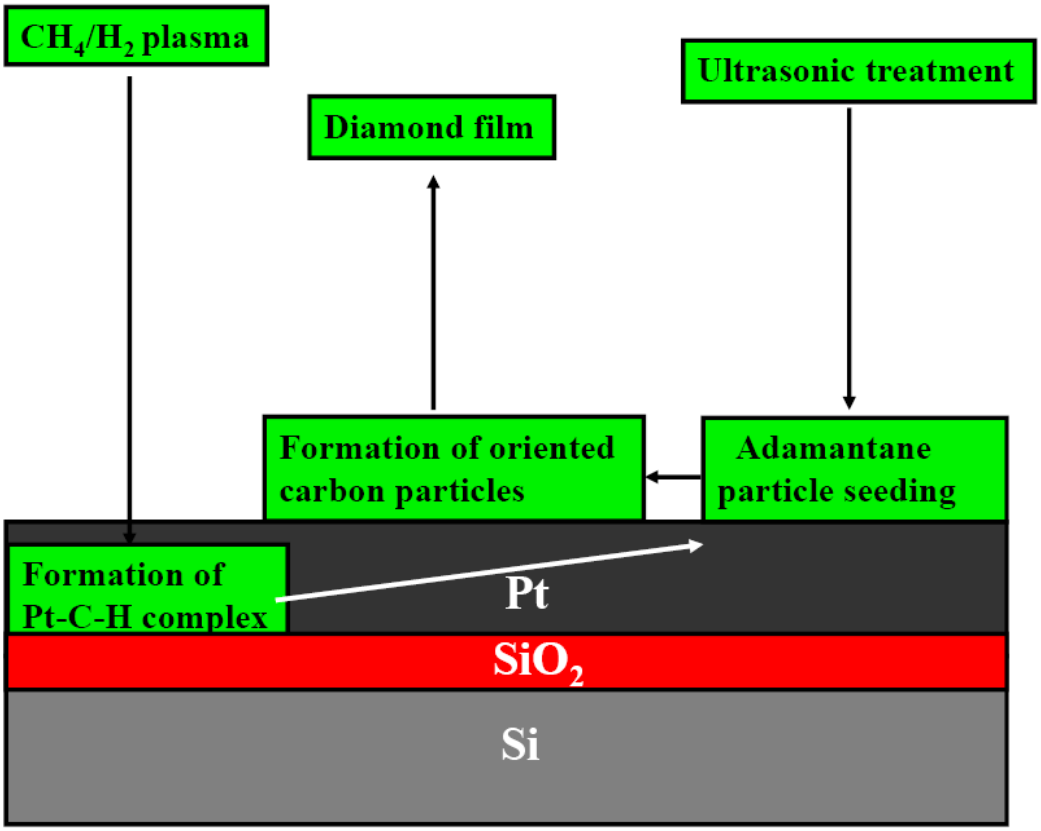

Figure 5.17: Schematic diagram of diamond growth on adamantane seeded on $Pt/SiO_2/Si$ substrates.

each case the structures on the surface are comparable to gas-phase analogues in which some CH bonds are replaced with C-Pt σ bonds [163]. The hydrogen is highly soluble in transition metals. Therefore, during ultrasonic process the adamantine is seeded (adsorbed) on the $Pt/SiO_2/Si$ surface, as shown in Figure 5.2 (a). In the CVD, hydrogen ion and the hydrocarbon radicals from the plasma (1% CH_4 in H_2 plasma) with the seeded adamantane might form the Pt-C-H complex. From the C 1s signals in XPS spectra (Figures 5.11, 5.12, and 5.14), it is shown that CO bond is present on the surface. It seems that Pt behaves as a catalyst and support the CO bond formation in the early stage (2 min) of deposition as shown in Figure 5.11 (b). Therefore, CO bonding can overcome the evaporation rate of adamantane and enhance the density. In general, hexane has high

evaporation properties. However, since Pt can adsorb the hydrocarbons, chemical reaction may not only take place with adamantane but also with hexane (C_6H_{14}). Previous studies have shown that the hexane can react with Pt [164]. The melting point of Pt (~1772°C) is much higher than the growth temperatures used in this study. The solid solubility of C in Pt is less than 1at.% at 650°C according to the Pt-C binary phase diagram [165]. Therefore, it is unlikely that the dissolution medium is a pure form of Pt or Pt-C solid solution. It is rather appropriate to consider the Pt-C-H ternary system in order to understand the SEM observations as the present CVD growth of diamond was conducted in a predominantly hydrogen plasma environment. Hydrogen in its atomic form has a small atomic radius, easily dissolves in Pt, and would weaken the bond strength and lower the effective melting point of the ternary system. Roy and co-workers claimed the importance of the metal-C-H systems in their observation of diamond growth from Ni-C and Cu-C mixtures in hydrogen plasma [166]. After 15 min treatment, the adsorbed Pt-C-H complex may promote the formation of some carbon particles which then act as nuclei for growth of diamond film in the presence of CVD plasma (1% CH_4 in H_2 plasma).

5.6 Summary

We have confirmed that diamond films are successfully grown on adamantane-seeded Pt/SiO_2/Si substrates by MPCVD from the gaseous mixture of methane and hydrogen. The seeded adamantane might first transform into nanodiamond and some unidentified carbon particles in the early stage of deposition within 2 min. After further deposition of 5-15 min, the existence of sp^3 carbon and graphite phases are evident, while no adamantane can be identified. With long time deposition in 120 min, diamond formation is observed. The SiO_2 layer between Pt and Si prevents not only silicidation reaction but also avoid to the formation of silicon carbide. The density synthesized diamond on Pt/SiO_2/Si is higher than that of without Pt/SiO_2/Si.

Chapter 6
Conclusions and Future Works

6.1 Conclusions

In this study, we have successfully synthesized diamond films by MPCVD using adamantane precursor at low temperature. The deposited films are characterized by scanning electron microscopy, Raman spectrometry, x-ray diffraction, x-ray photoelectron spectroscopy, and transmission electron microscopy. The synthesized diamond was not only in good quality but also was in good yield. The using of Pt on Si substrate enhances the diamond density. The presence of oxide layer prevents the formation of silicidation. The primary results of this thesis are summarized as follows:

1. In this study, diamond films have been synthesized on adamantane-coated silicon {100} substrate at low temperature by microwave plasma chemical vapor deposition from a gaseous mixture of methane and hydrogen gases without the application of a bias voltage to the substrates. Prior to adamantane coating, the Si substrates were not pretreated such as abraded/scratched. The substrate temperatures were ~ 400 to ~530 °C during diamond deposition. The diamond density was varied with microwave power. Characterization results provide definitive evidence for high-crystalline quality diamond film, which is synthesized on a SiC rather than clean Si substrate. The SiC was not uniformly distributed on the Si surface. The diamond films exhibit a low-threshold (55 V/μm) and high current-density (1.6 mA/cm^2) field-emission (FE) properties.

2. This study also demonstrates the synthesis of diamond films by microwave plasma chemical vapor deposition (MPCVD) on Pt/SiO_2/Si substrate. The Pt deposited on SiO_2/Si at room temperature was seeded with adamantane in hexane solution by ultrasonic treatment. It is shown that diamond formation is enhanced with adamantane on Pt/SiO_2/Si. During deposition, the adamantane may transform into

nanodiamond phase, graphite, and other carbon phases, which can then act as nuclei for diamond formation. The presence of oxide intermediate layer between Pt and Si prevent silicidation as well as SiC in diamond deposition.

6.2 Future Works

We have shown that the chemical precursor (adamantane) plays a major role in the formation of diamond at relatively low temperature and pressure in microwave plasma CVD because their structure is similar to diamond. Adamantane can be evaporated even at ambient atmosphere. The high evaporation rate at room temperature is one of the major disadvantages of using chemical precursor (adamantane) in CVD. Therefore, the major challenge with using adamantane is how to control the evaporation rate. Another major issue is how to obtain uniform distribution of adamantane on the substrate surface and to understand the exact mechanism of diamond nucleation and growth from adamantane. The diamond deposition in lower temperature (below 100°C) and pressure is still not succeeded. If we can succeed to prevent adamantane from evaporation during CVD, it may be possible to deposit diamond at <100°C. Using novel materials (Pt, Pd, Ir, and Au etc.) as substrate is an expensive route for diamond growth. Therefore, cost is one of the big issues for diamond deposition.

References

[1] B. X. Yang, W. Zhu, J. Ahn, and H. S. Tan, “Carburization and bias effects on textured (100) diamond thin films by microwave plasma enhanced chemical vapor deposition”, 151 (1995) 319.

[2] R. Spitzla, V. Raiko, R. Heiderhoff, H. Gnaser, and J. Engemann, “MPCVD diamond deposition on bias pretreated porous silicon”, Diamond & Relat. Mater. 4 (1995) 563.

[3] S. Bohr, R. Haubner, and B. Lux, “Influence of nitrogen additions on hot-filament chemical vapor deposition of diamond”, Appl. Phys. Lett. 68 (1996) 1075.

[4] R. Kröger, L. Schäfer, C.-P. Klages, and R. Six, “Enhanced Diamond Film Growth by Hot-Filament CVD Using Forced Convection”, Physica Status Solidi (a) 154 (1996) 33.

[5] F. Xiong, Y.Y. Wang, V. Leppert, and R.P.H. Chang, “Pulsed laser deposition of amorphous diamond-like carbon films with ArF (193 nm) excimer laser”, J. Mater. Res. 8 (1993) 2265.

[6] H. Huck, A. Jech, E. B. Halac, J. Nicolai, M. A. R. de Benyacar, and R. Righini, “Mass-separated ion beam deposition of diamond-like thin films” Nuclear Instruments and Methods in Physics Research Section B: Beam Interactions with Materials and Atoms 84 (1994) 62.

[7] X. Z. Zhao, R. Roy, K. A. Cherian, and A. Badzian, “Hydrothermal growth of diamond in metal–C–H2O systems”, Nature 385 (1997) 513.

[8] Y. Ando, S. Tobea, T. Saito, J. Sakurai, H. Tahara, and T. Yoshikawa, “Enlargement of the diamond deposition area in combustion flame method by traversing substrate”, Thin Solid Films 457 (2004) 217.

[9] Y. C. Lee, S. J. Lin, D. Pradhan, I. N. Lin, “Improvement on the growth of ultrananocrystalline diamond by using pre-nucleation technique”, Diamond & Relat. Mater. 15 (2006) 353.

[10] K. Tsugawa, M. Ishihara, J. Kim, Y. Koga, and M. Hasegawa, “Nucleation Enhancement of Nanocrystalline Diamond Growth at Low Substrate Temperatures by Adamantane Seeding”, J. Phys. Chem. C, 114 (2010) 3822.

[11] M. D. Whitfield, B. Audic, C. M. Flannery, L. P. Kehoe, G. M. Crean, and R. B. Jackman, “Acoustic wave propagation in free standing CVD diamond: Influence of

film quality and temperature" Diamond Relat. Mater. 8 (1999) 732.

[12] P. M. Martineau, M. P. Gaukroger, K. B. Guy, S. C. Lawson, D. J. Twitchen, I. Friel, J. O. Hansen, G. C. Summerton, T. P. G. Addison, and R. Burns, "High crystalline quality single crystal chemical vapour deposition diamond", J. Phys.: Condense. Matter 21 (2009) 364205.

[13] C. S. Yan, H. K. Mao, W. Li, J. Qian, Y. Zhao, and R. J. Hemley, "Ultraharddiamond single crystals from chemical vapor deposition", Phys. Stat. Sol. (a) 201 (2004) R25.

[14] V. Vaijayanthimala and H-C Chang, "Functionalized fluorescent nanodiamonds for biomedical applications", Nanomedicine 4 (2009) 47.

[15] H. Liu and D. S. Dandy, "Diamond chemical vapor deposition: nucleation and early growth stages", Noyes publications

[16] D. B. Oakes, J. E. Butler, K. A. Snail, W. A. Carrington, and L. M. Hanssen, "Diamond synthesis in oxygen-acetylene flames: Inhomogeneities and the effects of hydrogen addition", J. Appl. Phys. 69 (1991) 2602

[17] D. G. Lee and R. K. Singh, "Synthesis of (111) oriented diamond thin films by electrophoretic deposition process", Appl. Phys. Lett. 70 (1997) 1542.

[18] Y. X. Han, H. Ling, J. Sun, M. Zhao, T. Gebre, and Y.F. Lu, "Enhanced diamond nucleation on copper substrates by graphite seeding and CO2 laser irradiation", Applied Surface Science 254 (2008) 2054.

[19] H. G. Chen and L. Chang, "Diamond nucleation on Ni3Al substrate using bias enhanced nucleation method", Diamond Relat. Mater. 14 (2005) 183.

[20] V. Buck, F. Deuerler, H. Kluwe, and B. Schmiler, "Influence of chemical pretreatment of hardmetal substrates for diamond deposition", Int. J. Refr. Met. Hard mater. 20 (2002) 101.

[21] M. R. Shen, H. Wang, Z. Y. Ning, C. Ye, Z. Q. Gan, and Z. X. Ren,"Enhanced diamond nucleation on pretreated silicon substrates", Thin Solid Films 30 (1997) 77.

[22] R.J. Meilunas, R.P.H. Chang, "Diamond nucleation on surfaces using carbon clusters", J. Mater. Res. 9 (1994) 61.

[23] D. Das and R. N. Singh, "A review of nucleation, growth and low temperature synthesis of diamond thin films", Int. Mater. Rev. 52 (2007) 29.

[24] F. P. Bundy, H. T. Hall, H. M. Strong, and R. H. Wentorf, "Man-made diamonds"

Nature, 176 (1955) 51.

[25] H. W. Kroto, J. R. Heath, S. C. O. Brien, R. F. Curl, and R. E. Smalley, “C60: Buckminsterfullerene” Nature 318 (1985) 162.

[26] S. Iijima, “Helical microtubules of graphitic carbon” Nature 354 (1991) 56.

[27] R. Bacon, “Growth, structure, and properties of graphite whiskers”, J. Appl. Phys. 31 (1960) 283.

[28] S. Aisenberg and R. Chabot, “Ion-Beam deposition of thin films of diamondlike carbon”, J. Appl. Phys. 42 (1971) 2953.

[29] J. E. Dahl, S. G. Liu, and R. M. K. Carlson, “Isolation and Structure of Higher Diamondoids, Nanometer-Sized Diamond Molecules”, Science 299 (2003) 96.

[30] K. S. Novoselov, A. K. Geim, S. V. Morozov, D. Jiang, Y. Zhang, S. V. Dubonos, I. V. Grigorieva, and A. A. Firsov, “Electric field Effect in atomically thin carbon films”, Science 306 (2004) 666.

[31] H. Pierson, “Handbook of Carbon, Graphite, Diamond and Fullerenes”, Noynes, New Jersey 1993.

[32]K. Kobashi, “Diamond Films: Chemical vapor deposition for oriented and heteroepitaxial growth”, Elsevier 2005.

[33] R. S. Kalyoncu, “GRAPHITE”, Graphite (2000) 35.1.

[34] K. E. Spear and J. P. Dismukes, “Synthetic Diamond: Emerging CVD science and Technology”, Wiley, Pennington, NJ, 1994.

[35] B. Dischler and C. Wild, “Low-pressure synthetic diamond: Manufacturing and Applications”, Springer, Heidelberg 1998.

[36] J. Isberg, J. Hammersberg, E. Johansson, T. Wikström, D. J. Twitchen, A. J. Whitehead, S. E. Coe, G. A. Scarsbrook, “High Carrier Mobility in Single-Crystal Plasma-Deposited Diamond”, Science 297 (2002) 1670.

[37] T. Sharda and S. Bhattacharyya, “Diamond Nanocrystals”, Encyclopedia of nanoscience & Nanotechnology 2 (2004) 337.

[38] R. Abbaschian, H. Zhu, and C. Clarke, “High pressure–high temperature growth of diamond crystals using split sphere apparatus”, Diamond Relat. Mater. 14 (2005) 1916.

[39] R. F. Davis, “Diamond Films and Coating Development, Properties, and

Applications”, Noyes Publications, Park Ridge, New Jersey, 1992.

[40] P. S. DeCarli and J. C. Jamieson, "Formation of Diamond by Explosive Shock”, Science 133 (1961) 1821.

[41] N. R. Greiner, D. Phillips, J. Johnson, and F. Volk, “Diamonds in detonation soot” Nature 333 (1988) 440.

[42] S. Osswald, A. Gurga, F. Kellogg, K. Cho, G. Yushin, and Y. Gogotsi, “Plasma pressure compaction of nanodiamond”, Diamond Relat. Mater. 16 (1967) 2007.

[43] 宋建民，”鑽石合成” 全華科技圖書股份有限公司 (2000).

[44] J. C. Angus, H. A. Will, and W. S. Stanko, “Growth of Diamond Seed Crystals by Vapor Deposition”, J. Appl. Phys. 39 (1968) 2915.

[45] P. K. Bachmann, D. Leers, and H. Lydtin, “Towards a general concept of diamond chemical vapour deposition”, Diamond Relat. Mater. 1 (1991) 1.

[46] R. Messier and P. K. Bachmann, "Emerging technology of diamond thin films”, C & EN (1989) 20.

[47] N. Ohtake and M. Yoshikawa, “Diamond Film Preparation by Arc Discharge Plasma Jet Chemical Vapor Deposition in the Methane Atmosphere”, J. Electrochem. Soc., 137 (1990) 717.

[48] S. Yugo, K. Semoto, K. Hoshina, T.kirnura, and H. Nakai, "A modeling of diamond nucleation”, Diamond Relat. Mater. 4 (1995) 903.

[49] D. G. Bhatt, D. G. Johnson, A. P. Malshe, H, Naseem, W. D. Brown, L. W. Schaper, and C. H. Shen, “A preliminary investigation of the effect of post-deposition polishing of diamond films on the machining behavior of diamond-coated cutting tools”, Diamond Relat. Mater. 4 (1995) 921.

[50] A. K. Gangopadhyay and M. A. Tamor, Friction and wear behavior of diamond films against steel and ceramics”, Wear 169 (1993) 221.

[51] J. Filik, “Fundamental Studies on the Deposition and Characterisation of Novel Diamond-Like Materials” Ph.D thesis (2006).

[52] D. He, L. Shao, W. Gong, E. Xie, K. Xu, and G. Chen, “Electron transport and electron field emission of nanodiamond synthesized by explosive detonation”, Diamond Relat. Mater. 9 (2000) 1600.

[53] S.-T. Lee, Z. D. Lin, and X. Jiang, “CVD diamond films: nucleation and growth”,

Mater. Sci. Eng., 25 (1999)123.

[54] G. Manickam, “Deposition of diamond films on steel substrates for tribological applications”, (1980).

[55] S. Yugo, T. Kanai, T. Kimura, and T. Muto, "Generation of diamond nuclei by electric field in plasma chemical vapor deposition”, Appl. Phys. Lett. 58 (1991) 1036.

[56] M. Aoki, H. Kawarada, and M. Katoh, “Plasma-enhanced diamond nucleation on Si”, Jpn. J. Appl. Phys. 33 (1996) 194.

[57] R. Stöckel, M. Stammler, K. Janischowsky, K. Ley, M. Albrecht, and H. P. Stunk, “Diamond nucleation under bias conditions”, J. App. Phys. 83 (1998) 531.

[58] J. Ma, “Exploration of the gas phase chemistry in microwave activated plasmas used for diamond chemical vapour deposition”, (2008).

[59] J. E. Butler, R. L. Woodin, L. M. Brown, and P. Fallon, “Thin Film Diamond Growth Mechanisms [and Comment]’ Philos. Trans. R. Soc. London 342 (1993) 209.

[60] B. J. Garrison, E. J. Dawnkaski, D. Srivastava, and D. W. Brenner, “Molecular Dynamics Simulations of Dimer opening on a Diamond {001}(2x1) Surface”, Science 255 (1992) 835.

[61] S. Skokov, B. Weiner, and M. Frenklach, “Elementary Reaction Mechanism of Diamond Growth from Acetylene”, J. Phys. Chem. 98 (1994) 8.

[62] A. P. Marchand, “Diamondoid Hydrocarbons--Delving into Nature's Bounty”, Science 299 (2003) 52.

[63] A. T. Balaban and P. V. R. Schleyer, “Systematic classification and nomenclature of diamond hydrocarbons—I:Graph-theoretical enumeration of polymantanes”, Tetrahedron 34 (1978) 3599.

[64] S. Landa, and V. Machacek, “Adamantane, a new hydrocarbon extracted from petroleum”, Chem. Commun. 5 (1933) 1.

[65] J. E. P. Dahl, J. M. Moldowan, T. M. Peakman, J. C. Clardy, E. Lobkovsky, M. M. Olmstead, P. W. May, T. J. Davis, J. W. Steeds, K. E. Peters, A. Pepper, A. Ekuan, and R. M. K. Carlson, “Isolation and Structural Proof of the Large Diamond Molecule, Cyclohexamantane (C26H30)”, Angew. Chem. Int. Ed. 42 (2003) 2040.

[66] V. Prelog and R. Seiwerth, “Über die Synthese des Adamantans”, Ber. Dtsch. Chem. Ges., 74 (1941) 1644.

[67] P. V, R. Schleyer, "A Simple Preparation of Adamantane", *J. Am. Chem. Soc.* **79** (1957) 3292.

[68] C. Cupas, P. V. R. Schleyer, and D. J. Trecker, "Congressane", J. Am. Chem. Soc. 87 (1965) 917.

[69] S. Hala, S. Landa, and V. Hanus, "Islolation of Tetracyclo[6.3.1.$0^{2,6}$.$0^{5,10}$] dodecane and Pentacyclo[7.3.1.1.^{4,12}.$0^{2,7}$.$0^{6,11}$] tetradecane (Diamantane) from Petroleum", Angew. Chem. Internat. Edit. 5 (1966) 1045.

[70] V. Z. Williams, P. V. R. Schleyer, G. J. Gleicher, and L. B. Rodewald, "Triamantane", J. Am. Chem. Soc. 88 (1966) 3862.

[71] R. Lin and Z. A. Wilk, "Natural occurrence of tetramantane ($C_{22}H_{28}$), pentamantane ($C_{26}H_{32}$) and hexamantane ($C_{30}H_{36}$) in a deep petroleum reservoir", Fuel 74 (1995) 1512.

[72] J. E. Dahl, S. G. Liu, and R. M. K. Carlson,"Isolation and Structure of Higher Diamondoids, Nanometer-Sized Diamond Molecules", Science 299 (2003) 96.

[73] V. Vijayakumar A. B. Garg, B. K. Godwal, and S. K. Sikka, "Pressure induced phase transitions and equation of state of adamantane", J. Phys.: Condens. Matter 13 (2001) 1961.

[74] N. Polfer, B. G. Sartakov, and J. Oomens, "The infrared spectrum of the adamantyl cation", Chemical Physics Letters 400 (2004) 201.

[75] A. Giraud, T. Jenny, E. Leroy, O. M. Kuttel, L. Schlapbach, P. Vanelle, and Luc Giraud, "Chemical Nucleation for CVD Diamond Growth", J. Am. Chem. Soc. 123 (2001) 2271.

[76] S.-M. Wang, "The study of growth of diamond nano-platelet arrays on (111) textured diamond-film substrates", (2009).

[77] T. Yamada, T. Yokoyama, and A. Sawabe, "Electron emission from hydrogenated and oxidized heteroepitaxial diamond doped with boron" Diamond Relat. Mater. 11 (2002) 780.

[78] J. K. Yan and L. Chang, "Chemical vapour deposition of oriented diamond nanocrystallites by a bias-enhanced nucleation method", Nanotechnology 17 (2006) 5544.

[79] N. Yang, H. Uetsuka, E. Osawa, and C. E. Nebel, "Vertically Aligned Diamond

Nanowires for DNA Sensing", Angew. Chem. Int. Ed. 47 (2008) 5183.

[80] G. Dearnaley and J. H. Arps, Biomedical applications of diamond-like carbon (DLC) coatings: A review", Surf. Coat. Technol. 200 (2005) 2518.

[81] H. G. Chen and L. Chang, Growth of diamond nanoplatelets on nanocrystalline diamond substrates", Diamond Relat. Mater. 18 (2009) 141.

[82] M. S. You, F. C. N. Hong, Y. R. Jeng, and S. M. Huang, "Low temperature growth of highly transparent nanocrystalline diamond films on quartz glass by hot filament chemical vapor deposition", Diamond Relat. Mater. 18 (2009) 155.

[83] B. Walkowiak, W. Okroj, H. Jerczynska, and Z. Pawlowska, "Micron-sized diamond particles are internalized by endothelial cells", Diamond Relat. Mater. 18 (2009) 651.

[84] S. D. Wolter, M. T. McClure, J. T. Glass, and B. R. Stoner, "Bias-enhanced nucleation of highly oriented diamond on titanium carbide (111) substrates", Appl. Phys. Let. 66 (1995) 2810.

[85] E. Leroy, O. M. Kuttel, L. Schlapbach, L. Giraud, and T. Jenny, "Chemical vapor deposition of diamond growth using a chemical precursor", Appl. Phys. Lett. 73 (1998) 1050.

[86] R. J. Meilunas, R. P. H. Chang, S. Liu, and M. M. Kappes, "Nucleation of diamond films on surfaces using carbon clusters", Appl. Phys. Lett., 59 (1991) 3461.

[87] P. N. Barnes and R. L. C. Wu, "Nucleation enhancement of diamond with amorphous films", Appl. Phys. Lett. 62 (1993) 37.

[88] Z. Feng, K. Komvopoulos, D. B. Bogy, J. W. Ager, S. Anders, A. Anders, Z. Wang, and I. G. Brown, "Effect of pretreatment process parameters on diamond nucleation on unscratched silicon substrates coated with amorphous carbon films", J. Appl. Phys. 79 (1996) 485.

[89] A. A. Morrish and P. E. Pehrsson, "Effects of surface pretreatments on nucleation and growth of diamond films on a variety of substrates", Appl. Phys. Lett. 59 (1991) 417.

[90] M. Umeno, M. Noda, H. Uchida, and H. Takeuchi, "Deposition of DLC film from adamantane by using pulsed discharge plasma CVD". Diamond Relat. Mater. 17 (2008) 684.

[91] S. Matsumoto and Y. Matsui, "Electron microscopic observation of diamond

particles grown from the vapour phase", J. Mater. Sci. 18 (1983) 1785.

[92] A. Stacey, I. Aharonovich, S. Prawer, and J. E. Butler, "Controlled synthesis of high quality micro/nano-diamonds by microwave plasma chemical vapor deposition", Diamond Relat. Mater. 18 (2009) 51.

[93] N. A. Braga, C. A. A. Cairo, E. C. Almeida, M. R. Baldan, and N. G. Ferreiraa, "From micro to nanocrystalline transition in the diamond formation on porous pure titanium", Diamond Relat. Mater. 17 (2008) 1891.

[94] E. M. Schaller, O. M. Kuettel, and L. Schlapbach, "X-Ray Photoelectron Diffraction of the Silicon-Diamond Interface", Phys. Stat. Sol. (a) 153 (1996) 415.

[95] S. Gsell, S. Berner, T. Brugger, M. Schreck, R. Brescia, M. Fischer, T. Greber, J. Osterwalder, and B. Stritzker, "Comparative electron diffraction study of the diamond nucleation layer on Ir(001)", Diamond Relat. Mater. 17 (2008) 1029.

[96] J. Stiegler, A. Bergmaier, J. Michler, S. Laufer, G. Dollinger, and E. Blank, "The effect of nitrogen on low temperature growth of diamond films", Thin Solid Films 352 (1999) 29.

[97] W. Fortunato, A. J. Chiquito, J. C. Galzerani, and J. R. Moro, "A comparative study of p-type diamond films using Raman and transport measurements", Thin Solid Films 476 (2005) 246.

[98] L. Wang, Y. Wang, J. Zhou, and S. Ouyang, "Diamond films produced by microwave plasma chemical vapor deposition at low temperature and their characterization" Mater. Sci. Eng. A 475 (2008) 17.

[99] L. Dong, B. Ma, and G. Dong**, "**Diamond deposition at low temperature by using CH_4/H_2 gas mixture", Diamond Relat. Mater. 11 (2002) 1697.

[100] I. Schmidt and C. Benndorf, "Low temperature CVD diamond deposition using halogenated precursors—deposition on low melting materials: Al, Zn and glass", Diamond Relat. Mater. 10 (2001) 347.

[101] Y. Liou, A. Inspektor, R. Weimer, D. Knight, and R. Messier, "The effect of oxygen in diamond deposition by microwave plasma enhanced chemical vapor deposition", J. Mater. Res. 5 (1990) 2305.

[102] J. Filik , J. N. Harvey, N. L. Allan , P. W. May, J. E. P. Dahl , S. Liu, and R. M. K. Carlson, "Raman spectroscopy of diamondoids", Spectrochimica Acta A 64 (2006)

681.

[103] L. G. Bulusheva, A. V. Okotrub, I. A. Kinloch, I. P. Asanov, A. G. Kurenya, A. G. Kudashov, X. Chen, and H. Song, “Effect of nitrogen doping on Raman spectra of multi-walled carbon nanotubes”, Phys. stat. sol. (b) 245 (2008) 1971.

[104] M. Mermoux, B. Marcus, G. M. Swain, and J. E. Butler, “A Confocal Raman Imaging Study of an Optically Transparent Boron-Doped Diamond Electrode”, J. Phys. Chem. B 106, (2002) 10816.

[105] T. Sharda, T. Soga, T. Jimbo, and M. Uembo, “Growth of nanocrystalline diamond films by biased enhanced microwave plasma chemical vapor deposition”, Diamond Relat. Mater. 10 (2001) 1592.

[106] T. Lin, Y. Yu, A. T .S. Wee, Z. X. Shen, and K. P. Loh, “Compositional mapping of the argon–methane–hydrogen system for polycrystalline to nanocrystalline diamond film growth in a hot-filament chemical vapor deposition system”, Appl. Phys. Lett. 77 (2000) 2692.

[107] L. Fayette, B. Marcus, M. Mermoux, G. Tourillon, K. Laffon, P. Parent, and F. LeNormand, “Local order in CVD diamond films: Comparative Raman, x-ray-diffraction, and x-ray-absorption near-edge studies”, Phys. Rev. B 57 (1998) 14123.

[108] T. Kawato and K.-I. Kondo, “Effects of oxygen on CVD diamond synthesis”, Jap. J. Appl. Phys. 26 (1987) 1429.

[109] J. E. Krzanowski and J. Wormwood, “Microstructure and mechanical properties of Mo–Si–C and Zr–Si–C thin films: Compositional routes for film densification and hardness enhancement”, Surf. Coat. Technol. 201 (2006) 2942.

[110] E. Vanhove, J. de Sanoit, J. C. Arnault, S. Saada, C. Mer1, P. Mailley, P. Bergonzo, and M. Nesladek, “Stability of H-terminated BDD electrodes: an insight into the influence of the surface preparation”, Phys. Stat. Sol. (a) 204 (2007) 2931.

[111] R. Boukherroub, D. D. M. Wayner, G. I. Sproule, D. J. Lockwood, and L. T. Canham, “Stability Enhancement of Partially-Oxidized Porous Silicon Nanostructures Modified with Ethyl Undecylenate[1]”, Nano Lett. 1 (2001) 713.

[112] E. J. Corat, N. G. Ferreira, V. J. Trava-Alroldi, N. F. Leite, R. C. M. Barros, and K. Iha, “Diamond seed consolidation onto untreated silicon substrate”, J. Mater. Sci. Lett. 16 (1997) 197.

[113] T. Hirai, Y. Kanno, and Y. Takagi, “Effect of Water Contained in Acetone on Nanocrystalline Diamond Particles or Film synthesis”, Jpn. J. Appl. Phys. 47 (2008) 738.

[114] D. Roy, Z. H. Barber, and T. W. Clyne, “Ag nanoparticle induced surface enhanced Raman spectroscopy of chemical vapor deposition diamond thin films prepared by hot filament chemical vapor deposition”, J. Appl. Phys. 91 (2002) 6085.

[115] A. C. Ferrari and J. Robertson, “Origin of the 1150-cm^{-1} Raman mode in nanocrystalline diamond”, Phys. Rev. B 63 (2001) 121405.

[116] T. Lo´pez-Rios, E. Sandre, S. Leclereq, and E. Sauvain, “Polyacetylene in diamond films evidenced by surface enhanced Raman scattering”, Phys. Rev. Lett. 76 (1996) 4935.

[117] Q. Zhang, S. F. Yoon, J. Ahn, Rusli, and Y. P. Guo, “The effects of nitrogen flow on the Raman spectra of polycrystalline diamond films”, Microelectronics Journal 29 (1998) 875.

[118] B. Marcus, L. Fayette, M. Mermoux, L. Abello, and G. Lucazeau, “Analysis of the structure of multicomponent carbon films by resonant Raman scattering”, J. Appl. Phys. 76 (1994) 3463.

[119] J. Birrell, J. E. Gerbi, O. Auciello, J. M. Gibson, J. Johnson, and J. A. Carlisle, “Interpretation of the Raman spectra of ultrananocrystalline diamond”, Diamond Relat. Mater. 14 (2005) 86.

[120] A.T. Sowers, B. L. Ward, S. L. English, and R. J. Nemanich, “Field emission properties of nitrogen-doped diamond films”, J. Appl. Phys. 86 (1999) 3973.

[121] M. Bechelany, A. Brioude, D. Cornu, G. Ferro, and P. Miele, “A Raman Spectroscopy Study of Individual SiC Nanowires”, Adv. Funct. Mater. 17 (2007) 939.

[122] J. Wasyluk, T. S. Perova, S. A. Kukushkin, A. V. Osipov, N. A. Feoktistov, and S. A. Grudinkin, “Raman Investigation of Different Polytypes in SiC Thin Films Grown by Solid-Gas Phase Epitaxy on Si (111) and 6H-SiC Substrates”, Materials Science Forum 645 (2010) 359.

[123] S. Intarasiri, A. Hallen, J. Lu, J. Jensen, L. D. Yu, K. Bertilsson, M. Wolborski, S. Singkarat, and G. Possnert, “Crystalline quality of 3C-SiC formed by high-fluence

C^+-implanted Si", Appl. Surf. Sci. 253 (2007) 4836.

[124] S. Takabayashi, K. Okamoto, H. Sakaue, T. Takahagi, K. Shimada, and T. Nakatani, "Annealing effect on the chemical structure of diamondlike carbon", J. Appl. Phys. 104 (2008) 043512.

[125] W. R. L. Lambrecht, C. H. Lee, B. Segall, J. C. Angus, Z. Li, and M. Sunkara, "Diamond nucleation by hydrogenation of the edges of graphitic precursors", Nature 364 (1993) 607.

[126] Y. X. Han, H. Ling, J. Sun, M. Zhao, T. Gebre, and Y. F. Lu, "Enhanced diamond nucleation on copper substrates by graphite seeding and CO_2 laser irradiation". Appl. Surf. Sci. 254 (2008) 2054

[127] R. N. Tiwari, J. N. Tiwari, and L. Chang, "The synthesis of diamond films on adamantane-coated Si substrate at low temperature", Chem. Eng. J. 158 (2010) 641.

[128] S. Nakashima and H. Harima, "Raman Investigation of SiC Polytypes", Phys. Stat. Solidi A 162 (1997) 39.

[129] C. Y. Lee, J. S. Lin, N. I. Lin, and H. F. Cheng, "Effect of boron doping on the electron-field-emission properties of nanodiamond films", J. Appl. Phys. 97 (2005) 054310.

[130] H. R. Fowler and L. Nordheim, "Electron Emission in Intense Electric Fields", Proc. R Soc. London Ser. A 119 (1928) 173.

[131] P. T. Joseph, N. H. Tai, C. H. Chen, H. Niu, H. F. Cheng, W. F. Pong, and I. N. Lin, "On the mechanism of enhancement on electron field emission properties for ultrananocrystalline diamond films due to ion implantation", J. Phys. D: Appl. Phys. 42 (2009) 105403.

[132] S. Arora and V. D. Vankar, Field emission characteristics of microcrystalline diamond films: Effect of surface coverage and thickness", Thin Solid Films 515 (2006) 1963.

[133] W. A. Clay, T. Sasagawa, M. Kelly, J. E. Dahl, R. M. K. Carlson, N. Melosh, and Z.-X. Shen, "Diamondoids as low-k dielectric materials" Appl. Phys. Lett. 93 (2008) 172901.

[134] B. Atakan, K. Lummer, and K. K. Hoinghaus, "Diamond deposition in acetylene-oxygen fames: nucleation and early growth on molybdenum substrates for different

pretreatment procedures", Phys. Chem. Chem. Phys. 1 (1999) 3151.

[135] Y. X. Han, H. Ling, J. Sun, M. Zhao, T. Gebre, and Y.F. Lu, "Enhanced diamond nucleation on copper substrates by graphite seeding and CO_2 laser irradiation", Appl. Surf. Sci. 254 (2008) 2054.

[136] W. R. L. Lambrecht, C. H. Lee, B. Segall, J. C. Angus, Z. Li, and M. Sunkara, "Diamond nucleation by hydrogenation of the edges of graphitic precursors", Nature 364 (1993) 607.

[137] T. Saito, S. Tsuruga, N. Ohya, K. Kusakabe, S. Morooka, H. Maeda, A. Sawabe, and K. Suzuki, " Epitaxial nucleation of diamond on an iridium substrate by bias treatment, for microwave plasma-assisted chemical vapor deposition" 7 (1998) 1381.

[138] T. Tachibana, Y. Yokota, K. Miyata, K. Kobashi, and Y. Shintani, "Heteroepitaxial diamond growth process on platinum (111)", Diamond Relat. Mater. 6 (1997) 266.

[139] T. Tachibana, Y. Yokota, K. Hayashi, K. Miyata, K. Kobashi, and Y. Shintani, "Parametric study of bias-enhanced nucleation of diamond on platinum in microwave plasma", 9 (2000) 251.

[140] Y. Shintani, "Growth of highly (111) oriented, highly coalesced diamond films on platinum (111) surface: A possibility of heteroepitaxy", J. Mater. Res. 11 (1996) 2955.

[141] T. Tachibana, Y. Yokota, K. Miyata, T. Onishi, K. Kobashi, M. Tarutani, Y. Takai, R. Shimizu, and Y. Shintani, "Diamond films heteroepitaxially grown on platinum (111)", Phys. Rev. B 56 (1997) 15967.

[142] Y. Hayashi, Y. Matsushita, T. Soga, M. Umeno, and T. Jimbo, "The formation of a (111) texture of the diamond film on Pt/TiO2/SiO*x*/Si substrate by microwave plasma chemical vapor deposition", Diamond Relat. Mater. 11 (2002) 409.

[143] J. Oomens, N. Polfer, O. Pirali, Y. Ueno, R. Maboudian, P. W. May, J. Filik, J. E. Dahl, S. Liu, and R. M. K. Carlson, "Infrared spectroscopic investigation of higher diamondoids", Journal of Molecular Spectroscopy 238 (2006) 158.

[144] R. M. Corn, V. L. Shannon, R. G. Synder, and H. L. Strauss, "Orientational dynamics and disorder of solid adamantane as studied by infrared spectroscopy", J. Chem. Phys. 81(1984) 5231.

[145] T. Zheng, N. Nishiyama, Y. Egashira, and K. Ueyama, “Surfactant-mediated synthesis of Pt nanoparticles/nanoporous carbons composite”, Studies in Surface Science and Catalysis 162 (2006) 561.

[146] M. Tarakci, K. Korkmaz, Y. Gencer, and M. Usta, “Plasma electrolytic surface carburizing and hardening of pure iron”, Surf. Coat. Technol. 199 (2005) 205.

[147] K. W. Sun and C. Y. Wang, “Optical properties of a single free standing nanodiamond”, Journal of Physics: Conference Series 92 (2007) 012031.

[148] S. Costa, E. B. Palen, M. Kruszynska, A. Bachmatiuk, and R. J. Kalenczuk, “Characterization of carbon nanotubes by Raman spectroscopy”, Mater. Sci. Pol. 2 (2008) 433.

[149] B. Scheibe, E. B. Palen, and R. J. Kalenczuk, “Oxidation and reduction of multiwalled carbon nanotubes—preparation and characterization”, Materials Characterization 61 (2010) 185.

[150] K. Kobashi, “Diamond Films: Chemical Vapor Deposition for oriented and Heteroepitaxial growth Elsevier (2005).

[151] S. Takabayashi, K. Okamoto, K. Shimada, K. Motomitsu, H. Motoyama, T. Nakatani, H. Sakaue, H. Suzuki, and T. Takahagi, “Chemical Structural Analysis of Diamondlike Carbon Films with Different Electrical Resistivities by X-ray Photoelectron Spectroscopy”, Jap. J. Appl. Phys. 47 (2008)3376.

[152] G. Dagli and N.-H. Sung, “Properties of Carbon/Graphite Fibers Modified by Plasma Polymerization”, Polymer Composites, 10 (1989) 109.

[153] T. P. Smirnova, A. M. Badalyan, V. O. Borisov, L. V. Yakovkina, V. V. Kaichev, A. N. Shmakov, A. V. Nartova, V. I. Rakhlin, and A. N. Fomina, “Plasma Enhanced Chemical Vapor Deposition of Silicon Carbonitride Films from Volatile Silyl Derivatives of 1,1-Dimethylhydrazine”, High Energy Chemistry 37 (2003) 303.

[154] R. I. Kvon, A. I. Boronin, S .K. Shaikhutdinov, and R. A. Buyanov, “XPS and STM study of carbon deposits at the surface of platinum (110)”, Applied Surface Science 120 (1997) 239.

[155] M. Delamar, G. Dbsarmot, O. Fagebaume, R. Hitmi, and J. Pinson, “Modification of carbon fiber surfaces by electrochemical reduction of Aryl diazonium salts: application to carbon epoxy composites”, Carbon 35 (1997) 801.

[156] R. Boukherroub, D. D. M. Wayner, G. I. Sproule, D. J. Lockwood, and L. T. Canham, "Stability Enhancement of Partially-Oxidized Porous Silicon Nanostructures Modified with Ethyl Undecylenate[1]", Nano Lett. 1 (2001) 713.

[157] K. G. Saw and J. d. Plessis, "The X-ray photoelectron spectroscopy C 1s diamond peak of chemical vapour deposition diamond from a sharp interfacial structure", Materials Letter 58 (2004) 1344.

[158] S.-E. Ong, S. Zhang, H. Du, and D. Sun, "Relationship between bonding structure and mechanical properties of amorphous carbon containing silicon", Diamond Relat. Mater. 16 (2007) 1628.

[159] M. Ahmed, J. A. Byrne, and J. A. D. McLaughlin, "Glycine Adsorption onto DLC and N-DLC Thin Films Studied by XPS and AFM", e-J. Surf. Sci. Nanotech. 7 (2009) 217.

[160] G. Parravano, "Equilibrium hydrogen transfer between benzene and C_6 hydrocarbons over supported metal catalysts", J. Catalysis 16 (1970) 1.

[161] E. M. Crabb and M.K. Ravikumar, "Synthesis and characterisation of carbon-supported PtGe electrocatalysts for CO oxidation", Electrochimica Acta 46 (2001) 1033.

[162] H. O. strom, H. Ogasawara, L.-A. Naslund, L. G. M. Pettersson, and A. Nilsson, "Physisorption-Induced C-H Bond Elongation in Methane", PRL 96 (2006) 146104.

[163] T. Jacob and W. A. Goddard III, "Chemisorption of (CH_x and C_2H_y) Hydrocarbons on Pt(111) Clusters and Surfaces from DFT Studies", J. Phys. Chem. B 109 (2005) 297.

[164] K. Matusek and Z. Paal, "Reactions of n-Hexane and n-Nonane on Pt Catalysts and hydrogenating off hydrocarbonaceous adspecies after reaction', React. Kinet. Catal. Lett. 67 (1999) 241.

[165] T. B. Massalski, H. Okamoto, P. R. Subramanian, L. Kacprzak, "Binary Alloy Phase Diagram", ASM International, Ohio (1990) 794.

[166] R. Roy, H. S. Dewan, and P. Ravindranathan, "Diamond synthesis via a low-pressure solid-state-source process", Mater. Res. Bull. 28 (1993) 861.

Appendix

List of Publications

Journal Papers:

1. **Rajanish N. Tiwari** and Li Chang "Enhanced diamond nucleation on Pt/Si substrates by chemical precursor" manuscript under preparation.
2. **Rajanish N. Tiwari,** S. R. Sahoo, I. N. Lin, and Li Chang "The Synthesis of ultrananocrystalline diamond film on AC/Si substrate by chemical vapor deposition" manuscript under preparation.
3. **Rajanish N. Tiwari** and Li Chang "Adamantane precursor for the synthesis of icosahedral diamond particles" (Under review).
4. **Rajanish N. Tiwari**, Jitendra N. Tiwari, J. S. Meena, and Li Chang "Electrical characterization of metal-insulator-metal capacitor comprising a low-k film at room temperature" (revised).
5. **Rajanish N. Tiwari** and Li. Chang "Etching of GaN by microwave plasma of hydrogen" ***Semicond. Sci. Technol***. 25 (2010) 035010.
6. **Rajanish N. Tiwari,** Jitendra N. Tiwari, and Li Chang "The synthesis of diamond films on adamantane-coated Si substrate at low temperature" ***Chem Eng. J.*** 158 (2010) 641-645.
7. **Rajanish N. Tiwari** and Li Chang **"**Chemical Precursor for the Synthesis of Diamond Films at Low Temperature" ***Appl. Phys. Express*** 3 (2010) 045501-3.
8. **Rajanish N. Tiwari** and Li Chang "Growth, microstructure, and field emission properties of synthesized diamond film on adamantane-coated silicon substrate by microwave plasma chemical vapor deposition" ***Journal of Applied Physics*** 107 (2010) 103305-7.
9. **Rajanish N. Tiwari**, Wei-Chun Chen, Wei-Lin Wang and Li Chang "Diamond plates on dome-like particles: preparation, characterization and Field emission property" ***Journal of Applied Crystallography*** 43 (2010) 883-889.
10. Jitendra N. Tiwari, Fu-Ming Pan, Te-Ming Chen, **Rajanish N. Tiwari** and Kun-Lin Lin "Electrocatalytic activity of Pt nanoparticles electrodeposited on amorphous carbon coated silicon nanocones" ***J. Power Sources*** 195 (2010) 729-735.

11. Wei-Chun Chen, Wei-Lin Wang, **Rajanish N. Tiwari** and Li Chang *"*Growth and characterization of diamond films on TiN/Si(100) by microwave plasma chemical vapor deposition*"* ***Diamond related materials*** 18 (2009) 124-127.
12. Jitendra N. Tiwari, Fu-Ming Pan, **Rajanish N. Tiwari**, and S.K. Nandi "Facile synthesis of continuous Pt island networks and their electrochemical properties for methanol electrooxidation" ***Chem. Commun.*** 48 (2008) 6516-6518.
13. Jitendra N. Tiwari, Jagan Singh Meena, Chung-Shu Wu, **Rajanish N. Tiwari**, and Fu-Hsiang Ko, "Highly reliable, nanoscale and eco-friendly thin film composite materials as a gate dielectric layer for next generation flexible MIM capacitors" ***ChemSusChem*** DOI: 10.1002/ cssc.201000118 (accepted).
14. Jitendra N. Tiwari, **Rajanish N. Tiwari**, and Kun-Lin Lin, "Synthesis of Pt nanopetals on High Ordered Silicon Nanocones for Enhanced Methanol Electrooxidation Activity" ***ACS Appl. Mater. Interfaces*** 2 (2010) 2231-2237.

International Conference:

I. **Rajanish N. Tiwari**, Li Chang "Synthesis of diamond using adamantane precursor in chemical vapor deposition" ***Diamond 2009***· 20th Anniversary Conference 6-10 September 2009, Athens, Greece.
II. **Rajanish N. Tiwari**, Wei-Chun Chen and Li Chang "Formation of polycrystalline globular diamond particles on TiC/Si". ***NDNC-2008,*** Taipei, Taiwan
III. **Rajanish N. Tiwari** and Li Chang "Deposition of Icosahedral diamond particles on adamantane-coated Si substrate by MPCVD" ***Diamond 2010,*** Budapest, Hungry (accepted).
IV. Wei-Chun Chen, **Rajanish N. Tiwari** and Li Chang "Growth and characterization of diamond films on TiN/Si(100) by MPECVD" ***NDNC-2008,*** Taipei, Taiwan.
V. Jitendra N. Tiwari, Te-Ming Chen, **Rajanish N. Tiwari** and Fu-Ming Pan "Oxygen Reduction Reaction Activity of Pt Nanoparticles Electrodeposited on Amorphous Carbon Coated Silicon Nanocones"***214th ECS Meeting*** - Honolulu, HI, Abstract # 963